Mathematisches Forschungsinstitut Oberwolfach

Computational Inverse Problems for Partial Differential Equations

Organised by
Liliana Borcea, Ann Arbor
Thorsten Hohage, Göttingen
Barbara Kaltenbacher, Klagenfurt

14 May – 20 May 2017

ABSTRACT. The problem of determining unknown quantities in a PDE from measurements of (part of) the solution to this PDE arises in a wide range of applications in science, technology, medicine, and finance. The unknown quantity may e.g. be a coefficient, an initial or a boundary condition, a source term, or the shape of a boundary. The identification of such quantities is often computationally challenging and requires profound knowledge of the analytical properties of the underlying PDE as well as numerical techniques. The focus of this workshop was on applications in phase retrieval, imaging with waves in random media, and seismology of the Earth and the Sun, a further emphasis was put on stochastic aspects in the context of uncertainty quantification and parameter identification in stochastic differential equations. Many open problems and mathematical challenges in application fields were addressed, and intensive discussions provided an insight into the high potential of joining deep knowledge in numerical analysis, partial differential equations, and regularization, but also in mathematical statistics, homogenization, optimization, differential geometry, numerical linear algebra, and variational analysis to tackle these challenges.

Introduction by the Organisers

The workshop was attended by 49 participants from eight countries (15 from outside Europe), eight of them women, as well as nine of them PhD students and PostDocs. The scientific program consisted of 23 long and 4 short talks with extensive discussions, includig one evening talk after the Wednesday excursion to Sankt Roman.

Additionally, a diverse group of participants joined for regular evening discussions on deep learning in model-based inverse problems. Topics included the potential of these methods to (a) learn better regularization; (b) learn model correction in situations where the forward model is inexact, e.g., due to model reduction.

The talks, which covered a broad range of methods and applications and often lead to lively discussion, were gathering around the following focus areas:

Imaging with waves: The reconstruction of an unknown wave speed inside some domain from boundary observations arises in many applications ranging from geophysical prospection to ultrasound imaging. One issues here is multiple scattering leading to artifacts when using linearized reconstruction algorithms. A novel method that was shown to erase multiple scattering, is based on appropriate construction of exterior initial Cauchy data through scattering control. Another approach presented at the meeting relies on reduced order modeling, which can actually be carried out using the measured data only.

In the context of inverse source problems and inverse scattering in time harmonic wave equations, reconstruction algorithms and stability as well as convergence rate estimates were shown. Some of them resulted from uncertainty principles for certain Fourier type transforms, some of them from a monotonicity relation between sets contained in the support of the scatterer and the Neumann-Dirichlet operator. Others used Tikhonov regularization under appropriate regularity conditions on the solution. In the context of electromagnetic waves, imaging of small scatterers was discussed, with resolution results on the Kirchhoff imaging functionals that extend the scalar acoustic case. An important topic in inverse scattering is the computation of transmission eigenvalues, since they carry information on the refractive index of non-absorbing media. Also forward modeling plays an important role here, e.g. the derivation of appropriate radiation conditions or the characterization of shape derivatives as a crucial prerequisite for computationally solving the inverse problem.

Uncertainty quantification: Incomplete information on the geometry of the domain on which the governing PDE holds, modeling errors due to domain truncation, and noise in the data are examples of sources of uncertainty that propagates into the computational solutions of inverse problems. Bayesian approaches allow to quantify such uncertainties, as was demonstrated in the context of electrical impedance tomography, quantitative photoacoustic tomography, modeling of ice sheet flow, among others. Key challenges in the computational solution of infinite dimensional Bayesian inverse problems governed by PDEs include the choice of appropriate prior distributions, efficient solution of PDE constrained optimization problems for evaluating the MAP estimator, approximation of the posterior covariance, and the treatment of correlated non-zero-mean noise.

Phase retrieval: In many practical inverse scattering and wave imaging applications, only intensity measurements are available, whereas phase information is inaccessible to direct observation. Certain wave imaging tasks allow to exploit illumination and frequency diversity in order to recover complete interferometric data, from which the image can be obtained in a robust manner. In X-ray phase contrast

imaging, stability results can be achieved under support constraints on the image. Also uniqueness questions as well as error estimates and explicit reconstruction formulas for phaseless inverse medium scattering problems were discussed.

Stochastic differential equations: A strong link between this focus area and the first one was given by a talk on high-order statistics for the random paraxial wave equation, in which the slowly varying envelope satisfies an SDE, the Itô-Schrödinger equation. This, among other results, leads to a stochastic motivation for correlation based imaging. A rather different field of application is modeling of neural activity of the brain by stochastic PDEs or function valued SDEs, which was presented together with a statistical analysis, including, e.g., the derivation of (approximate) 1-d SDEs for certain quantities of interest.

A couple of talks dealt with the problem of estimating parameters — drift and diffusion — in stochastic differential equations. One of them gave an overview on convergence rates results for drift and/or diffusion estimators in the continuous and high frequency observation regime as compared to the more challenging and so far less explored low frequency regime of coarsely spaced observation times. These observation settings were also considered in a different presentation from a Bayesian perspective. An alternative approach to drift and diffusion estimation that is well suited for the low frequency – actually even for the single time – observation case relies to a reformulation of the problem via the Fokker Planck (or Kolmogorov) equation, a deterministic PDE for the transition density.

Seismic imaging: Extracting information on the interior of the earth from seismic waves is a classical source of inverse problems. Related techniques, in particular full waveform inversions, can be used to reconstruct interior quantities in the Sun such as flows and sound speed using correlation data of the line-of-sight velocities on the Solar surface.

Kirchhoff migration is a standard seismic imaging technique based on a ze-roth order imaging functional. Alternative, appropriately constructed first order imaging functionals were shown to allow for better recovery of singularities. Full waveform inversion, requires efficient optimization tools that are capable of avoiding local minima. This can, e.g., be achieved by means of multilevel algorithms, whose stability constants and hence radii of attraction can be controlled by scale and frequency.

Beyond these focus areas we also had a number of talks on mixed topics in computation inverse problems for PDEs such as the *reconstruction of singularities of the conductivity* in electrical impedance tomography, based on complex geometric optics solutions and a radial Fourier transform, that enables to establish and exploit relations to X-ray tomography. Further the inverse problem of *recovering microscale properties of materials from effective or homogenized parameters*, where the spectral measure in the integral representation of the homogenized parameters plays a crucial role was considered. In addition *hybrid techniques* such as photocoustic or acousto-optic imaging that enable enhanced biomedical imaging and lead to coupled systems for different physical quantities like light and sound were discussed.

Workshop: Computational Inverse Problems for Partial Differential Equations

Table of Contents

Abstracts

Scattering control and inverse problem for the wave equation with piecewise smooth wave speed

MAARTEN DE HOOP

(joint work with Peter Caday, Vitaly Katsnelson, Paul Kepley, Lauri Oksanen, Gunther Uhlmann)

We consider the wave equation with an unknown, piecewise smooth, wave speed on a bounded domain. The wave speed contains a discrete set of conormal singularities. We assume that we can probe the domain from outside with arbitrary Cauchy initial data and observe the wavefield outside the domain for sufficiently large times. We introduce the notion of an almost directly transmitted wave constituent generated by "localized" Cauchy initial values in an exact setting and a microlocal framework. We show that one can obtain exterior Cauchy initial data through scattering control that generate this constituent, at a time equal to some geodesic distance from the boundary of the domain erasing the multiple scattering that would probe the deeper part of the domain. This holds up to a harmonic extension of the first component of the (interior) Cauchy data at the above mentioned time. The scattering control can be implemented as an iteration of Neumann type, involving instantaneous time mirrors, which converges on a set that is dense in the space of all exterior Cauchy initial data. We then prove uniqueness, that is, the recovery of the locations of the discontinuities and the wave speeds in between them.

In parallel, we consider the inverse boundary value problem for the wave equation with a smooth wave speed, using partial data. We present an algorithm for reconstruction derived from the boundary control method via wavefield reconstruction and the reconstruction of the transformation from semi-geodesic to Cartesian coordinates. The reconstruction holds in some region near the boundary, but it possible to iterate it in a layer stripping fashion. The layer stripping alternates between local reconstruction and so-called redatuming.

REFERENCES

[1] Maarten V. de Hoop and Paul Kepley and Lauri Oksanen, *On the Construction of Virtual Interior Point Source Travel Time Distances from the Hyperbolic Neumann-to-Dirichlet Map*, SIAM Journal on Applied Mathematics **76** (2016), 805–825.
[2] Peter Caday, Maarten V. de Hoop, Vitaly Katsnelson and Gunther Uhlmann, *Scattering Control for the Wave Equation with Unknown Wave Speed*, arXiv:1701.01070.

Back-projected reduced-order models for solving inverse acoustic scattering problems

Mikhail Zaslavsky

(joint work with Vladimir Druskin, Alexander Mamonov)

We consider a problem of imaging the acoustic velocity in the scalar wave equation, in some domain of interest, from the measurements of its solutions in the time domain on an array of transducers located on the boundary of said domain. This problem is known to be highly non-linear, mostly because of multiple reflections between (unknown) scatterers. When more than one reflector is present, first reflections (primaries) from them are typically mixed together with multiply-reflected wavefields (multiples). This creates additional events in the data compared to linearized case with primaries only. Linear imaging methods may interpret these events as extra reflectors that are not present in the actual medium. In this work we developed artifact-free imaging algorithm based on the theory of model order reduction. In particular, we construct an approximate wave equation propagator that is derived to satisfy certain data interpolation conditions, as explained later. If the data is discretely sampled in time, then the reduced order model (ROM) interpolating the data is an orthogonal projection of the propagator on the (Krylov) subspace spanned by the wavefield snapshots taken precisely at the data sampling instants. Computing the projection requires an orthogonalization of wavefiled snapshots to be performed. Since the wavefields are not known inside the domain of interest, the orthogonalization is performed implicitly. It is a non-linear operation that is crucial to our approach, as it allows to suppress the effects of multiple reflections and probe the medium of interest with localized wavefields.

Consider a scalar wave equation for the acoustic pressure $p(x,t)$

$$(1) \qquad p_{tt} = c(x)^2 \Delta p + q_t(t)\phi(x)e(x), \quad -\infty < t < \infty, \quad x \in \Omega,$$

where Ω is the domain of interest in $\mathbb{R}^d$, $d = 2, 3$. Domain Ω can be either infinite or finite. Here we assume Ω is finite with boundary $\mathcal{B} = \partial\Omega$ split into the *accessible* $\mathcal{B}_A$ and *inaccessible* $\mathcal{B}_I = \mathcal{B} \setminus \mathcal{B}_A$ parts respectively. We also assume that the *acoustic velocity* $c(x)$ is piecewise smooth in Ω.

Wave equation (1) is driven by the source term comprised of a wavelet $q(t)$, source weighting function $\phi(x)$ and a distribution $e(x)$. Source distribution $e(x)$ is supported on the accessible boundary supp $e \subset \mathcal{B}_A$

Assuming that all sources and receivers are collocated, the components of the measured data on $\mathcal{B}_A$ are given by

$$(2) \qquad \mathbf{D}_{i,j}(t) = \int_\Omega \psi(x)e_i(x)u(x,t)dx, \quad t > 0,$$

where $u(x,t) = \frac{1}{2}\left(p(x,t) + p(x,-t)\right)$, $\psi(x)$ is a spatial receiver weighting function and $p(x,t)$ is the solution of 1 for $e = e_j(x)$.

The data can be equivalently rewritten as

$$(3) \qquad \mathbf{D}(t) = \mathbf{b}^* \cos\left(t\sqrt{-\widehat{A}}\right)\mathbf{b}, \quad t > 0,$$

where $\widehat{A} = c(x)\Delta c(x)$ and

(4) $$\mathbf{b}(x) = [\widetilde{q}^{1/2}(-\widehat{A})\sqrt{\phi(x)\psi(x)}\mathbf{e}](x),$$

is the row-vector-valued *transducer function* $\mathbf{b} : \Omega \to \mathbb{R}^{1\times m}$.

At the core of our imaging approach is the construction of a reduced order model for the sampled data $\mathbf{D}^k$, $k = 0, \ldots, 2n-1$. To that end we need to transform the symmetrized data (3) using the fact that the data is sampled uniformly in time. Specifically, it is clear

(5)
$$\mathbf{D}^k = \mathbf{D}(t_k) = \mathbf{b}^* \cos\left(k\tau\sqrt{-\widehat{A}}\right)\mathbf{b} = \mathbf{b}^* \cos\left(k \arccos\left[\cos\tau\sqrt{-\widehat{A}}\right]\right)\mathbf{b}$$
$$= \mathbf{b}^* T_k(P)\mathbf{b},$$

where T_k are Chebyshev polynomials of the first kind of degree k and P is the *propagator*

(6) $$P = \cos\left(\tau\sqrt{-\widehat{A}}\right).$$

We seek the reduced order model in the form (5), namely

(7) $$\widetilde{\mathbf{F}}^k = \widetilde{\mathbf{B}}^* T_k(\widetilde{\mathbf{P}})\widetilde{\mathbf{B}},$$

where $\widetilde{\mathbf{P}} \in \mathbb{R}^{mn\times mn}$ is the reduced order propagator and $\widetilde{\mathbf{B}} \in \mathbb{R}^{mn\times m}$ is the reduced order transducer matrix.

To compute the reduced order propagator and transducer matrices we solve the following interpolation problem

(8) $$\widetilde{\mathbf{F}}^k = \mathbf{D}^k, \quad k = 0, \ldots, 2n-1.$$

It can be shown [2] that the reduced order propagator $\widetilde{\mathbf{P}} \in \mathbb{R}^{mn\times mn}$ and transducer matrix $\widetilde{\mathbf{B}} \in \mathbb{R}^{mn\times m}$ that solve the interpolation problem

(9) $$\mathbf{D}^k = \widetilde{\mathbf{B}}^* T_k(\widetilde{\mathbf{P}})\widetilde{\mathbf{B}}, \quad k = 0, \ldots, 2n-1,$$

are orthogonal projections

(10) $$\widetilde{\mathbf{P}} = (\mathbf{U}\mathbf{L}^{-1})^*(P\mathbf{U}\mathbf{L}^{-1}) = (\mathbf{L}^{-1})^*(\mathbf{U}^* P\mathbf{U})\mathbf{L}^{-1}, \quad \widetilde{\mathbf{B}} = (\mathbf{U}\mathbf{L}^{-1})^*\mathbf{b},$$

of the true propagator (6) and transducer function (4) on the Krylov subspace $colspan(\mathbf{U})$. Here $\mathbf{U} = (\mathbf{b}, \cos\left(\tau\sqrt{-\widehat{A}}\right)\mathbf{b}, \ldots, \cos\left((n-1)\tau\sqrt{-\widehat{A}}\right)\mathbf{b})$ is a tall matrix of snapshots and $\mathbf{L}\mathbf{L}^* = \mathbf{U}^*\mathbf{U}$. Though we don't have access to $\mathbf{U}$, we still can compute $\mathbf{U}^* P\mathbf{U}$ and $\mathbf{L}$ via the given data $\{\mathbf{D}^k\}_{k=0}^{2n-1}$ only. Indeed, it can be easily verified (see [1]) that $(k;l)$-th blocks of these matrices can be computed as

$$(\mathbf{U}^*\mathbf{U})_{k,l} = (\widehat{\mathbf{u}}^k)^*\widehat{\mathbf{u}}^l = \mathbf{b}^* T_k(P)T_l(P)\mathbf{b} = \frac{1}{2}\left(\mathbf{b}^* T_{k+l}(P)\mathbf{b} + \mathbf{b}^* T_{|k-l|}(P)\mathbf{b}\right).$$

and

$$(\mathbf{U}^*(P\mathbf{U}))_{k,l} = (\widehat{\mathbf{u}}^k)^*(P\widehat{\mathbf{u}}^l) = \frac{1}{4}\left(\mathbf{D}^{k+l+1} + \mathbf{D}^{|k-l+1|} + \mathbf{D}^{|k+l-1|} + \mathbf{D}^{|k-l-1|}\right),$$

Hence, having the measured data $\{\mathbf{D}^k\}_{k=0}^{2n-1}$ only without access to snapshots, we still can compute the orthogonal projection of the propagator onto the subspace of snapshots. Once the reduced order propagator $\widetilde{\mathbf{P}}$ is computed from the sampled data, we can use it for inversion and imaging. In this work we target to approximation of the difference $g(x_i, x_i, \tau) - g_0(x_i, x_i, \tau)$ of the Green's functions for the true unknown medium and for some known background with velocity $c_{(o)}(x)$ that is assumed to capture kinematics of the problem. If in the vicinity of a point $x \in \Omega$ the unknown medium $c(x)$ contains a reflector, then the difference will be large. Otherwise, $c(x) \approx c_{(o)}(x)$ and $g(x_i, x_i, \tau) - g_0(x_i, x_i, \tau) \approx 0$. If the subspace of snapshots is rich enough then the back-projected propagator $\mathbf{U}\mathbf{L}^{-1}\widetilde{\mathbf{P}}(\mathbf{U}\mathbf{L}^{-1})^*$ approximates $g(x_i, x_i, \tau)$ when being probed by delta-functions $\delta(x - x_i)$ from the left and from the right. However, we don't have access to $\mathbf{U}$. Hence, we propose to approximate $g(x_i, x_i, \tau) - g_0(x_i, x_i, \tau)$ by *ROM backprojection imaging functional*

$$(11) \qquad \mathcal{I}_{BP}(x) = [\mathbf{U}_{(o)}(x)\mathbf{L}_{(o)}^{-1}] \left(\widetilde{\mathbf{P}} - \widetilde{\mathbf{P}}_{(o)} \right) [(\mathbf{U}_{(o)}(x)\mathbf{L}_{(o)}^{-1})^*], \quad x \in \Omega,$$

Imaging via $\mathcal{I}_{BP}(x)$ can be related to imaging of the Schrödinger potential of the Liouville-transformed equation (1) (see [2] for details).

In Figure 1 we demonstrate the performance of the algorithm for example of imaging hydraulic fractures (exact model is shown on the left). The sources-receivers array is located on top of the domain. As clearly seen, results obtained using conventional linear approach (middle figure) exhibits numerous artifacts due to multiple reflections. Imaging via $\mathcal{I}_{BP}(x)$, in turn, captures the fracture pattern very well.
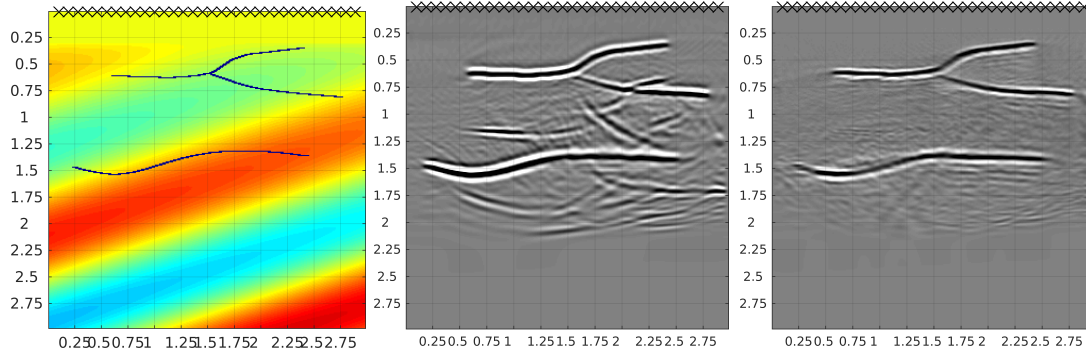
FIGURE 1. For the model consisting of two extended reflectors $c(x)$ in the known layered background (left) we compared images produced using backprojection and RTM functionals $\mathcal{I}_{BP}$ (right) and $\mathcal{I}_{RTM}$ (middle), respectively. Locations x_j, $j = 1, \ldots, m$, of $m = 32$ point-like transducers are black $\times$. All distances in km, velocities in km/s.

REFERENCES

[1] V. Druskin, A. Mamonov, A. Thaler, M. Zaslavsky, *Direct, nonlinear inversion algorithm for hyperbolic problems via projection-based model reduction*, SIAM Journal on Imaging Sciences **9** (2016), 684–747.

[2] V. Druskin, A. Mamonov, A. Thaler, M. Zaslavsky, *A nonlinear method for imaging with acoustic waves via reduced order model backprojection*, arXiv:1704.06974 [math.NA] (2017).

Uncertainty principles for inverse source problems, far field splitting and data completion

ROLAND GRIESMAIER

(joint work with John Sylvester)

Modelling the propagation of time-harmonic acoustic or electromagnetic waves by the Helmholtz equation, the far field of such a wave radiated by a compactly supported source f coincides up to a constant with the Fourier transform of the source restricted to a sphere. Unique continuation of solutions to the Helmholtz equation implies that no two sources with disjoint supports can radiate the same far fields, so the subspaces of far fields radiated from disjoint compact sets intersect only at the origin, and therefore a far field radiated by a collection sources with disjoint supports has a unique splitting into a sum of far fields, each of which is radiated by an individual source. Similarly, because the Fourier transform of a compactly supported function is analytic, observations of the far field on any open subset of the sphere uniquely determine the far field on the entire sphere. This implies that far field splitting and data completion are theoretically possible, but, without further assumptions both are severely ill-posed inverse problems.

We recently investigated both data completion and far field splitting in two and three dimensions [4, 5]. Based on the singular value decomposition of the operator that maps sources supported in a ball to the far fields they radiate, we developed a *regularized Picard criterion*, which characterized the subspaces of nonevanescent far fields radiated by L^2 sources supported in a ball. These are the far fields that can be radiated by a limited power source, and at the same time have enough power to be detected by a sensor with limited sensitivity. We combined the regularized Picard criterion with an *uncertainty principle for the far field translation operator* to develop reconstruction algorithms and stability results for far field splitting. The *far field translation operator* maps the restricted Fourier transform of a compactly supported source $f(x)$ to the restricted Fourier transform of its translate $f(x + c)$, and our *uncertainty principle* is an upper bound on the cosine of the angle between two different subspaces of nonevanescent far fields, each of which is radiated from a different ball. The bound on the cosine implies a bound on the cosecant, and the cosecant is exactly the condition number of the linear splitting operator.

We also combined the regularized Picard criterion with another uncertainty principle for the operator that maps far fields to their Fourier components, and obtained reconstruction algorithms and stability estimates for recovering missing data segments of a far field radiated by a localized source. Both results can be

combined to simultaneously complete far fields and split them into the components radiated by well-separated localized sources. In both cases, the bounds depend simply on wavelength, diameter, and (in the case of splitting) distance between the sources.

Our main results are based on estimates of condition numbers for linear operators that split a vector into two or more components. The estimates are all of the same general form. Define the cosine of the angle θ between two subspaces V_1 and V_2 as

$$\cos\theta = \sup_{v_1 \in V_1, \, v_2 \in V_2} \left| \frac{\langle v_1, v_2 \rangle}{\|v_1\| \|v_2\|} \right|.$$

As long as $\cos\theta < 1$, the following result is straightforward to check.

Theorem 1. *Suppose that $v = v_1 + v_2$ with $v_1 \in V_1$ and $v_2 \in V_2$, then, for $i = 1, 2$,*

$$(1) \qquad \|v_i\|^2 \leq \frac{1}{1 - \cos^2\theta} \|v\|^2.$$

The inequality (1) asserts that the splitting operator that maps v to the pair (v_1, v_2) exists and its condition number is bounded by $\csc\theta$.

For far field splitting and data completion, V_1 and V_2 are finite dimensional subspaces of $L^2(S^d)$, $d = 2, 3$. We use a *regularized Picard criterion* to define the subspaces V_R^c of *nonevanescent far fields* radiated by sources supported in the ball of radius R centered at a point c (at wavenumber k). We showed that, in $\mathbb{R}^3$, the subspace V_R^c is the approximately $(kR)^2$ dimensional space spanned by $e^{ikc\cdot\phi}$ times the spherical harmonics of degree $n \leq kR$. For comparison, in $\mathbb{R}^2$, V_R^c has dimension $2kR + 1$ and is spanned by $e^{ikc\cdot\phi}$ times the complex exponentials $e^{in\phi}$ with $|n| \leq kR$.

We established estimates for the cosine of the angle between nonevanescent far fields radiated from well-separated balls. Specifically, in $\mathbb{R}^3$, if

$$|kc_2 - kc_1| > 2\left(kR_1 + kR_2 + \frac{3}{2}\right),$$

the cosine of the angle θ between the subspaces $V_{R_1}^{c_1}$ and $V_{R_2}^{c_2}$ satisfies

$$(2) \qquad \cos\theta \lesssim \frac{(kR_1)^{\frac{3}{2}}(kR_2)^{\frac{3}{2}}}{|kc_2 - kc_1|},$$

where the symbol $\lesssim$ means that the left-hand side is less than or equal to the right hand side times a constant that is independent of k, R_i, and c_i, $i = 1, 2$. In $\mathbb{R}^2$, the analogous inequality is

$$(3) \qquad \cos\theta \lesssim \frac{(kR_1)^{\frac{1}{2}}(kR_2)^{\frac{1}{2}}}{|kc_2 - kc_1|^{\frac{1}{2}}},$$

and an example in [4] using a line source shows that the dependence on k, R_i, and c_i, $i = 1, 2$, in (3) is sharp. An example in [5], which calculates the inner product of the far fields radiated by constant sources supported on translated disks in $\mathbb{R}^3$,

gives a cosine estimate

$$\cos\theta \gtrsim \frac{kR_1 kR_2}{|kc_2 - kc_1|} \sin(|kc_2 - kc_1|)$$

so we don't yet know if the dependence in (2) is sharp, or if it is possible to replace the $3/2$ power in (2) by the first power.

We also showed that the cosine of the angle θ between the subspaces V_R^c and $L^2(\Omega)$, the subspace of functions in $L^2(S^2)$ supported in $\Omega \subset S^2$, satisfies the inequality

$$(4) \qquad \cos\theta \lesssim \sqrt{\frac{|\Omega|}{4\pi}(kR)^2}\,,$$

where $|\Omega|$ is the area of Ω. An example in [5] shows that the dependence on k, R, and $|\Omega|$ is sharp. The analogy in two dimensions, with $|\Omega|$ equal to the length of Ω, is

$$(5) \qquad \cos\theta \lesssim \sqrt{\frac{|\Omega|}{2\pi}kR}\,,$$

which is also sharp.

These estimates have been used to establish stability estimates for reconstruction algorithms for far field splitting and data completion in [4, 5] (see also [2, 3]).

We end this report by explaining why we refer to the inequalities (2), (3), (4), and (5) as uncertainty principles. Let V_T denote the L^2 functions supported in T and $V_{\widehat{W}}$ denote the L^2 functions whose transforms are supported in W. By *transforms*, we mean either the Fourier transform on the line, the Fourier series on the circle, or the N-point discrete Fourier transform[1].

Theorem 2. *If there is a nonzero f that belongs to $V_T \cap V_{\widehat{W}}$, then*

$$C \leq |T||W|\,,$$

where the constant C is 2π for the Fourier transform on the line and the circle, and $C = N$ for the N-point DFT.

The contrapositive of Theorem 2 is the following.

Theorem 3. *If $|T||W| < C$, then $V_T \cap V_{\widehat{W}} = \{0\}$.*

We reformulate this as follows.

Theorem 4. *If $f \in V_T$ and $g \in V_{\widehat{W}}$, then*

$$(6) \qquad |\langle f, g \rangle| \leq \sqrt{\frac{|T||W|}{C}} \|f\| \|g\|\,.$$

Setting $f = g$ in (6) recovers Theorems 3 and 2. Where Theorem 3 guarantees the existence of a splitting operator, Theorem 4 explicitly estimates its norm,

---

[1]This example in [1] motivated this work.

which is $\csc\theta$. In the case of the Fourier transform, Theorem 2 as stated is vacuous, because a compactly supported function cannot have a compactly supported Fourier transform[2]. Theorem 4 does not suffer this inconvenience.

REFERENCES

[1] D. L. DONOHO AND P. B. STARK, *Uncertainty principles and signal recovery*, *SIAM J. Appl. Math.*, 49 (1989), 906–931.
[2] R. Griesmaier, M. Hanke, and J. Sylvester, *Far field splitting for the Helmholtz equation*, SIAM J. Numer. Anal. **52** (2014), 343–362.
[3] R. Griesmaier and J. Sylvester, *Far field splitting by iteratively reweighted ℓ^1 minimization*, SIAM J. Appl. Math. **76** (2016), 705–730.
[4] R. Griesmaier and J. Sylvester, *Uncertainty principles for inverse source problems, far field splitting, and data completion*, SIAM J. Appl. Math. **77** (2017), 154–180.
[5] R. Griesmaier and J. Sylvester, *Uncertainty principles for three-dimensional inverse source problems*, submitted.

Tikhonov Regularization for Inverse Medium Scattering in Banach Spaces

FREDERIC WEIDLING

(joint work with Thorsten Hohage)

This talk is concerned with the problem of the recovery of the potential q in the Schrödinger equation

$$\left(-\Delta + q(x)\right)u(x) = E\,u(x).$$

at fixed energy E from measurements of the corresponding Green's function $g = F(q)$ on a sphere assuming that the potential is bounded and absorbing with compact support inside the measurement sphere. To deal with the ill-posedness of the problem given noisy measurements $g^\delta = F(q) + \xi$ with $\|\xi|L^2\| \leq \delta$ we apply Tikhonov regularization

$$q_\alpha^\delta \in \operatorname{argmin} T_{\alpha,g^\delta}(q) \qquad \text{with} \qquad T_{\alpha,g^\delta}(f) = \frac{1}{2\alpha}\|F(q) - g^\delta|L^2\|^2 + \mathcal{R}(q).$$

to obtain a stable reconstruction of the true potential $q^\dagger$. Here we use as a penalty term

$$\mathcal{R}(q) = \iota_K(q) + \iota_{\|\cdot|L^\infty\|\leq C_\infty}(q) + \frac{1}{2}\|q|B_{p,p}^0\|^2$$

where ι_C is the indicator function of the set C, K is the set of all functions with support contained in a fixed ball and nonnegative imaginary part and $B_{p,p}^0$ is a Besov space with $1 < p \leq 2$. The Besov norm is in our case defined via a weighted sum of wavelet coefficients see [1]. The idea behind this approach is to enforce sparsity of the solution in the corresponding wavelet basis.

The first question that arises is whether the Tikhonov functional is indeed regularizing. We prove that this in fact the case relying mainly on the support

---

[2]Theorem 2 can easily be modified to a useful statement about functions *essentially supported* in certain subsets [1].

constraint and L^∞ bound to be able to use results in [2]. Another main issue is to determine how close the minimizer of the Tikhonov functional q_α^δ is to the true potential $q^\dagger$. To answer this question we use the theory of *variational source conditions* which for the problem under consideration has the form

$$(1) \qquad \langle q^*, q^\dagger - q \rangle \leq \frac{1}{2}\Delta_{\frac{1}{2}\|\cdot|B_{p,p}^0\|^2}(q, q^\dagger) + \psi(\|F(q) - F(q^\dagger)|L^2\|^2)$$

for all $q \in K$ with $\|q|L^\infty\| \leq C_\infty$. Here $\Delta_{\frac{1}{2}\|\cdot|B_{p,p}^0\|^2}$ denotes the Bregman distance with respect to $\frac{1}{2}\|\cdot|B_{p,p}^0\|^2$ and $q^* \in \partial\frac{1}{2}\|q^\dagger|B_{p,p}^0\|^2$. For reasons why we consider variational source conditions see [3] and references therein. Here we aim at making the dependence on E of the function ψ explicit. This is inspired by known stability estimates for the problem under consideration which show that the exponential ill-posedness of the problem (see [4]) becomes a Hölder instability in the high energy limit, see [5] and references therein.

Here we prove the following theorem:

Theorem 1. *Let $E \geq 1$ and $q^\dagger \in K$ with $\|q^\dagger|L^\infty\| \leq C_\infty$ and $\|q^\dagger|B_{p,\infty}^s\| \leq C_s$. Then there exists a constant $c > 0$ such that a variational source condition holds true for all $q \in K$ with $\|q|L^\infty\| \leq C_\infty$ with ψ given by*

$$\psi(\delta^2) = c\left(E^3\delta^{\frac{1}{2}} + \left(E + \ln^2(3 + \delta^{-2})\right)^{-\mu}\right), \quad where \;\; \mu = \min\left\{s(p-1), \frac{2}{4-p}\right\}.$$

The dependence of c on C_∞ and C_s can be made explicit. The theorem has the following two important implications.

Corollary 2. *With the notation of Theorem 1:*

(1) Convergence rate: *Let $q^\dagger$ as above and q_α^δ be the minimizer of the Tikhonov functional for optimal α, then*

$$\|q^\dagger - q_\alpha^\delta|B_{p,p}^0\|^2 \leq c\psi(\delta^2).$$

(2) Stability estimate: *Let q_1 and q_2 fulfill the requirements on $q^\dagger$, then*

$$\|q_1 - q_2|B_{p,p}^0\|^2 \leq c\psi(\|F(q_1) - F(q_2)|L^2\|^2).$$

Concerning the proof of Theorem 1 we rely on a generalization of a strategy proven in [6] to spaces which are convex of power type. This strategy relies on splitting the left hand side of (1) into two parts, one of which can be estimated using smoothness of q^* and the second one with properties of the forward operator.

For the first estimate an important step is to characterize the smoothness of q^* in terms of the smoothness of $q^\dagger$.

Theorem 3. *Let $s > 0$, $1 < p \leq 2$ and $q^* \in \partial\frac{1}{2}\|q^\dagger|B_{p,p}^0\|^2$. Then $q^\dagger \in B_{p,\infty}^s$ if and only if $q^* \in B_{p',\infty}^{s(p-1)}$ where $\frac{1}{p} + \frac{1}{p'} = 1$.*

For the second part it turns out that one has to estimate the largest Fourier coefficient of $q^\dagger - q$ in a ball of a certain radius. Here we proceed similar to [7] to show the following:

Lemma 4. *Let $E \geq 1$ and $q_1, q_2 \in K$ such that $\|q_j | L^\infty\| \leq C_\infty$ for $j = 1, 2$. Then for fixed radius $\varrho > 0$ there exists constants $a, c > 0$ such that for all t large enough the estimate*

$$\left\| \widehat{q_1 - q_2} | L^\infty(B(\varrho)) \right\| \leq c \left(e^{at} E^3 \|F(q_1) - F(q_2) | L^2\| + \frac{1}{\sqrt{E + t^2}} \|q_1 - q_2 | L^2\| \right)$$

holds true.

The proof of this result relies on well-known results in scattering theory [8, 9]. To derive the energy dependence, which has not been done in [7], we use in addition results in [10].

With the help of the previous two results, interpolation and a proper choice of the free parameters one then proves Theorem 1.

REFERENCES

[1] H. Triebel, *Theory of function spaces III*, Birkhäuser, 2006.
[2] A. Lechleiter, K. S. Kazimierski and M. Karamehmedović, *Tikhonov regularization in L^p applied to inverse medium scattering*, Inverse Problems **29** (2013), 075003.
[3] T. Hohage and F. Weidling, *Verification of a variational source condition for acoustic inverse medium scattering problems*, Inverse Problems **31** (2015), 075006.
[4] N. Mandache, *Exponential instability in an inverse problem for the Schrödinger equation* Inverse Problems **17** (2001), 1435–1445.
[5] M. I. Isaev and R. G. Novikov, *Effectivized Hölder-logarithmic stability estimates for the Gel'fand inverse problem*, Inverse Problems **30** (2014), 095006.
[6] T. Hohage and F. Weidling, *Characterizations of Variational Source Conditions, Converse Results, and Maxisets of Spectral Regularization Methods*, SIAM Journal on Numerical Analysis **55** (2017), 598–620.
[7] P. Hähner and T. Hohage, *New stability estimates for the inverse acoustic inhomogeneous medium problem and applications.* SIAM J. Math. Anal. **33** (2001), 670–685.
[8] R. Weder, *Generalized Limiting Absorption Method and Multidimensional Inverse Scattering Theory*, Mathematical Methods in the Applied Sciences **14** (1991), 509–524.
[9] R. Novikov and G. Khenkin, *The $\bar\partial$-equation in the multidimensional inverse scattering problem*, Russ. Math. Surv. **3** (1987), 109–180.
[10] D. Baskin and E. A. Spence and J. Wunsch, *Sharp High-Frequency Estimates for the Helmholtz Equation and Applications to Boundary Integral Equations*, SIAM J. Math. Anal. **48**, 229–267.

Reconstruction of a compact perturbation of a periodic structure – Preliminary Results

ANDREAS KIRSCH

(joint work with Armin Lechleiter)

We consider the following scattering problem in the half plane $\mathbb{R}^2_+ = \{x \in \mathbb{R}^2 : x_2 > 0\}$: We are given the wave number $k > 0$, the index of refraction $n \in L^\infty(\mathbb{R}^2_+)$ which is assumed to be 2π−periodic with respect to x_1 and equal to one for $x_2 > h$, a perturbation $q \in L^\infty(\mathbb{R}^2_+)$ with compact support in the layer $W := \mathbb{R} \times (0, h)$, and the incident field $u^i(x) = \Phi(x, y) - \Phi(x, y^*)$. Here, y is the source location with $y_2 > 0$ and $y^* = (y_1, -y_2)^\top$, and $\Phi(x, y) = \frac{i}{4} H_0^{(1)}(k|x - y|)$ denotes the

fundamental solution of the Helmholtz equation. The (direct) scattering problem is to determine the total field $u^t = u^i + u^s$ as the sum of the incident field u^i and the scattered field u^s such that

(1) $$\Delta u^t + k^2 n \, (1 + q) \, u^t = 0 \quad \text{for } x_2 > 0 \,, \quad u^t = 0 \quad \text{for } x_2 = 0 \,.$$

Furthermore, u^s has to satisfy some kind of radiation condition, and the main concern of this talk is to derive its correct form. A natural candidate is the upward propagation radiation condition UPRC; that is, u^s has the form

$$u^s(x) \; = \; 2 \int_{\Gamma_h} u^s(y) \, \frac{\partial}{\partial y_2} \Phi(x, y) \, ds(y) \,, \; x_2 > h \,, \quad \text{were } u^s|_{\Gamma_h} \in L^\infty(\Gamma_h)$$

and $\Gamma_h := \mathbb{R} \times \{h\}$. However, this UPRC is not sufficient as we will see.

First, we consider the unperturbed situation $q = 0$. We transform the problem into a source problem by choosing $\xi \in C^\infty(\mathbb{R}^2)$ with $\xi(x) = 0$ for $|x - y| \leq \varepsilon/2$ and $\xi(x) = 1$ for $|x - y| \geq \varepsilon$ and set $u = u^s + \xi u^i$. Then u solves

(2) $$\Delta u + k^2 n \, u = -f \quad \text{for } x_2 > 0 \,, \quad u = 0 \quad \text{for } x_2 = 0 \,,$$

for some $f \in L^2(\mathbb{R}^2_+)$ with compact support.

We look for quasi-periodic solutions of the homogeneous problem ($f = 0$); that is, for solutions ϕ of (2) for $f = 0$ with $\phi(x_1 + 2\pi, x_2) = \phi(x)e^{i2\pi\alpha}$ for all $x \in W$. Parameters $\alpha \in (-1/2, 1/2]$ for which non-trivial α-quasi-periodic solutions of (2) exist which satisfy also a Rayleigh expansion in the form

$$\phi(x) \; = \; \sum_{m \in \mathbb{Z}} a_m \, e^{i(m+\alpha)x_1 + i\sqrt{k^2 - (m+\alpha)^2}(x_2 - h)} \,, \quad x_2 > h \,,$$

for some $a_m \in \mathbb{C}$ are called *exceptional values*. We make the first assumption:

Assumption 1: Let $k = k_0 + \kappa$ with $k_0 \in \mathbb{N}_0$ and $\kappa \in (-1/2, 1/2]$. Then $\pm\kappa$ are not exceptional values.

It is well known that, in general, these exceptional values exist but there are only finitely many of these. We collect them in the set $\{\hat{\alpha}_j : j \in J\}$ where J is finite (or empty). Furthermore, the corresponding functions ϕ are evanescent; that is, they decay exponentially as x_2 tends to infinity. For every $j \in J$ we set $Q^\infty = (0, 2\pi) \times (0, \infty)$ and

$$X_j \; = \; \left\{ \phi \in H^1(Q^\infty) : \begin{array}{l} \Delta\phi + k^2 n\phi = 0 \text{ for } x_2 > 0 \,, \; \phi = 0 \text{ for } x_2 = 0 \,, \\ \phi \text{ is } \hat{\alpha}_j\text{-quasi-periodic and evanescent.} \end{array} \right\}$$

Then every X_j is finite dimensional. For every $j \in J$ we choose a basis $\{\phi_{\ell,j} : \ell = 1, \ldots, m_j\}$ of X_j by solving the eigenvalue problem

$$-i \int_{Q^\infty} \overline{\psi} \, \frac{\partial \phi_{\ell,j}}{\partial x_1} \, dx \; = \; \lambda_{\ell,j} \, k \int_{Q^\infty} n \, \phi_{\ell,j} \, \overline{\psi} \, dx \quad \text{for all } \psi \in X_j \,,$$

with eigenvalues $\lambda_{\ell,j} \in \mathbb{R}$ for $\ell = 1, \ldots, m_j$ and $j \in J$.

Assumption 2: $\lambda_{\ell,j} \neq 0$ for all ℓ and $j \in J$.

The sign of the eigenvalues determine the modes which travel to the right and left, respectively. Therefore, we set $L_j^{\pm} = \{\ell : \lambda_{\ell,j} \gtrless 0\}$. Now we are able to prove the following *limiting absorption principle.*

Theorem Let Assumptions 1 and 2 hold, and let $u_\varepsilon \in H^1(\mathbb{R}_+^2)$ be the unique solution of (2) where k is replaced by $k + i\varepsilon$. Then u_ε converges to u_0 in $H_{loc}^1(\mathbb{R}_+^2)$ where u_0 satisfies (2), the UPRC, and has a decomposion into the form $u_0 = u^{(1)} + u^{(2)}$ where $u^{(1)} \in H^1(\mathbb{R} \times (0, H))$ for every $H > h$ and $u^{(2)}$ has the form

$$u^{(2)}(x) \;=\; \psi^+(x_1) \sum_{j \in J} \sum_{\ell \in L_j^+} a_{\ell,j}^+ \, \phi_{\ell,j}(x) \;+\; \psi^-(x_1) \sum_{j \in J} \sum_{\ell \in L_j^-} a_{\ell,j}^- \, \phi_{\ell,j}(x)$$

for some $a_{\ell,j}^{\pm} \in \mathbb{C}$. Here, $\psi^{\pm}$ are given by

$$\psi^{\pm}(x_1) \;:=\; \frac{1}{2} \left[1 \;\pm\; \frac{2}{\pi} \int\limits_0^{x_1/2} \frac{\sin t}{t} \, dt \right], \quad x_1 \in \mathbb{R}.$$

We note that $\lim_{x_1 \to \infty} \psi^+(x_1) = 1$ and $\lim_{x_1 \to -\infty} \psi^+(x_1) = 0$ and $\psi^- = 1 - \psi^+$. By this theorem we have shown the existence of the Green's function $G(x, y)$ since we can apply this limiting absorption principle to every point y in $\mathbb{R}_+^2$. Now we include the perturbation q and consider (1).

Theorem Let Assumptions 1 and 2 hold.

(a) Let $u^t = u^i + u^s$ be a solution of (1) such that u^s satisfies the radiation condition of the previous theorem. Then the restriction of u^t to $D := \operatorname{supp} q$ solves the Lippmann-Schwinger integral equation

$$(3) \qquad u^t(x) \;=\; u^i(x) \;+\; k^2 \int_D q(y) \, u^t(y) \, G(x, y) \, dy, \quad x \in D.$$

(b) Let $u^t \in L^2(D)$ be a solution of (3). Then its extension by the right hand side to $\mathbb{R}_+^2$ is a solution of the scattering problem (1) such that u^s satisfies the radiation condition of the previous theorem.

(c) The integral equation is uniquely solvable in $L^2(D)$ for sufficiently small $k^2 \int_D q(y) \, dy$.

Therefore, this theorem provides well-posedness of the direct scattering problem. It is the aim of future work to study the corresponding inverse scattering problem to determine properties of the perturbation q from the knowledge of the scattered field outside (and far away) of the perturbation.

REFERENCES

[1] A. Kirsch, A. Lechleiter, *The Limiting Absorption Principle and a Radiation Condition for the Scattering by a Periodic Layer*, submitted.
[2] A. Kirsch, A. Lechleiter, *A Radiation Condition arizing from the Limiting Absorption Principle for a Closed Full- or Half-Waveguide Problem*, in preparation.

Data-to-Born transform for inversion and imaging with waves

ALEXANDER V. MAMONOV

(joint work with Liliana Borcea, Vladimir Druskin, Mikhail Zaslavsky)

Inverse problems for the coefficients of wave equations are highly nonlinear due to both kinematic and multiple scattering effects. Meanwhile, many conventional inversion algorithms assume that the dependency of the scattered waves on the medium properties is approximately linear. The linearization, known as the Born approximation, is not accurate in strongly scattering media, where the waves undergo multiple reflections before reaching the measurement sensors. This results in artifacts in the reconstructions obtained under the Born approximation assumption. Here we present an algorithm that removes the multiple scattering effects from the data measured at an array of sensors based on the techniques of model order reduction. The transformed data can then be fed to conventional linearized inversion workflows.

The method relies heavily on the tools of linear algebra, so for simplicity of exposition we treat all continuum quantities as discretized on a very fine grid with N nodes. All matrix-valued quantities are denoted by bold letters. Consider the first order form of the initial value problem for the symmetrized acoustic wave equation

$$(1) \qquad \partial_t \begin{pmatrix} \mathbf{P} \\ \mathbf{U} \end{pmatrix} = \begin{pmatrix} \mathbf{0} & -\mathbf{L}_q \\ \mathbf{L}_q^T & \mathbf{0} \end{pmatrix} \begin{pmatrix} \mathbf{P} \\ \mathbf{U} \end{pmatrix}, \quad t > 0, \quad \mathbf{P}(0) = \mathbf{B}, \quad \mathbf{U}(0) = \mathbf{0}.$$

Here the wavefields are driven by an array of m sources, the columns of the initial condition matrix $\mathbf{B} \in \mathbb{R}^{N \times m}$. The columns of the matrix-valued function of time $\mathbf{P} : \mathbb{R}_+ \to \mathbb{R}^{N \times m}$ contain the acoustic pressure wavefields for all m sources. The matrices $\mathbf{L}_q$, and $\mathbf{L}_q^T$ are the fine grid discretizations of the operators

$$(2) \quad L_q = \sqrt{c(x)}\Big(-\nabla \cdot + \frac{1}{2}\nabla q(x)\cdot\Big)\sqrt{c(x)} \text{ and } L_q^T = \sqrt{c(x)}\Big(\nabla + \frac{1}{2}\nabla q(x)\Big)\sqrt{c(x)},$$

where the non-reflective wave speed $c(x)$ is assumed known, and our objective is to image the acoustic impedance $\sigma(x) = e^{q(x)}$.

The solution of (1) is given by $\mathbf{P}(t) = \cos\Big(t\sqrt{\mathbf{L}_q \mathbf{L}_q^T}\Big)\mathbf{B}$. We assume that the sources are collocated with receivers, so the receiver matrix is also $\mathbf{B}$, and we can write the data collected at the array of m receivers as

$$(3) \qquad\qquad \mathbf{D}(t) = \mathbf{B}^T \cos\Big(t\sqrt{\mathbf{L}_q \mathbf{L}_q^T}\Big)\mathbf{B} \in \mathbb{R}^{m \times m}.$$

Typically, the data is sampled discretely in time, say uniformly at $t_k = k\tau$. This allows us to write the sampled data $\mathbf{D}_k = \mathbf{D}(k\tau) = \mathbf{B}^T T_k(\mathscr{P})\mathbf{B}$, using Chebyshev polynomials of the first kind T_k and the propagator

$$(4) \qquad\qquad \mathscr{P} = \cos\Big(\tau\sqrt{\mathbf{L}_q \mathbf{L}_q^T}\Big).$$

Given the sampled data $\mathbf{D}_k$, we construct a reduced order model (ROM) for the propagator and the source-receiver matrix $\mathbf{B}$. The ROM is given by a pair of

matrices $\widetilde{\mathscr{P}} \in \mathbb{R}^{mn \times mn}$, $\widetilde{\mathbf{B}} \in \mathbb{R}^{mn \times m}$ that satisfy the data interpolation conditions

$$(5) \qquad \mathbf{D}_k = \widetilde{\mathbf{B}}^T T_k(\widetilde{\mathscr{P}})\widetilde{\mathbf{B}}, \quad k = 0, 1, \ldots, 2n - 1.$$

Using the properties of Chebyshev polynomials we can show [1, 2, 3] that the ROM (5) can be computed entirely from the knowledge of the sampled data $\mathbf{D}_k$, $k = 0, 1, \ldots, 2n - 1$.

While the ROM can be used to image $\sigma(x)$ directly [1, 2], here we follow [3] to transform the multiple scattering data $\mathbf{D}_k$ to its single-scattering (Born) approximation. To that end we need to obtain a quantity that is (approximately) linear with respect to $q(x) = \ln\sigma(x)$. Discrete data sampling also induces the sampling of the wavefields into the snapshots $\mathbf{P}_k = \mathbf{P}(k\tau)$ that satisfy exactly a second-order time stepping scheme

$$(6) \qquad \frac{1}{\tau^2}\Big[\mathbf{P}_{k+1} - 2\mathbf{P}_k + \mathbf{P}_{k-1}\Big] = -\xi(\mathscr{P})\mathbf{P}_k,$$

with a positive definite

$$(7) \qquad \xi(\mathscr{P}) = \frac{2}{\tau^2}\big(\mathbf{I} - \mathscr{P}\big) = \mathcal{L}_q\mathcal{L}_q^T,$$

where we use Taylor series expansion to see that the factors satisfy $\mathcal{L}_q = \mathbf{L}_q + O(\tau^2)$, i.e. they are approximately linear with respect to q. But the ROM $\widetilde{\mathscr{P}}$ is an approximation of the propagator $\mathscr{P}$, so the block Cholesky factors of

$$(8) \qquad \xi(\widetilde{\mathscr{P}}) = \frac{2}{\tau^2}\big(\mathbf{I} - \widetilde{\mathscr{P}}\big) = \widetilde{\mathbf{L}}_q\widetilde{\mathbf{L}}_q^T \in \mathbb{R}^{mn \times mn},$$

are also approximately linear in q.

Once we obtain the ROM $\widetilde{\mathscr{P}}$ from the sampled data $\mathbf{D}_k$ and thus the block Cholesky factor $\widetilde{\mathbf{L}}_q$ of (8), we can perform the same computation for some reference impedance, say $\sigma \equiv 1$ corresponding to $q \equiv 0$, to obtain $\widetilde{\mathbf{L}}_0$ from the sampled reference data $\mathbf{D}_k^0$. To compute the Born approximation around the reference impedance we consider the perturbation of the block Cholesky factor

$$(9) \qquad \widetilde{\mathbf{L}}^\varepsilon = \widetilde{\mathbf{L}}_0 + \varepsilon\big(\widetilde{\mathbf{L}}_q - \widetilde{\mathbf{L}}_0\big),$$

approximately linear in q, and the correspondingly perturbed propagator ROM

$$(10) \qquad \widetilde{\mathscr{P}}^\varepsilon = \mathbf{I} - \frac{\tau^2}{2}\widetilde{\mathbf{L}}^\varepsilon\widetilde{\mathbf{L}}^{\varepsilon T}.$$

Then the transformed single scattering data $\mathbf{F}_k$ is given by

$$(11) \qquad \mathbf{F}_k = \mathbf{D}_k^0 + \widetilde{\mathbf{B}}^T\left[\frac{d}{d\varepsilon}T_k\left(\widetilde{\mathscr{P}}^\varepsilon\right)\Big|_{\varepsilon=0}\right]\widetilde{\mathbf{B}},$$

where the derivative can be computed using the three-term recurrence for Chebyshev polynomials. We refer to (11) as the Data-to-Born (DtB) transform. This highly nonlinear procedure transforms the multiple scattering sampled data $\mathbf{D}_k$ to its single scattering approximation $\mathbf{F}_k$ taken about the reference impedance.

In Figure 1 we demonstrate the performance of the DtB transform on the simulated data for a 2D model with linear wave speed and $\sigma(x)$ with three reflectors.
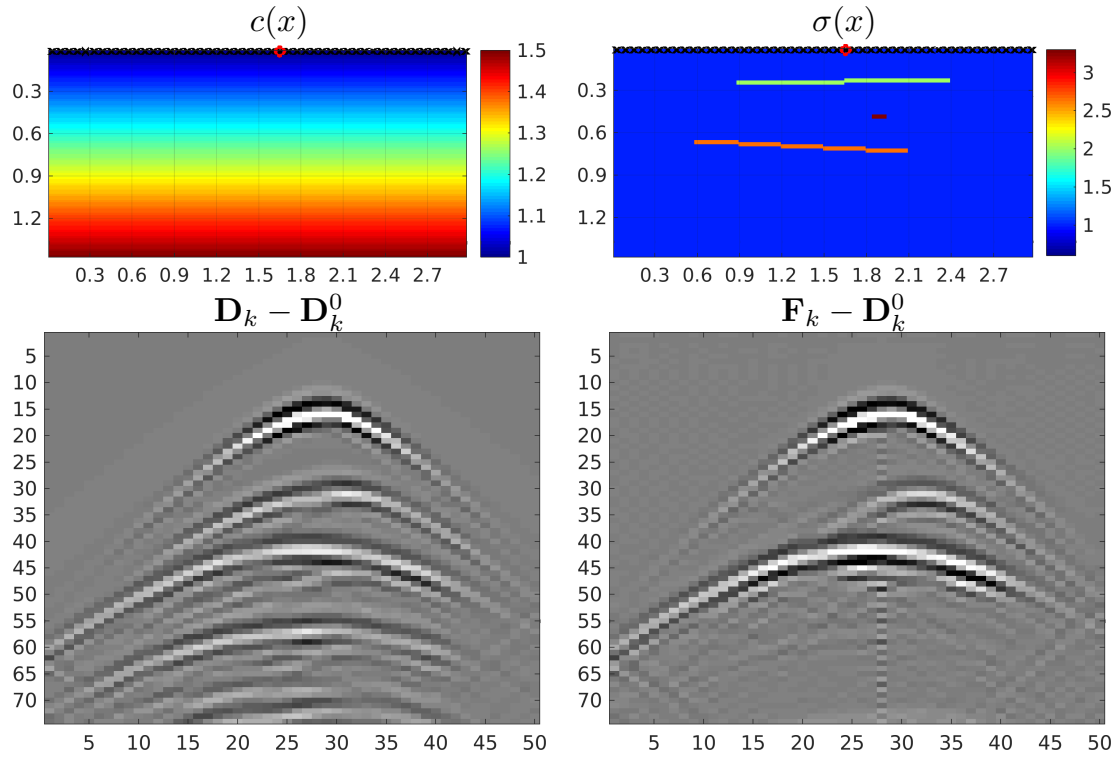
FIGURE 1. Numerical example 2D model and DtB transform. Top row: wave speed $c(x)$ in km/s and acoustic impedance $\sigma(x)$ in kg/sm^2, all distances in km, $m = 50$ sources/receivers are $\times$. Bottom row: sampled data (left) and DtB transform (right) for a single receiver (red $\circ$) with the surface wave $\mathbf{D}_k^0$ removed; horizontal axis: receiver index, vertical axis: sample time index k.

In the original data $\mathbf{D}_k$ we observe a number of events, arrivals of the scattered waves to the receiver array, including the primary and multiple reflected waves, which we reference in the order of arrival. We observe that the second event is a combination of a primary arrival from the small reflector and a secondary arrival from the topmost reflector. All events after the third one are multiple reflections. The DtB transform successfully removes all the multiple reflection events. Specifically, in the second event it extracts the primary reflection from the small reflector by suppressing the secondary reflection from the top reflector.

REFERENCES

[1] A.V. Mamonov, V. Druskin, M. Zaslavsky, *Nonlinear seismic imaging via reduced order model backprojection.* SEG Technical Program Expanded Abstracts: 2015, pp. 4375–4379.
[2] V. Druskin, A.V. Mamonov, A.E. Thaler, M. Zaslavsky, *Direct, nonlinear inversion algorithm for hyperbolic problems via projection-based model reduction.* SIAM Journal on Imaging Sciences 9(2):684–747, 2016.
[3] L. Borcea, V. Druskin, A.V. Mamonov, M. Zaslavsky, *Untangling nonlinearity in inverse scattering with data-driven reduced order models*, 2017, arXiv:1704.08375 [math.NA]

Stochastic boundary models and geometric uncertainties

Jari Kaipio

(joint work with Daniela Calvetti, Paul Hadwin, Janne Huttunen, Erkki Somersalo)

Inverse problems induced by partial differential equations and related boundary value problems are notoriously sensitive to geometric uncertainties, and this topic has received recent attention [3, 4, 2]. Furthermore, real world inverse problems practically always necessitate truncation of the (computational) domain; and on these boundaries, the boundary conditions depend on the material coefficients *outside* the computational domain. Here, we constrain ourselves to electrical impedance tomography with the complete electrode model which is the real world counterpart of the inverse conductivity problem of Cálderon [1]

Consider the inverse conductivity problem of feeding currents into a body/ domain (volume conductor) via electrodes and measuring the resulting potentials on the electrodes. The forward problem is induced by the the boundary value problem (complete electrode model)

$$
\begin{aligned}
\nabla \cdot (\sigma \nabla u) &= 0 \quad \text{in } \Omega \\
u + z_\ell \sigma \frac{\partial u}{\partial \nu} &= U_\ell \quad \text{on } e_\ell, \quad \ell = 1, \dots, L \\
\int_{e_\ell} \sigma \frac{\partial u}{\partial \nu} dS &= I_\ell \quad \text{on } e_\ell, \ \ell = 1, \dots, L \\
\sigma \frac{\partial u}{\partial \nu} &= 0 \quad \text{on } \partial\Omega \backslash \cup_{\ell=1}^L e_\ell
\end{aligned}
$$

where z_ℓ are the contact impedances, u is the electric potential, e_ℓ are the electrodes and σ is the electrical conductivity.

Let the domain Ω consist of two subdomains, Ω_1 and Ω_2, where the former is of interest and the task is to estimate the (probability) distribution of σ_1 so that the computations are carried out in Ω_1 only, as in the figure below.

The variational form of the complete electrode model was derived in [8] and the extension of modelling part of the boundary with a (deterministic) Dirichlet-to-Neumann (DtN) operator in [7].

Here, we model the unknown conductivity as a random field over the entire Ω [9]. In [5, 6], it was shown that the DtN operator depends on the conductivity σ_2 *outside* Ω_1 and the DtN can thus be interpreted as a stochastic operator. The
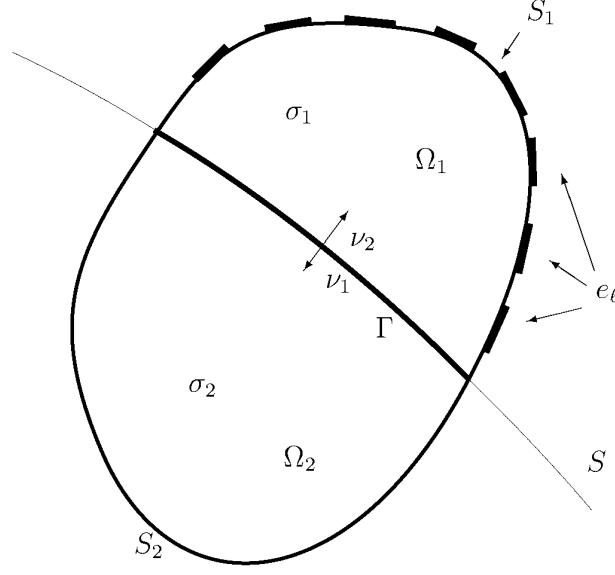
FIGURE 1. Decomposition of the domain.

variational form with the DtN on the truncation boundary Γ is of the form

$$
\begin{aligned}
B[\sigma_1, \Lambda]((v, U), (u, V)) &= \sum_{\ell=1}^{L} V_\ell I_\ell \\
B[\sigma_1, \Lambda]((v, U), (u, V)) &= \int_{\Omega_1} \sigma_1 \nabla u \cdot \nabla v \, dx + \sum_{\ell=1}^{L} \frac{1}{z_\ell} \int_{e_\ell} (v - V_\ell)(u - U_\ell) \, dS \\
&\quad + \int_{\Gamma} v \Lambda u \, dS
\end{aligned}
$$

where $(u, U), (v, V) \in \dot{H} = H/\mathbb{R}$ and $H = H^1(\Omega_1) \times \mathbb{R}^L$ and $\Lambda = \Lambda_{\sigma_2}$ is the DtN operator $\Lambda_{\sigma_2} u = \sigma_1 \partial_n u$ on Γ.

After discretization of the variatinonal form, the DtN operator takes the form of a matrix whose elements are random variables whose joint distribution is induced by the distribution $\pi(\sigma_2)$ of the random field σ_2.

Here, we construct a series approximation for the discretized DtN operator $\Lambda \in \mathbb{R}^{N \times N}$

$$
\Lambda = \Lambda_0 + \sum_{k=1}^{p} \beta_k \Lambda_k + \tilde{\Lambda}
$$

where $\beta = (\beta_1, \ldots, \beta_p)$ are random variables and we determine $\Lambda_0, \ldots, \Lambda_p$ so that $\tilde{\Lambda}$ is small in some sense. We choose to minimize the expectation of the Frobenius norm

$$
\mathbb{E}\|\tilde{\Lambda}\|_F^2
$$

over $\pi(\sigma_2)$ which results in a Karhunen-Loéve type decomposition [6]. The inverse problem is then to model the posterior density $\pi(\sigma_1, \beta \,|\, V)$ and compute point and

spread estimates [10]. For the computational model, we need the basis operators $\Lambda_0, \ldots \Lambda_p$ which are provided by a Monte Carlo simulation over $\pi(\sigma_2)$, and we approximate $\pi(\beta)$ as normal.

An example of results from laboratory measurements are given in Fig. 2.
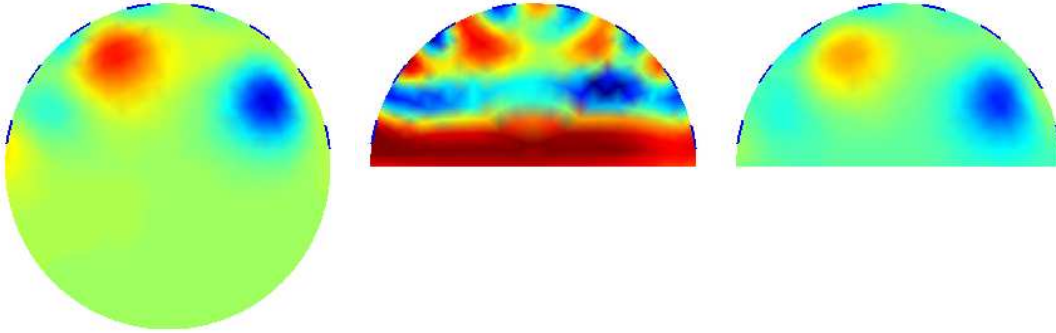
FIGURE 2. Left: reconstruction in the entire domain Ω, center: reconstruction in Ω_1 with homogeneous Neumann conditions used on Γ, right: the stochastic DtN used on Γ.

REFERENCES

[1] Calderon AP (1980) On an inverse boundary value problem. In Seminar on Numerical Analysis and Its Applications to Continuum Physics (Rio de Janeiro, 1980), 65–73.
[2] Nissinen A, Kolehmainen V, Kaipio JP (2011) Compensation of Modelling Errors Due to Unknown Domain Boundary in Electrical Impedance Tomography. IEEE Trand Med Imag **30** 231-242.
[3] Kolehmainen V, Lassas M, Ola P (2010) Calderon's inverse problem with an imperfectly known boundary and reconstruction up to a conformal deformation. SIAM J Math Anal **42** 1371-1381.
[4] Kolehmainen V, Lassas M, Ola P (2007) The inverse conductivity problem with an imperfectly known boundary in three dimensions. SIAM J Appl Math **67** 1440-1452.
[5] Calvetti D, Hadwin P, Huttunen J, Isaacson D, Kaipio JP, McGivney D, Somersalo E, Volzer J (2015) Artificial boundary conditions and domain truncation in electrical impedance tomography. Part I: Theory and preliminary results. Inverse Probl Imaging **9** 749 - 766.
[6] Calvetti D, Hadwin P, Huttunen J, Kaipio JP, Somersalo E (2015) Artificial boundary conditions and domain truncation in electrical impedance tomography. Part II: Stochastic extension of the boundary map. Inverse Probl Imaging **9** 767-789.
[7] Jonsson E (1999) Electrical conductivity reconstruction using nonlocal boundary conditions. SIAM J Appl Math **59** 1582-1598.
[8] Somersalo E, Isaacson D and Cheney M (1992) Existence and uniqueness for electrode models for electric current computed tomography. SIAM J. Appl. Math. **52** 1023–1040.
[9] Roininen L, Huttunen J, Lasanen S (2014) Whittle-Matérn priors for Bayesian statistical inversion with applications in electrical impedance tomography. Inverse Probl Imaging **8** 561-586.
[10] Kaipio J, Somersalo E (2005) *Statistical and Computational Inverse Problems.* Applied Mathematical Sciences 160, Springer.

Practical aspects in computational methods for Bayesian inverse problems governed by PDEs

Georg Stadler

(joint work with Yair Daon, Omar Ghattas, Tobin Isaac, Noemi Petra)

My presentation focused on challenges arising in the development of computational methods for infinite-dimensional Bayesian inverse problems governed by PDEs. As driving application, I considered the inference of a spatially distributed coefficient in the basal Robin boundary condition of the Antarctic ice sheet. The data for this inference are satellite observations of the flow on the top surface of the ice sheet, and the governing PDE describing the gravity-driven flow of ice is an instantaneous nonlinear incompressible Stokes equation [3]. Inferring the basal boundary condition together with the corresponding uncertainty is the crucial starting point for predicting the contribution of the continental ice sheets to future sea level rise under various climate forcing scenarios.

I first discussed the definition of prior distributions for infinite-dimensional parameters, such as, for instance, the uncertain Robin coefficient field for the Antarctica ice sheet inference problem. Building on theoretic results [6] and computational experience [1, 3], we use a Gaussian normal distribution defined over the Hilbert space of square integrable functions as prior. This Gaussian is characterized by its mean and its covariance operator, for which we choose the negative square of an elliptic (Laplacian-like) PDE operator. This choice is motivated by the connection between stochastic PDEs and Gaussian random fields [4], and by the availability of fast solvers for elliptic PDE operators. These solvers allow for the fast application of the covariance operator, its inverse and its square root to vectors, as required to evaluate the likelihood and to draw samples from the distribution.

However, these PDE operators require a choice of boundary conditions, and this choice can have a strong influence on the prior distribution. This influence is usually undesired. For instance, the commonly used homogeneous Neumann boundary conditions tend to result in increased correlation close to the boundary compared to the interior of the domain. As a remedy, in [2], we propose two techniques that allow to ameliorate these boundary effects in the definition of Gaussian priors based on elliptic PDE operators. The first approach we propose combines the elliptic PDE operator with a Robin boundary condition, where a varying Robin coefficient is computed from an optimization problem. The second approach normalizes the pointwise variance by rescaling the covariance operator. Numerical results on simple domains as well as the Antarctica domain illustrate that these methods largely mitigate undesired boundary effects in the prior while the computational efficiency that results from the choice to define covariance operators using elliptic PDE operators is retained. An alternative approach to mitigate undesired boundary effects is to extend the computational domain, e.g., [5]. This typically requires to assemble discretized PDE operators, which can be infeasible for large-scale problems.

As a second theme of my talk, I presented approximations of the posterior distribution for the basal Robin coefficient in the Antarctic ice flow inference problem. This inference is formulated as Bayesian inverse problem (or inverse uncertainty quantification problem). The uncertainty in the inferred coefficient is due to the ill-posedness of the problem and the limited observational data. In particular in infinite (upon discretization, high) dimensions and in the presence of expensive-to-evaluate governing equations (here, a nonlinear Stokes equation), characterizing the solution of a Bayesian inverse problem (i.e., the posterior probability distribution), is extremely challenging. Hence, one often has to resort to approximations. A first approximation is to compute the maximum a posterior (MAP) estimate, which amounts to the solution of a PDE-constrained optimization problem that is similar to the problems being solved in regularization-based deterministic inverse problem approaches. I presented results for this optimization problem using an inexact Newton-conjugate-gradient algorithm, where first and second derivatives of this PDE-constrained optimization problem are computed using adjoints. A next level of posterior approximation is a Gaussian approximation around the MAP estimate, with posterior covariance operator given by the inverse of the Hessian of the optimization problem for the MAP estimate. To make this approximation computationally feasible, I presented a method that exploits that the posterior covariance can typically be derived as a low rank update of the prior covariance. This low rankness reflects that the amount of information one can learn from observations is typically limited in ill-posed problems [1, 3]. I discussed the use of randomized singular value decomposition methods to compute these low rank approximation, and showed samples as well as pointwise variance plots from this Gaussianized posterior distribution for the inference of the basal boundary coefficient of the Antarctica ice sheet. Finally, I briefly discussed challenges and limitations of sampling algorithms. While in principle, sampling algorithms allow to fully explore posterior distributions, they become computationally extremely expensive in high dimensions with complex-to-evaluate parameter-to-observable maps.

References

[1] T. Bui-Thanh, O. Ghattas, J. Martin, and G. Stadler, *A computational framework for infinite-dimensional Bayesian inverse problems Part I: The linearized case, with application to global seismic inversion*, SIAM Journal on Scientific Computing **35(6)**, (2013), A2494–A2523.

[2] Y. Daon, and G. Stadler, *Mitigating the influence of boundary conditions on covariance operators derived from elliptic PDEs*, arXiv:1610.05280 (2016).

[3] T. Isaac, N. Petra, G. Stadler, and O. Ghattas, *Scalable and efficient algorithms for the propagation of uncertainty from data through inference to prediction for large-scale problems, with application to flow of the Antarctic ice sheet*, Journal of Computational Physics **296** (2015), 348–368.

[4] F. Lindgren, H. Rue, and J. Lindström. *An explicit link between Gaussian fields and Gaussian Markov random fields: the stochastic partial differential equation approach*, Journal of the Royal Statistical Society: Series B (Statistical Methodology), **73(4)** (2011), 423–498.

[5] L. Roininen, J. M. J. Huttunen, and S. Lasanen, *Whittle-Matérn priors for Bayesian statistical inversion with applications in electrical impedance tomography*, Inverse Problems Imaging, **8(2)**, (2014), 561–586.

[6] A.M. Stuart, *Inverse problems: A Bayesian perspective*, Acta Numerica, **19** (2010), 451–559.

Bayesian approach to quantitative photoacoustic imaging

Tanja Tarvainen

(joint work with Aki Pulkkinen, Jari P. Kaipio, Ben T. Cox, Simon R. Arridge)

Quantitative photoacoustic tomography (QPAT) is an emerging imaging technique aimed at estimating the optical parameters inside tissues from photoacoustic images which are formed by combining optical information and ultrasonic propagation [1]. The two inverse problems of QPAT are: 1) reconstruct the initial acoustic pressure distribution from measured acoustic waves and 2) reconstruct the distributions of the optical parameters from the absorbed optical energy density. The first inverse problem is an inverse initial value problem of acoustics. There are a large number of reconstruction techniques available, see e.g. [2, 3] and the references therein. However, in cases in which the acoustic properties of the medium are varying, the inverse problem becomes significantly more challenging.

The second inverse problem in QPAT is the optical image reconstruction where the goal is to estimate the concentrations of chromophores. These can be obtained either by directly estimating the chromophore concentrations from photoacoustic images obtained at various wavelengths [4, 5, 6] or by first recovering the absorption coefficients at different wavelengths and then calculating the concentrations from the absorption spectra [4, 5]. As an alternative to the two-step approach, estimation of the optical parameters directly from the photoacoustic time-series has also been considered recently [7, 8, 9, 10].

In this work, the optical inverse problem of QPAT is studied. Modelling of the noise and errors due to the acoustic solver and incorporating this information into the solution of the optical inverse problem are investigated [11, 12]. That is, we consider estimation of a distribution of parameters x in a case of a hybrid tomography where the data is obtained as a solution of an another inverse problem.

Let us assume that all parameters are random variables. A discretised observation model with an additive noise model is

$$(1) \qquad\qquad y = A_h(x) + e$$

where $y = (y_1, \ldots, y_m)^{\mathrm{T}} \in \mathbb{R}^m$ is the data vector which, in this work, is the absorbed optical energy density distribution obtained as a solution of the acoustic inverse problem. Further, x is a discretised optical parameter distribution and A_h is a discretised forward model [13].

Let us approximate the unknown parameters x and noise e as mutually independent and Gaussian distributed $x \sim \mathcal{N}(x_*, \Gamma_x)$, $e \sim \mathcal{N}(e_*, \Gamma_e)$ where $x_* \in \mathbb{R}^N$ and $e_* \in \mathbb{R}^m$ are the means and $\Gamma_x \in \mathbb{R}^{N \times N}$ and $\Gamma_e \in \mathbb{R}^{m \times m}$ are the covariance

matrices. This yields to posterior density

$$(2) \qquad \pi(x|y) \propto \exp\left\{-\frac{1}{2}\|L_e(y - A_h(x) - e_*)\|^2 - \frac{1}{2}\|L_x(x - x_*)\|^2\right\}$$

where L_e and L_x are the Cholesky decompostions of the inverse of the covariance matrices for the noise and prior, $\Gamma_e^{-1} = L_e^{\mathrm{T}} L_e$ and $\Gamma_x^{-1} = L_x^{\mathrm{T}} L_x$, respectively.

In tomography, a practical solution for the inverse problem is obtained by calculating point estimates from the posterior density. In this work, we consider the *maximum a posteriori* (MAP) estimate. It is obtained as

$$(3) \qquad x_{\mathrm{MAP}} = \arg\min_x \left\{\frac{1}{2}\|L_e(y - A_h(x) - e_*)\|^2 + \frac{1}{2}\|L_x(x - x_*)\|^2\right\}.$$

Typically in tomographic inverse problems, the mean of the noise is assumed to be zero, $e_* = 0 \in \mathbb{R}^m$, and the covariance is assumed to be a diagonal matrix with known (constant) standard deviation σ, that is $\Gamma_e = \Gamma_\sigma = \mathrm{diag}(\sigma^2) \in \mathbb{R}^{m \times m}$. In this case, the MAP estimate is obtained as

$$(4) \qquad x_{\mathrm{MAP}} = \arg\min_x \left\{\frac{1}{2}\|\sigma^{-1}(y - A_h(x))\|^2 + \frac{1}{2}\|L_x(x - x_*)\|^2\right\}.$$

which we refer as the MAP estimate with the conventional noise model (MAP-CNM).

In QPAT, the solution method of the acoustic inverse problem affects how the noise of the acoustic data is transferred to the optical problem. Therefore, the noise of the optical inverse problem is necessarily not uncorrelated and it may have a non-zero mean. A more accurate noise model can be, for example, approximated as follows [12]. First, a set of noise samples of the acoustic measurements are simulated. Then, the inverse initial value problem is solved using these noise samples as data. As a result, noise samples of the optical inverse problem $e^{(l)}$ are obtained. The mean and the covariance of the noise model can then be approximated using these noise samples as

$$(5) \qquad\qquad e_* \quad = \quad \frac{1}{L}\sum_{l=1}^{L} e^{(l)}$$

$$(6) \qquad\qquad \Gamma_e \quad = \quad \frac{1}{L-1}\sum_{l=1}^{L} e^{(l)} e^{(l)\,\mathrm{T}} - e_* e_*^{\mathrm{T}}$$

where L is the number of the samples. These are then utilised in the solution of the minimisation problem (3). We refer to the solution of (3) together with (5)–(6) as the MAP estimate with an approximate noise model (MAP-ANM).

In practice, the numerical implementation of the acoustic inverse method affects also the data. Thus, the optical energy density distribution obtained as the solution of the acoustic inverse problem contains modelling error ε which can be due to e.g. discretisation of the geometry and time, implementation of the boundary conditions and smoothing of the data by the acoustic solver. Therefore, let us

write the observation model (1) in the form

$$\tilde{y} = A_h(x) + e$$
$$y + (\tilde{y} - y) = A_h(x) + e$$
$$(7) \qquad y = A_h(x) + \varepsilon + e$$

where $\varepsilon = y - \tilde{y}$ is the modelling error of the acoustic solver which describes the discrepancy between the 'ideal' data $\tilde{y}$ and the data y which contains errors due to the acoustic solver. Then, similarly as in the framework of Bayesian approximation error modelling [11], a Gaussian approximation is constructed for ε, and the total error $n = \varepsilon + e$ is approximated by a Gaussian distribution, thus $\varepsilon \sim \mathcal{N}(\varepsilon_*, \Gamma_\varepsilon)$ $n \sim \mathcal{N}(n_*, \Gamma_n)$ where $n_* = \varepsilon_* + e_*$ and $\Gamma_n = \Gamma_\varepsilon + \Gamma_e$. Furthermore, the mutual dependence of x and ε is ignored. The MAP estimate with the noise and error modelling (MAP-AEM) is obtained as

$$(8) \qquad x_{\mathrm{MAP}} = \arg \min_x \left\{ \frac{1}{2} \|L_n(y - A_h(x) - n_*)\|^2 + \frac{1}{2} \|L_x(x - x_*)\|^2 \right\}$$

where $\Gamma_n^{-1} = L_n^{\mathrm{T}} L_n$. The mean and covariance of the modelling error can be simulated for example as in [12].

References

[1] B. Cox, J. G. Laufer, S. R. Arridge, and P. C. Beard. Quantitative spectroscopic photoacoustic imgaging: a review. *J Biomed Opt*, 17(6):061202, 2012.

[2] M. Xu and L. V. Wang. Photoacoustic imaging in biomedicine. *Rev Sci Instrum*, 77:041101, 2006.

[3] P. Kuchment and L. Kunyansky. Mathematics of thermoacoustic tomography. *European Journal of Applied Mathematics*, 19:191–224, 2008.

[4] B. T. Cox, S. R., Arridge, and P. C. Beard. Estimating chromophore distributions from multiwavelength photoacoustic images. *J Opt Soc Am A*, 26(2):443–455, 2009.

[5] G. Bal and K. Ren. On multi-spectral quantitative photoacoustic tomography in a diffusive regime. *Inv Probl*, 28:025010, 2012.

[6] A. Pulkkinen, B. T. Cox, S. R. Arridge, J. P. Kaipio, and T. Tarvainen. A Bayesian approach to spectral quantitative photoacoustic tomography. *Inv Probl*, 30:065012, 2014.

[7] M. Haltmeier, L. Neumann, and S. Rabanser. Single-stage reconstruction algorithm for quantitative photoacoustic tomography. *Inv Probl*, 31:065005, 2015.

[8] H. Gao, J. Feng, and L. Song. Limited-view multi-source quantitative photoacoustic tomography. *Inv Probl*, 31:065004, 2015.

[9] T. Ding, K. Ren, and S. Vallélian. A one-step reconstruction algorithm for quantitative photoacoustic imaging. *Inv Probl*, 31:095005, 2015.

[10] A. Pulkkinen, B. T. Cox, S. R. Arridge, H. Goh, J. P. Kaipio, and T. Tarvainen. Direct estimation of optical parameters from photoacoustic time series in quantitative photoacoustic tomography. *IEEE Trans Med Imag*, 35(11):2497–2508, 2016.

[11] J. Kaipio and E. Somersalo. *Statistical and Computational Inverse Problems*. Springer, New York, 2005.

[12] T. Tarvainen, A. Pulkkinen, B. T. Cox, J. P. Kaipio, and S. R. Arridge. Bayesian image reconstruction in quantitative photoacoustic tomography. *IEEE Trans Med Imag*, 32(12):2287–2298, 2013.

[13] T. Tarvainen, B. T. Cox, J. P. Kaipio, and S. R. Arridge. Reconstructing absorption and scattering distributions in quantitative photoacoustic tomography. *Inv Probl*, 28:084009, 2012.

Imaging with intensity-only measurements

ALEXEI NOVIKOV

(joint work with Miguel Moscoso, George Papanicolaou, ChysoulaTsogka)

We propose an illumination strategy for interferometric imaging that allows for robust depth recovery from intensity-only measurements. For an array with colocated sources and receivers, we show that all the possible interferometric data for multiple sources, receivers and frequencies can be recovered from intensity-only measurements provided that we have sufficient source location and frequency illumination diversity. There is no need for phase reconstruction in this approach. Using interferometric imaging methods we show that in homogeneous media there is no loss of resolution when imaging with intensities-only. If in these imaging methods we reduce incoherence by restricting the multifrequency interferometric data to nearby array elements and nearby frequencies we obtain robust images in weakly inhomogeneous background media with a somewhat reduced resolution.

We consider an active array of size a consisting of N transducers separated by a distance h which is of the order of the central wavelength λ_0 of the probing signals. The transducers emit probing signals of different frequencies ω_l, $l = 1, \ldots, S$, from positions $\boldsymbol{x}_s$ and record the reflected intensities at positions $\boldsymbol{x}_r$, $s, r = 1, 2, \ldots, N$. The goal is to determine the positions $\boldsymbol{y}_j$ and reflectivities $\alpha_j \in \mathbb{C}$, $j = 1, \ldots, M$, of a set of M point-scatterers within a region of interest, called the image window (IW), which is at a distance L form the array.

Holographic Imaging. A holographic imaging approach with intensity-only measurements is presented in [6, 4]. The main idea is to exploit illumination diversity by designing illumination strategies that recover the missing phase information from intensity-only measurements. It was shown in [6, 4] how by using an appropriate protocol of illuminations and the polarization identity, the single frequency matrix $\boldsymbol{M}(\omega) = \boldsymbol{P}(\omega)^* \boldsymbol{P}(\omega)$ can be determined from intensity-only measurements at that frequency. Here $\boldsymbol{P}(\omega) = [P(\boldsymbol{x}_r, \boldsymbol{x}_s; \omega)]_{r,s=1}^N$ is the full array response matrix of the imaging system, including phases, with $\boldsymbol{x}_r, \boldsymbol{x}_s$ the receiver and source locations, and ω the radian frequency. The matrix $\boldsymbol{M}(\omega)$ is called the time reversal matrix as it arises in ultrasonic time reversal experiments [3]. We will refer to $\boldsymbol{M}(\omega)$ as the single frequency interferometric data matrix. Once we have this data matrix we can image with the DORT method [7] which uses the eigenvectors of $\boldsymbol{M}(\omega)$, or MUSIC [8], which also uses the eigenvectors of $\boldsymbol{M}(\omega)$. Here DORT and MUSIC are the acronyms: Decomposition de l'Operateur de Retournement Temporel (Decomposition of the Time Reversal Operator), and Multiple Signal Classification, respectively. These are phase-sensitive imaging methods that involve only phase differences contained in $\boldsymbol{M}(\omega)$ and, therefore, they provide interferometric information. The illumination strategies in [6, 4] are a form of digital holography since the resulting image does have phase information. Imaging with $\boldsymbol{M}(\omega)$ at a single frequency ω is not robust relative to small perturbations in the unknown phases unless the array is very large. The perturbations can come from medium inhomogeneities or from the discretization of the image window.

Having $\boldsymbol{M}(\omega_l)$ at multiple frequencies ω_l, $l = 1, 2, \ldots, S$ still may not provide robustness with respect to depth in the image. Methods that use the eigenvectors frequency by frequency, as in MUSIC, are not robust.

Interferometric robust imaging. It is known [2] that we can get image robustly if we have interferometric data

$$(1) \qquad d((\boldsymbol{x}_r, \boldsymbol{x}_{r'}), (\boldsymbol{x}_s, \boldsymbol{x}_{s'}), (\omega, \omega')) = \overline{P(\boldsymbol{x}_r, \boldsymbol{x}_s, \omega)} P(\boldsymbol{x}_{r'}, \boldsymbol{x}_{s'}, \omega')$$

at multiple frequency pairs (ω, ω'), receiver location pairs $(\boldsymbol{x}_r, \boldsymbol{x}_{r'})$ and source location pairs $(\boldsymbol{x}_s, \boldsymbol{x}_{s'})$. The main result of [5] is that we can recover such data $d((\boldsymbol{x}_r, \boldsymbol{x}_{r'}), (\boldsymbol{x}_s, \boldsymbol{x}_{s'}), (\omega, \omega'))$ for pairs of arguments from intensity-only measurements. Here receivers and transmitters are colocated in the same array. When the imaging system has separate transmitting and receiving arrays then we can recover only single receiver elements, one receiver at a time,

$$(2) \qquad d((\boldsymbol{x}_r, \boldsymbol{x}_r), (\boldsymbol{x}_s, \boldsymbol{x}_{s'}), (\omega, \omega')) = \overline{P(\boldsymbol{x}_r, \boldsymbol{x}_s, \omega)} P(\boldsymbol{x}_r, \boldsymbol{x}_{s'}, \omega')$$

for all pairs of frequencies, and source locations from intensity-only measurements.

In a homogeneous medium, imaging with $d((\boldsymbol{x}_r, \boldsymbol{x}_{r'}), (\boldsymbol{x}_s, \boldsymbol{x}_{s'}), (\omega, \omega'))$ can be done by

$$
\begin{aligned}
(3) \qquad I^{Interf}(\boldsymbol{y}^s) \;\; &= \sum_{\boldsymbol{x}_s, \boldsymbol{x}_{s'}} \sum_{\boldsymbol{x}_r, \boldsymbol{x}_{r'}} \sum_{\omega_l, \omega_{l'}} d((\boldsymbol{x}_r, \boldsymbol{x}_{r'}), (\boldsymbol{x}_s, \boldsymbol{x}_{s'}), (\omega_l, \omega_{l'})) \\
&\quad \times G_0(\boldsymbol{x}_r, \boldsymbol{y}^s, \omega_l) G_0(\boldsymbol{x}_s, \boldsymbol{y}^s, \omega_l) \overline{G_0(\boldsymbol{x}_{r'}, \boldsymbol{y}^s, \omega_{l'}) G_0(\boldsymbol{x}_{s'}, \boldsymbol{y}^s, \omega_{l'})}
\end{aligned}
$$

with $G_0(\boldsymbol{x}_r, \boldsymbol{y}^s, \omega_l)$ the free space Green's function for the Helmholtz equation, and $\boldsymbol{y}^s$ a point in the image window IW. Replacing the data by its expression (1) we note that $I^{Interf}(\boldsymbol{y}^s)$ equals the square of the Kirchhoff Migration imaging function

$$
\begin{aligned}
(4) \qquad I^{Interf}(\boldsymbol{y}^s) \;\; &= \left| \sum_{\boldsymbol{x}_s} \sum_{\boldsymbol{x}_r} \sum_{\omega_l} \overline{P(\boldsymbol{x}_r, \boldsymbol{x}_s, \omega_l)} G_0(\boldsymbol{x}_r, \boldsymbol{y}^s, \omega_l) G_0(\boldsymbol{x}_s, \boldsymbol{y}^s, \omega_l) \right|^2 \\
&= \left| I^{KM}(\boldsymbol{y}^s) \right|^2.
\end{aligned}
$$

Here, the Kirchhoff migration functional

$$(5) \qquad I^{KM}(\boldsymbol{y}^s) = \sum_{\boldsymbol{x}_s} \sum_{\boldsymbol{x}_r} \sum_{\omega_l} \overline{P(\boldsymbol{x}_r, \boldsymbol{x}_s, \omega_l)} G_0(\boldsymbol{x}_r, \boldsymbol{y}^s, \omega_l) G_0(\boldsymbol{x}_s, \boldsymbol{y}^s, \omega_l)$$

is simply the back propagation of the array response matrix in a homogeneous medium, both for source and receiver points. Note that it is the *square* of the Kirchhoff migration functional that we obtain with intensity-only measurements.

The main result can now be restated as follows. For colocated source and receivers on a single array, we can obtain full-phase, holographic images from intensity-only measurements by exploiting illumination and frequency diversity. That is, in a homogeneous medium there is no loss of resolution when imaging only with intensities if we have sufficient source and frequency illumination diversity.

Single receiver multifrequency interferometric imaging (SRINT). Restricting the data to intensity-only measurements at a single receiver, we obtain $d((\boldsymbol{x}_r, \boldsymbol{x}_r), (\boldsymbol{x}_s, \boldsymbol{x}_{s'}), (\omega_l, \omega_{l'}))$. Using only data from a single receiver, we introduce the following single receiver coherent interferometric imaging (SRINT) functional

$$
\begin{aligned}
I^{SRINT}(\boldsymbol{y}^s) \quad = &\sum_{\substack{\boldsymbol{x}_s, \boldsymbol{x}_{s'} \\ |\boldsymbol{x}_s - \boldsymbol{x}_{s'}| \le X_d}} \sum_{\substack{\omega_l, \omega_{l'} \\ |\omega_l - \omega_{l'}| \le \Omega_d}} d((\boldsymbol{x}_r, \boldsymbol{x}_r), (\boldsymbol{x}_s, \boldsymbol{x}_{s'}), (\omega_l, \omega_{l'})) \\
& \times G_0(\boldsymbol{x}_r, \boldsymbol{y}^s, \omega_l) G_0(\boldsymbol{x}_s, \boldsymbol{y}^s, \omega_l) \overline{G_0(\boldsymbol{x}_r, \boldsymbol{y}^s, \omega_{l'}) G_0(\boldsymbol{x}_{s'}, \boldsymbol{y}^s, \omega_{l'})} .
\end{aligned}
$$

(6)

Note that there is no sum over receivers here. We only have one receiver at $\boldsymbol{x}_r$.

The performance of the proposed interferometric method is explored with numerical simulations in an optical (digital) microscopy regime. We observe in the simulations that in homogeneous media we can image with the same resolution as if phases where recorded and the method is robust with respect to the discretization of the image window. When the ambient medium is weakly inhomogeneous the interferometric approach removes some of the uncertainty in the data due to the fluctuating phases, which tends to stabilize the images and this is seen clearly in the simulations. We also compare the performance of the interferometric approach with MUSIC which is shown to be sensitive to phase errors and does not provide robust results unless the illuminating and receiving arrays are large [1]. The fact that the SRINT imaging functional, which uses data obtained with intensity-only measurements, gives images that are robust to weak fluctuations in the ambient medium is another main result in this paper. It is surprising that such robust, holographic imaging can be obtained with intensity-only measurements.

REFERENCES

[1] A. Chai, M. Moscoso and G. Papanicolaou, *Array imaging of localized objects in homogeneous and heterogeneous media*, Inverse Problems, 32 (2016), 104003.
[2] L. Borcea, G. Papanicolaou and C. Tsogka, *Interferometric array imaging in clutter*, Inverse Problems, 21 (2005), pp. 1419–1460.
[3] M. Fink and C. Prada, *Time reversal mirrors*, Inverse Problems, 17 (2001), pp. R1–R38.
[4] M. Moscoso, A. Novikov and G. Papanicolaou, *Coherent imaging without phases*, SIAM Journal of Imaging Sci., 9 (2016), pp. 1689–1707.
[5] M. Moscoso, A. Novikov, G. Papanicolaou and C.Tsogka, *Multifrequency interferometric imaging with intensity-only measurements*, SIAM J. Imaging Sci., to appear.
[6] A. Novikov, M. Moscoso and G. Papanicolaou, *Illumination strategies for intensity-only imaging*, SIAM Journal of Imaging Sci., 8 (2015), pp. 1547–1573.
[7] C. Prada, S. Manneville, D. Spoliansky and M Fink, *Decomposition of the time reversal operator: Detection and selective focusing on two scatterers*, J. Acoust. Soc. Am., 99 (1996), pp. 2067–2076.
[8] R. O. Schmidt, *Multiple Emitter Location and Signal Parameter Estimation*, IEEE Trans. Antennas Propag., 34 (1986), pp. 276–280.

Inverse scattering without phase information

ROMAN NOVIKOV, ALEXEY AGALTSOV

We consider direct and inverse scattering for the Schrödinger equation of quantum mechanics and for the Helmholtz equation of acoustics or electrodynamics. In addition, only scattering data without phase information can be measured directly in practice in quantum mechanics and in some other cases. Note that in quantum mechanics this limitation is related to the probabilistic interpretation of the wavefunction proposed originally by Max Born in 1926.

In this connection we report on non-uniqueness, uniqueness and reconstruction results for inverse scattering without phase information. We are motivated by recent and very essential progress in this domain.

In particular, in the first part of this talk we present the results of [6], [7], [8] and in the second part of the talk we present the results of [1] and [2].

For more information, see [1], [2], [6], [7], [8], and references therein. In particular, among preceeding works we would like to mention [3], [4], [5].

REFERENCES

[1] A. D. Agaltsov, R. G. Novikov, *Error estimates for phaseless inverse scattering in the Born approximation at high energies*, The Journal of Geometric Analysis, doi:10.1007/s12220-017-9872-6; arXiv:1604.06555v2.

[2] A. D. Agaltsov, A. Gillman, T. Hohage, R. G. Novikov, *An iterative approach to monochromatic phaseless inverse scattering*, in preparation.

[3] T. Aktosun, P. Sacks, *Inverse problem on the line without phase information*, Inverse Problems **14** (1998), 211–224.

[4] A. A. Govyadinov, G. Y. Panasyuk, J. C. Schotland, *Phaseless three-dimensional optical nanoimaging*, Physical Review Letters **103** (2009), 213901.

[5] M. V. Klibanov, *Phaseless inverse scattering problems in three dimensions*, SIAM J. Appl. Math. **74** (2014), no. 2, 392–410.

[6] R. G. Novikov, *Phaseless inverse scattering in the one dimensional case*, Eurasian Journal of Mathematical and Computer Applications **3** (2015), no. 1, 64–70.

[7] R. G. Novikov, *Formulas for phase recovering from phaseless scattering data at fixed frequency*, Bulletin des Sciences Mathématiques **139** (2015), no. 8, 923–936.

[8] R. G. Novikov, *Explicit formulas and global uniqueness for phaseless inverse scattering in multidimensions*, The Journal of Geometric Analysis **26** (2016), no. 1, 346–359.

Stability estimates for linearized near-field phase retrieval in X-ray phase contrast imaging – A well-posed phase retrieval problem

SIMON MARETZKE

(joint work with Thorsten Hohage)

In classical X-ray radiography, an image of an unknown sample is obtained by measuring the partial attenuation of transmitted X-rays. Phase contrast techniques are sensitive also to the *refraction* of X-rays by the scattering interaction with the illuminated sample. The refraction parameter δ of the refractive index

$n = 1 - \delta + \mathrm{i}\beta$ in the hard X-ray regime is typically up to three orders of magnitude larger than the attenuative part β. Consequently, X-ray phase contrast imaging enables significantly improved contrast, thereby extending the scope of X-ray imaging to microscale light-element samples such as biological cells. Spatial variations of δ is encoded as phase shifts in the transmitted X-rays wave field. However, the phase of the wave field cannot be observed directly, as X-ray detectors are limited to measuring intensities. Phase contrast imaging thus involves a *phase retrieval* problem, which is typically ill-posed and even non-unique.
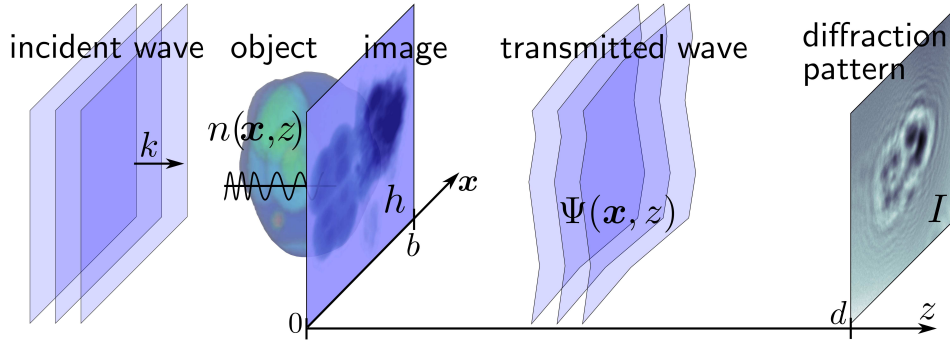
FIGURE 1. Physical model of propagation-based X-ray phase contrast imaging (also known as inline holography).

We consider the setup of (propagation-based) X-ray phase contrast imaging. The physical model is essentially that of phaseless Helmholtz scattering, as sketched in Figure 1: an object is illuminated by a plane wave for a single incident direction and wavenumber k. We make use the *projection approximation*, assuming that the scattering interaction can be modeled by geometrical optics. The object parameters δ, β are then encoded as line-integrals in the exit wave field at $z = 0$:

$$(1) \qquad \Psi(\boldsymbol{x}, 0) = \exp(h(\boldsymbol{x})) \quad \text{with} \quad h(\boldsymbol{x}) = -\mathrm{i}k \int_{\mathbb{R}} \big(\delta(\boldsymbol{x}, z) - \mathrm{i}\beta(\boldsymbol{x}, z)\big)\mathrm{d}z$$

A diffraction pattern (or *hologram*) is measured by a detector in the plane $z = d > 0$ behind the object. By diffraction of the propagating wave field, the refractive phase shifts are partially encoded into measurable intensities. We describe the propagation from the exit plane $z = 0$ to the detector $z = d$ by the free-space solution to the Helmholtz equation within the *paraxial approximation*. $\Psi(\cdot, d)$ is then related to $\Psi(\cdot, 0)$ via the *Fresnel propagator* $\mathcal{D}$ ($\mathcal{F}$: Fourier transform):

$$(2) \qquad \mathrm{e}^{-\mathrm{i}kd}\Psi(\cdot, d) = \mathcal{D}\left(\Psi(\cdot, 0)\right) := \mathcal{F}^{-1}\left(\exp\left(-\frac{\mathrm{i}|\cdot|^2}{2N_{\mathrm{F}}}\right) \cdot \mathcal{F}\left(\Psi(\cdot, 0)\right)\right)$$

The parameter $N_{\mathrm{F}} := kb^2/d$ is the Fresnel number of the setup (scaled by 2π).

In total, we have the following forward model for the reconstruction of the complex-valued image h from measured intensities I:

$$(3) \qquad I = F(h) := |\Psi(\cdot, d)|^2 = |\mathcal{D}\left(\exp(h)\right)|^2$$

The underlying projection- and paraxial approximations have been shown to be well-satisfied in the hard X-ray regime of very large wavenumbers $k \to \infty$ [4].

We consider a commonly-used linearization of (3) for weakly scattering samples, known as the *contrast transfer function* (CTF) model, see e.g. [1, 3, 9]:

$$(4) \quad F(h) = 1 + T + \mathcal{O}(h^2), \quad T(h) = 2\mathrm{Re}\,(\mathcal{D}(h)) \quad (\mathrm{Re: \ pointwise \ real \ part})$$

Although the $\mathbb{R}$-linear forward map T is clearly not injective as a map $L^2(\mathbb{R}^2, \mathbb{C}) \to L^2(\mathbb{R}^2, \mathbb{C})$, it has been shown in [5] that the linearized inverse problem (and also the nonlinear one) is uniquely solvable if we restrict to images h with a *compact support*. Such a constraint arises naturally within the ray-optical model (1).

In the present work [7], we analyze stability of image reconstruction $h \mapsto I$ for the linearized forward model in (4) under support constraints. Our approach is strongly inspired by *Gabor holography* [2]: the starting point is the formula

$$(5) \quad T(h) = 2\mathrm{Re}\,(\mathcal{D}(h)) = \mathcal{D}(h) + \overline{\mathcal{D}(h)} = \mathcal{D}(h) + \mathcal{D}^{-1}(\overline{h}).$$

Applying $\mathcal{D}$ to the data then yields $\mathcal{D}T(h) = \mathcal{D}^2(h) + \overline{h}$, i.e. a sum of the sharp *twin-image* $\overline{h}$ (complex-conjugate) and a wavy pattern from the doubly propagated image. If the support constraint $\mathrm{supp}(h) \subset \Omega \subset \mathbb{R}^2$ holds, we may thus eliminate the twin-image contribution by restricting to $\mathbb{R}^2 \setminus \Omega$. Stability-wise, this implies

$$(6) \quad \|T(h)\|_{L^2}^2 \overset{\mathcal{D} \text{ unitary}}{=} \|\mathcal{D}T(h)\|_{L^2}^2 \geq \|\mathcal{D}T(h)|_{\mathbb{R}^2 \setminus \Omega}\|_{L^2}^2 \overset{\overline{h}|_{\mathbb{R}^2 \setminus \Omega} = 0}{=} \|\mathcal{D}^2(h)|_{\mathbb{R}^2 \setminus \Omega}\|_{L^2}^2,$$

i.e. the inversion of T cannot be more ill-posed or ill-conditioned than reconstructing h from incomplete Fresnel data $\mathcal{D}^2(h)|_{\mathbb{R}^2 \setminus \Omega}$. Using the representation

$$(7) \quad \mathcal{D}^2(h) = \mathrm{e}^{-\mathrm{i}\pi/2} N_{\mathrm{F}} n_{\mathrm{F}}^{\frac{1}{2}} \cdot \mathcal{F}(n_{\mathrm{F}}^{\frac{1}{2}} \cdot h) \left(\frac{N_{\mathrm{F}}}{2}(\cdot) \right), \quad n_{\mathrm{F}}^{\frac{1}{2}}(\boldsymbol{x}) := \exp\left(\frac{\mathrm{i}N_{\mathrm{F}}|\boldsymbol{x}|^2}{4} \right)$$

this can be further identified with a reconstruction from incomplete Fourier data:

$$(8) \quad \|T(h)\|_{L^2} \geq \|\mathcal{F}(n_{\mathrm{F}}^{\frac{1}{2}} \cdot h)|_{\mathbb{R}^2 \setminus \Omega_{\mathrm{F}}}\|_{L^2} \geq C\|h\|_{L^2} \quad C := \inf_{\substack{\|h\|_{L^2} = 1 \\ \mathrm{supp}(h) \subset \Omega}} \|\mathcal{F}(h)|_{\mathbb{R}^2 \setminus \Omega_{\mathrm{F}}}\|_{L^2}$$

with $\Omega_{\mathrm{F}} := \{(\frac{N_{\mathrm{F}}}{2})\boldsymbol{x} : \boldsymbol{x} \in \mathbb{R}^2\}$. The arising Fourier data completion problem is well-understood. In particular, for rectangular domains Ω the computation of the stability constant C in (6) can be related to the principal singular value of 1D-integral operator, for which estimates are available [8]. By incorporating these known results into (8), we arrive at the following startling stability result:

Theorem 1 (Well-posedness and stability estimate). *Let the support-domain Ω be given by a stripe of width 1, without loss of generality $\Omega := [-1/2; 1/2] \times \mathbb{R}$. Then the stability constant $C = C(\Omega, N_{\mathrm{F}})$ in (8) is strictly positive and satisfies*

$$(9) \quad C(\Omega, N_{\mathrm{F}}) \geq (2\pi N_{\mathrm{F}})^{\frac{1}{4}} \left(1 - \frac{3}{8N_{\mathrm{F}}} + \mathcal{O}\left(N_{\mathrm{F}}^{-2} \right) \right) \exp\left(-N_{\mathrm{F}}/8 \right).$$

Hence, the reconstruction of a complex-valued image $h \in L^2(\mathbb{R}^2)$ with $\mathrm{supp}(h) \subset \Omega$ from a single diffraction pattern $I = 1 + Th$ is well-posed.

Numerical computations indicate that the bound for the stability constant $C(\Omega, N_{\mathrm{F}})$ in (9) is surprisingly sharp. Due to the exponential decay with the Fresnel number N_{F}, solving the inverse problem may thus be terribly *ill-conditioned* for typical values $N_{\mathrm{F}} = 10^2 \ldots 10^4$ encountered in imaging practice – despite well-posedness. This is in accordance with experience from numerical reconstructions which turn out to be practically impossible for larger N_{F} but feasible in the deeply holographic regime of Fresnel numbers $N_{\mathrm{F}} \sim 10^2$ or less [6].

Using a different approach, we show that the stability estimates can be improved to *algebraic* rates $C(\Omega, N_{\mathrm{F}}) \sim N_{\mathrm{F}}^{-1}$ in two settings of high practical relevance:

   1 Image reconstruction for *single material objects* with proportional $\beta \propto \delta$, including the important special case of *non-absorbing objects* $\beta \approx 0$

   2 Recovery from *two* holograms I_1, I_2 acquired in different setups $N_{\mathrm{F},1}, N_{\mathrm{F},2}$

All in all, our analysis highlights the considerable value of support constraints in propagation-based X-ray phase contrast imaging, turning a highly non-unique phase retrieval problem into a *well-posed* one and ensuring practical stability of image reconstruction for sufficiently small Fresnel numbers N_{F}. The results may be relevant to several related wave-optical or quantum-mechanical inverse problems such as (phaseless) inverse scattering or wavefront reconstruction.

References

[1] P Cloetens, W Ludwig, J Baruchel, D Van Dyck, J Van Landuyt, JP Guigay, and M Schlenker. Holotomography: Quantitative phase tomography with micrometer resolution using hard synchrotron radiation X-rays. *Appl. Phys. Lett.*, 75(19):2912–2914, 1999.
[2] D. Gabor et al. A new microscopic principle. *Nature*, 161(4098):777–778, 1948.
[3] JP Guigay. Fourier-transform analysis of Fresnel diffraction patterns and in-line holograms. *Optik*, 49(1):121–125, 1977.
[4] P Jonas and AK Louis. Phase contrast tomography using holographic measurements. *Inverse Probl.*, 20(1):75, 2004.
[5] S Maretzke. A uniqueness result for propagation-based phase contrast imaging from a single measurement. *Inverse Probl.*, 31:065003, 2015.
[6] S Maretzke, M Bartels, M Krenkel, T Salditt, and T Hohage. Regularized Newton methods for X-ray phase contrast and general imaging problems. *Opt. Express*, 24(6):6490–6506, 2016.
[7] S Maretzke and T Hohage. Stability estimates for linearized near-field phase retrieval in X-ray phase contrast imaging. *SIAM J. Appl. Math.*, 77:384–408, 2017.
[8] D Slepian and E Sonnenblick. Eigenvalues associated with prolate spheroidal wave functions of zero order. *Bell Syst. Tech. J.*, 44(8):1745–1759, 1965.
[9] L Turner, B Dhal, J Hayes, A Mancuso, K Nugent, D Paterson, R Scholten, C Tran, and A Peele. X-ray phase imaging: Demonstration of extended conditions for homogeneous objects. *Opt. Express*, 12(13):2960–2965, 2004.

High-order statistics for the random paraxial wave equation. Application to correlation-based imaging

Josselin Garnier

In sensor array imaging an unknown medium is probed by waves emitted by an array of sources and recorded by an array of receivers. Sensor array imaging in a randomly scattering medium is usually limited because coherent signals recorded

by the receiver array and coming from a reflector to be imaged are weak and dominated by incoherent signals coming from multiple scattering by the medium. Stochastic and multiscale analysis allows to understand the direct problem and helps solving the inverse problem. We show in this talk how correlation-based imaging techniques can mitigate or even sometimes benefit from the multiple scattering of waves. Applications to seismic interferometry, non-destructive testing, and intensity correlation imaging in optics are discussed.

1. Wave propagation in random media

We consider the three-dimensional scalar wave equation:

$$\frac{1}{c^2(\vec{\boldsymbol{x}})}\frac{\partial^2 u}{\partial t^2}(t,\vec{\boldsymbol{x}}) - \Delta_{\vec{\boldsymbol{x}}}u(t,\vec{\boldsymbol{x}}) = F(t,\vec{\boldsymbol{x}}).$$

Here the source emits a time-harmonic signal and it is localized in the plane $z = 0$:

$$F(t,\vec{\boldsymbol{x}}) = \delta(z)f(\boldsymbol{x})e^{-i\omega t} \text{ with } \vec{\boldsymbol{x}} = (\boldsymbol{x},z),$$

and the speed of propagation is spatially heterogeneous

$$\frac{1}{c^2(\vec{\boldsymbol{x}})} = \frac{1}{c_o^2}\big(1 + \mu(\vec{\boldsymbol{x}})\big),$$

where μ is a zero-mean stationary random process with nice ergodic properties.

The time-harmonic field $\hat{u}$ such that $u(t,\vec{\boldsymbol{x}}) = \hat{u}(\vec{\boldsymbol{x}})e^{-i\omega t}$ is solution of the random Helmholtz equation

$$(\partial_z^2 + \Delta_\perp)\hat{u} + \frac{\omega^2}{c_o^2}\big(1 + \mu(\boldsymbol{x},z)\big)\hat{u} = -\delta(z)f(\boldsymbol{x}),$$

where $\Delta_{\vec{\boldsymbol{x}}} = \Delta_\perp + \partial_z^2$. The function $\hat{\phi}$ (slowly-varying envelope of a plane wave going along the z-axis) defined by

$$\hat{u}(\boldsymbol{x},z) = \frac{ic_o}{2\omega}e^{i\frac{\omega z}{c_o}}\hat{\phi}(\boldsymbol{x},z)$$

satisfies

$$\partial_z^2\hat{\phi} + \left(2i\frac{\omega}{c_o}\partial_z\hat{\phi} + \Delta_\perp\hat{\phi} + \frac{\omega^2}{c_o^2}\mu(\boldsymbol{x},z)\hat{\phi}\right) = 2i\frac{\omega}{c_o}\delta(z)f(\boldsymbol{x}).$$

In the paraxial regime "$\lambda \ll l_c, r_o \ll L$" (which means, the wavelength $2\pi c_o/\omega$ is much smaller than the correlation radius of the medium and the radius of the source, which are themselves much smaller than the typical propagation distance) the forward-scattering approximation in direction z is valid and $\hat{\phi}$ satisfies the Itô-Schrödinger equation [3]

$$d_z\hat{\phi} = \frac{ic_o}{2\omega}\Delta_\perp\hat{\phi}dz + \frac{i\omega}{2c_o}\hat{\phi}\circ dB(\boldsymbol{x},z), \qquad \hat{\phi}(z=0,\boldsymbol{x}) = f(\boldsymbol{x}),$$

where $\circ$ stands for the Stratonovich integral, $B(\boldsymbol{x},z)$ is a Brownian field, that is a Gaussian process with mean zero and covariance $\mathbb{E}[B(\boldsymbol{x},z)B(\boldsymbol{x}',z')] = \gamma(\boldsymbol{x} -$

$\boldsymbol{x}'$) $\min(z, z')$ with

$$\gamma(\boldsymbol{x}) = \int_{-\infty}^{\infty} \mathbb{E}[\mu(\mathbf{0}, 0)\mu(\boldsymbol{x}, z)]dz.$$

2. STATISTICS OF THE WAVE FIELD

By Itô's formula, the coherent (or mean) wave satisfies the Schrödinger equation with homogeneous damping:

$$\frac{\partial}{\partial z}\mathbb{E}[\hat{\phi}] = \frac{ic_o}{2\omega}\Delta_{\perp}\mathbb{E}[\hat{\phi}] - \frac{\omega^2\gamma(\mathbf{0})}{8c_o^2}\mathbb{E}[\hat{\phi}],$$

and therefore $\mathbb{E}\big[\hat{\phi}(\boldsymbol{x}, z)\big] = \hat{\phi}_0(\boldsymbol{x}, z)\exp(-z/Z_{\text{sca}})$, where $\hat{\phi}_0$ is the solution in the homogeneous medium and $Z_{\text{sca}} = 8c_o^2/[\gamma(\mathbf{0})\omega^2]$. The coherent wave amplitude decays exponentially with the propagation distance and the characteristic decay length is the *scattering mean free path* Z_{sca}. This result shows that any coherent imaging method (such as Kirchhoff migration or Reverse-Time migration) fails in random media when the propagation distance is larger than the scattering mean free path.

The mean Wigner transform defined by

$$W(\boldsymbol{x}, \boldsymbol{\xi}, z) = \int_{\mathbb{R}^2}\exp\big(-i\boldsymbol{\xi}\cdot\boldsymbol{y}\big)\mathbb{E}\left[\hat{\phi}\big(\boldsymbol{x} + \frac{\boldsymbol{y}}{2}, z\big)\overline{\hat{\phi}}\big(\boldsymbol{x} - \frac{\boldsymbol{y}}{2}, z\big)\right]d\boldsymbol{y},$$

is the angularly-resolved mean wave energy density. By Itô's formula, it solves a *radiative transport-like equation*

$$\frac{\partial W}{\partial z} + \frac{c_o}{\omega}\boldsymbol{\xi}\cdot\nabla_{\boldsymbol{x}}W = \frac{\omega^2}{4(2\pi)^2c_o^2}\int_{\mathbb{R}^2}\hat{\gamma}(\boldsymbol{\kappa})\big[W(\boldsymbol{\xi} - \boldsymbol{\kappa}) - W(\boldsymbol{\xi})\big]d\boldsymbol{\kappa},$$

starting from $W(\boldsymbol{x}, \boldsymbol{\xi}, z = 0) = W_0(\boldsymbol{x}, \boldsymbol{\xi})$, the Wigner transform of the initial field f. $\hat{\gamma}$ is the Fourier transform of γ and determines the scattering cross section of the radiative transport equation. This result shows that the fields observed at nearby points are correlated and their correlations contain information about the medium. Accordingly, one should use local cross correlations for imaging in random media [1, 2].

In order to quantify the stability of correlation-based imaging methods, one needs to study the fourth-order moment:

$$M_4(\boldsymbol{r}_1, \boldsymbol{r}_2, \boldsymbol{q}_1, \boldsymbol{q}_2, z) = \mathbb{E}\Big[\hat{\phi}\big(\frac{\boldsymbol{r}_1 + \boldsymbol{r}_2 + \boldsymbol{q}_1 + \boldsymbol{q}_2}{2}, z\big)\hat{\phi}\big(\frac{\boldsymbol{r}_1 - \boldsymbol{r}_2 + \boldsymbol{q}_1 - \boldsymbol{q}_2}{2}, z\big)$$
$$\times \overline{\hat{\phi}}\big(\frac{\boldsymbol{r}_1 + \boldsymbol{r}_2 - \boldsymbol{q}_1 - \boldsymbol{q}_2}{2}, z\big)\overline{\hat{\phi}}\big(\frac{\boldsymbol{r}_1 - \boldsymbol{r}_2 - \boldsymbol{q}_1 + \boldsymbol{q}_2}{2}, z\big)\Big].$$

By Itô's formula,

$$\frac{\partial M_4}{\partial z} = \frac{ic_o}{\omega}\big(\nabla_{\boldsymbol{r}_1}\cdot\nabla_{\boldsymbol{q}_1} + \nabla_{\boldsymbol{r}_2}\cdot\nabla_{\boldsymbol{q}_2}\big)M_4 + \frac{\omega^2}{4c_o^2}U_4(\boldsymbol{q}_1, \boldsymbol{q}_2, \boldsymbol{r}_1, \boldsymbol{r}_2)M_4,$$

with the generalized potential

$$U_4(\boldsymbol{q}_1, \boldsymbol{q}_2, \boldsymbol{r}_1, \boldsymbol{r}_2) = \gamma(\boldsymbol{q}_2 + \boldsymbol{q}_1) + \gamma(\boldsymbol{q}_2 - \boldsymbol{q}_1) + \gamma(\boldsymbol{r}_2 + \boldsymbol{q}_1) + \gamma(\boldsymbol{r}_2 - \boldsymbol{q}_1)$$
$$- \gamma(\boldsymbol{q}_2 + \boldsymbol{r}_2) - \gamma(\boldsymbol{q}_2 - \boldsymbol{r}_2) - 2\gamma(\boldsymbol{0}).$$

These moment equations have been known for a long time [8]. If we take the Fourier transform:

$$\hat{M}_4(\boldsymbol{\xi}_1, \boldsymbol{\xi}_2, \boldsymbol{\zeta}_1, \boldsymbol{\zeta}_2, z) = \iiiint_{\mathbb{R}^8} M_4(\boldsymbol{q}_1, \boldsymbol{q}_2, \boldsymbol{r}_1, \boldsymbol{r}_2, z)$$
$$\times \exp\big(-i\boldsymbol{q}_1 \cdot \boldsymbol{\xi}_1 - i\boldsymbol{r}_1 \cdot \boldsymbol{\zeta}_1 - i\boldsymbol{q}_2 \cdot \boldsymbol{\xi}_2 - i\boldsymbol{r}_2 \cdot \boldsymbol{\zeta}_2\big) d\boldsymbol{r}_1 d\boldsymbol{r}_2 d\boldsymbol{q}_1 d\boldsymbol{q}_2,$$

then in the regime "$\lambda \ll l_c \ll r_o \ll L$" the function $\hat{M}_4$ has the form

$$\hat{M}_4(\boldsymbol{\xi}_1, \boldsymbol{\xi}_2, \boldsymbol{\zeta}_1, \boldsymbol{\zeta}_2, z) = \Phi(K, A, f)(\boldsymbol{\xi}_1, \boldsymbol{\xi}_2, \boldsymbol{\zeta}_1, \boldsymbol{\zeta}_2, z) + R(\boldsymbol{\xi}_1, \boldsymbol{\xi}_2, \boldsymbol{\zeta}_1, \boldsymbol{\zeta}_2, z),$$

where the nonlinear function Φ is explicit and

$$\sup_{z \in [0,L]} \|R(\cdot, \cdot, \cdot, \cdot, z)\|_{L^1(\mathbb{R}^2 \times \mathbb{R}^2 \times \mathbb{R}^2 \times \mathbb{R}^2)} \simeq 0,$$

with

$$K(z) = (2\pi)^8 \exp\Big(-\frac{\omega^2}{2c_o^2} \gamma(\boldsymbol{0}) z\Big),$$

$$A(\boldsymbol{\xi}, \boldsymbol{\zeta}, z) = \frac{1}{2(2\pi)^2} \int_{\mathbb{R}^2} \Big[\exp\Big(\frac{\omega^2}{4c_o^2} \int_0^z \gamma\big(\boldsymbol{x} + \frac{c_o \boldsymbol{\zeta}}{\omega} z'\big) dz'\Big) - 1\Big] \exp\big(-i\boldsymbol{\xi} \cdot \boldsymbol{x}\big) d\boldsymbol{x}.$$

This result allows to quantify the scintillation index of the field (i.e. the relative variance of the intensity) [4], the coefficient of variation of the (smoothed) Wigner transform [5], and paves the way for original imaging modalities based on intensity correlations [7] or optimal methods for wave focusing through a randomly scattering medium [6].

References

[1] L. Borcea, G. Papanicolaou, and C. Tsogka, *Interferometric array imaging in clutter*, Inverse Problems **21** (2005), 1419–1460.

[2] L. Borcea, J. Garnier, G. Papanicolaou, and C. Tsogka, *Enhanced statistical stability in coherent interferometric imaging*, Inverse Problems **27** (2011), 085004.

[3] J. Garnier and K. Sølna, *Coupled paraxial wave equations in random media in the white-noise regime*, Ann. Appl. Probab. **19** (2009), 318–346.

[4] J. Garnier and K. Sølna, *Scintillation in the white-noise paraxial regime*, Comm. Part. Differ. Equat. **39** (2014), 626–650.

[5] J. Garnier and K. Sølna, *Fourth-moment analysis for beam propagation in the white-noise paraxial regime*, Archive on Rational Mechanics and Analysis **220** (2016), 37–81.

[6] J. Garnier and K. Sølna, *Focusing waves through a randomly scattering medium in the white-noise paraxial regime*, arXiv:1608.00154, to appear in SIAM J. Appl. Math.

[7] J. Garnier, *Ghost imaging in the random paraxial regime*, Inverse Problems and Imaging **10** (2016), 409–432.

[8] A. Ishimaru, *Wave Propagation and Scattering in Random Media*, Academic Press, San Diego, 1978.

Statistical problems in nerve axon equations

Wilhelm Stannat

When modeling neural activity in the brain, stochasticity on the molecular level, for example channel noise and synaptic noise, has to be taken into account. To this end a mathematical framework is introduce that allows to analyze in a mathematical rigorous way stochastic conductance based neural models describing the propagation of action potentials along the nerve axon under the impact of channel noise fluctuations. The resulting stochastic partial differential equations exhibit a rich phenomenology, like propagation failure, backpropagation, spontaneous pulse solutions and annihilation of pulses, that cannot be modelled with their deterministic counterparts.

1. Conductance-based neural models

The temporal evolution of the membrane potential $v(t,x)$ along the axon of a nerve cell can be modelled by a linear cable equation coupled to a set of equations describing the concentrations of ion channels, both excitatory and inhibitory, regulating v. For a mathematical introduction to this subject see [2]. In neuroscience these models are called conductance-based neural models and the prototypical example are the Hodgkin-Huxley equations:

$$(1) \qquad \tau \partial_t v = \lambda^2 \partial_{xx}^2 v - g_K n^4 (v - E_K) - g_{Na} m^3 h (v - E_{Na}) - g_L (v - E_L) + I$$

for $t \geq 0$ and $x \in [0, L]$, $L > 0$ fixed, coupled to three equations of the type

$$(2) \qquad \frac{dp}{dt} = \alpha_p(v)(1 - p) - \beta_p(v)p$$

for the concentrations of ions of three different types, $p \in \{m, n, h\}$, where m, n and h denote ion concentrations in activating sodium, activating potassium and inactivating sodium channels. τ and λ denote specific time and space constants, g_{Na}, g_K, g_L conductances and E_{Na}, E_K, E_L resting potentials of the respective currents and the reaction rates $\alpha_p(v)$ and $\beta_p(v)$ are functions of the following structure $\alpha_p(v) = a_1 \frac{v+A}{1-e^{-a_2(v+A_p)}}$ and $\beta_p(v) = b_1 e^{-b_2(v+B)}$ for certain parameters a_1, a_2, b_1, b_2, A and B. The coupled system is a reaction-diffusion system which is neither Lipschitz nor one-sided Lipschitz, but has the following two structural properties:

a) conditioned on fixed ion-channel concentrations $\mathbf{X} = (m, n, h)$ (1) becomes linear,
b) the equations for p are forward Kolmogorov equations preserving probabilities, i.e., $p_0(x) \in [0, 1]$ implies $p(t, x) \in [0, 1]$.

The function $I(t,x)$ denotes additional exterior current, for example of presynaptic neurons or sensory input and can mathematically be seen as a control. Depending on the value of I, the solution $v(t,x)$ to equation (1) can take the form of an action potential (AP) or spike, i.e. a sharp rise of the membrane potential followed by a sharp decrease and a recovery phase, traveling with constant speed

c along $[0, L]$. Moreover, the system undergoes a Hopf bifurcation w.r.t. the parameter I, separating the excitable regime, where the solution exhibits at most one AP, from the regime of periodic spiking.

2. STOCHASTIC CONDUCTANCE-BASED NEURAL MODELS

Despite this important feature, which was a great success of mathematical modelling of neural activity, (1) nevertheless does not take into account the variability in the ion concentrations due to the apparent random opening and closing of the individual ion channels, so called channel noise. The dynamical implications of channel noise are important and cannot be neglected in a thorough understanding of neural activity. Possible implications are spontaneous spiking, propagation failure, splitting and annihilation of APs and time jitter (see [1]). There are various possibilities for incorporating noise into (1). The simplest one is the so called current noise leading to the following stochastic partial differential equation

(3) $\quad \tau \partial_t v = \lambda^2 \partial_{xx} v - g_{Na} m^3 h(v - E_{Na}) - g_K n^4 (v - E_K) - g_L(v - E_L) + I + \sigma \partial_t \xi(t, x)$

where $\xi(t, x)$ denotes $L^2(0, L)$-valued Wiener noise, i.e.,

$$\xi(t, x) = \sum_{m=1}^{\infty} \sigma_m \beta_m(t) e_m(x)$$

for some orthonormal system $(e_m)_{m \geq 1}$ of $L^2(0, L)$, independent, 1d-Brownian motions $(\beta_m)_{m \geq 1}$ and ℓ^2-summable noise amplitudes $(\sigma_m)_{m \geq 1}$. Numerical simulations show that (3) exhibits a rich phenomenology, including the above mentioned implications of channel noise effects on the AP.

Current noise clearly is a purely phenomenological modelling of channel noise. A second possibility is to apply classical diffusion approximation to the Markovian dynamics of the ion concentrations, leading to so-called subunit noise

(4)
$$\partial_t p = (\alpha_p(v)(1 - p(t)) - \beta_p(v)p(t)) \, dt + \sqrt{\alpha(v)(1 - p(t)) + \beta(v)p(t)} \, \partial_t \xi_p(t, x) \, ,$$

turning (2) into a function-valued stochastic ordinary differential equation. A mathematical theory of variational, i.e. analytically weak, solutions of general stochastic conductance based neural models including both, current and subunit noise, has been developed in [4, 5], including a numerical analysis of lattice approximations.

3. STATISTICAL ANALYSIS OF STOCHASTIC CONDUCTANCE-BASED NEURAL MODELS

The statistical analysis of stochastic conductance-based neural models is important to understand the impact of channel noise on neural activity. Consider as an example the computation of the probability for the propagation failure of an action potential. To this end we introduce the following observable

$$\Phi(v) := \int_0^L v(x) - v_* \, dx \, , \qquad v_* = \text{resting potential}$$

and define a propagation failure on the time interval $[T_0, T]$ w.r.t. a given threshold θ if

$$\Phi(v(t)) < \theta \quad \text{for some} \quad t \in [T_0, T].$$

The quantity of interest therefore is the probability

$$p_\sigma := P_\sigma \left(\min_{T_0 \le t \le T} \Phi(v(t)) < \theta \right).$$

In [6], a statistical analysis of the estimator Φ has been performed in the case of the Hodgkin-Huxley model with current noise. It has been shown in particular that for small noise amplitude the probability p_σ can be approximated by a first passage time probability of the following 1d-stochastic differential equation

$$d\Phi(v(t)) = \kappa_* \left(c - \Phi(v(t)) \right) dt + \tilde\sigma d\beta(t).$$

Here, $c = \int_0^L \hat{v}(t, x) - v_* \, dx$ is independent of time, $\tilde\sigma^2 = \sigma^2 \frac{1}{t} \mathrm{Var}\left(\int_0^L \xi(t, x) \, dx \right)$ and β denotes a 1d-Brownian motion.

A second example for a statistical analysis is the derivation of a 1d-stochastic differential equation for the velocity $c(t)$ of the AP. A derivation of a dynamical equation first requires the identification of the position of the AP. To this end one can consider a reference profile v^{AP} and define the current position of the AP as a (local) minimum of $\|v(t, \cdot) - v^{AP}(\cdot + c)\|_{L^2(0,L)}$ w.r.t. c. Numerical illustrations then indicate that for small noise amplitude σ, $c(t)$ is approximately given as the solution of the stochastic differential equation

$$(5) \qquad dc(t) = c_{det} dt + \langle e^{\frac{c_{det}}{\lambda^2} \cdot} v^{AP}(\cdot + c_{det} t), \sigma \, d\xi(t) \rangle$$

where c_{det} is the velocity of the AP in the absence of noise ($\sigma = 0$). The analogue of (5) for the velocity of a traveling wave in a bistable stochastic reaction diffusion equation has been rigorously derived in [3] as a result of a multiscale analysis.

REFERENCES

[1] A. Faisal, L. Selen, D. Wolpert, *Noise in the nervous system*, Nature Reviews Neuroscience **9** (2008), 292–303.
[2] J. Keener, J. Sneyd, *Mathematical Physiology I: Cellular Physiology*, Springer, Berlin, 2nd Edition (2009).
[3] J. Krüger, W. Stannat, *A Multiscale-Analysis of Stochastic Bistable Reaction-Diffusion Equations*, arXiv:1701.01688 (2017).
[4] M. Sauer, W. Stannat, *Lattice Approximation for Stochastic Reaction Diffusion Equations with One-sided Lipschitz Condition*, Math. Comp. **84** (2015), 743–766.
[5] M. Sauer, W. Stannat, *Analysis and Approximation of Stochastic Nerve Axon Equations*, Math. Comp. **85** (2016), 2457–2481.
[6] M. Sauer, W. Stannat, *Reliability of signal transmission in stochastic nerve axon equations*, Journal of Computational Neuroscience **40** (2016), 103–111.

SDE estimation from discrete observations as inverse problems

Markus Reiss

(joint work with Jakub Chorowski, Emmanuel Gobet, Marc Hoffmann)

We consider time-homogeneous stochastic differential equations (SDEs) with drift b and diffusion matrix Σ:

$$dX_t = b(X_t) \, dt + \Sigma^{1/2}(X_t) \, dW_t, \quad X_0 = x_0.$$

Here, W denotes d-dimensional Brownian motion and $b : \mathbb{R}^d \to \mathbb{R}^d$, $\Sigma : \mathbb{R}^d \to \mathbb{R}^{d \times d}$ (with values in the positive definite matrices) are sufficiently regular to define a unique strong solution $(X_t, t \geq 0)$.

Let us first restrict to the one-dimensional case with $\Sigma = \sigma^2$. Then

$$\mathbb{E}\Big[\frac{X_{t+\Delta} - X_t}{\Delta} \,\Big|\, X_t \Big] \xrightarrow{\Delta \to 0} b(X_t),$$

$$\mathrm{Var}\Big(\frac{X_{t+\Delta} - X_t}{\sqrt{\Delta}} \,\Big|\, X_t \Big) \xrightarrow{\Delta \to 0} \sigma^2(X_t)$$

holds with convergence in probability (for regular b, σ^2). This is the basis for constructing estimators based on continuous or high-frequency observations of one sample path of X.

Continuous observations $(X_t, t \in [0, T])$. The quadratic variation of X is given by $\langle X \rangle_t = \int_0^t \sigma^2(X_s) \, ds$ such that $\sigma^2(x)$ is identifiable (meaning estimated without error) by using $\frac{d}{dt} \langle X \rangle_t = \sigma^2(X_t)$ for all x in the visited range $\{X_t \,|\, t \in [0, T]\}$. A standard kernel estimator for the drift is

$$\hat{b}(x) = \frac{\int_0^T K_h(x - X_t) \, dX_t}{\int_0^T K_h(x - X_t) \, dt}$$

with kernel for instance $K_h(x) = \frac{1}{2h} \mathbf{1}_{[-h,h]}(x)$.

High-frequency observations $(X_{n\Delta}, 0 \leq n \leq N)$, $\Delta = \Delta_N \to 0$, $N\Delta_N \to \infty$. Approximating the stochastic and deterministic integrals yields the estimators

$$\hat{b}(x) = \frac{\sum_{n=0}^{N-1} K_h(x - X_{n\Delta}) \frac{X_{(n+1)\Delta} - X_{n\Delta}}{\Delta}}{\sum_{n=0}^{N-1} K_h(x - X_{n\Delta})},$$

$$\hat{\sigma}^2(x) = \frac{\sum_{n=0}^{N-1} K_h(x - X_{n\Delta}) \frac{(X_{(n+1)\Delta} - X_{n\Delta})^2}{\Delta}}{\sum_{n=0}^{N-1} K_h(x - X_{n\Delta})}.$$

For *low-frequency observations* $(X_{n\Delta}, n = 0, \ldots N)$ with $\Delta > 0$ fixed and $N \to \infty$ these strategies are no longer feasible. Assuming reflecting boundary conditions on $[0, 1]$ (implying Neumann boundary conditions for the Markov generator) and ellipticity (σ^2 bounded away from zero), a stationary ergodic solution X exists with invariant density

$$\mu(x) = C\sigma^{-2}(x) \exp\Big(\int_0^x 2b(y)\sigma^{-2}(y) \, dy \Big), \quad x \in [0, 1],$$

observations	b	σ^2
continuous	$T^{-s/(2s+1)}$	known
high-frequency	$(N\Delta_N)^{-s/(2s+1)}$	$N^{-s/(2s+1)}$
low-frequency (1 unknown)	$N^{-s/(2s+3)}$	$N^{-s/(2s+1)}$
low-frequency (b, σ^2 unknown)	$N^{-s/(2s+5)}$	$N^{-s/(2s+3)}$

TABLE 1. Optimal convergence rates.

where $C > 0$ is a norming constant. If σ^2 is assumed to be known, we can solve for b in this formula (taking derivatives) and use a kernel estimator for the invariant density:

$$\hat{\mu}(x) = \frac{1}{N+1} \sum_{n=0}^{N} K_h(x - X_{n\Delta}).$$

Similarly, we can estimate σ^2 in the case of known b.

In the more realistic case with both, b and σ^2 unknown, we rely instead on the Markov transition semigroup $(P_t^{b,\sigma^2})_{t \geq 0}$ with self-adjoint generator on $L^2(\mu)$

$$L^{b,\sigma^2} f(x) = \tfrac{1}{2}\sigma^2(x)f''(x) + b(x)f'(x) = \frac{1}{\mu(x)}(Sf')'(x),$$

where μ is the invariant density and $S = \tfrac{1}{2}\sigma^2\mu$. The spectral approach consists in estimating the first non-trivial eigenfunction-eigenvalue pair (u_1, κ_1) of the transition operator P_Δ^{b,σ^2} (matrix discretisation via approximation spaces) and to use $L^{b,\sigma^2} u_1 = \nu_1 u_1$ with $\nu_1 = \Delta^{-1} \log \kappa_1$ by functional calculus in $L^2(\mu)$. We obtain the identification formulas

$$\sigma^2(x) = \frac{2\nu_1 \int_0^x u_1 \mu}{u_1'(x)\mu(x)}, \quad b(x) = \frac{\nu_1 (u_1'(x) \int_0^x u_1 \mu)'}{u_1'(x)^2 \mu(x)}.$$

Remark that for σ^2 the first derivative of the eigenfunction u_1 appears and for b even the second derivative. A detailed analysis yields the convergence rates for $\mathbb{E}[\|\hat{b} - b\|_{L^2}]$, $\mathbb{E}[\|\hat{\sigma}^2 - \sigma^2\|_{L^2}]$ in Table 1, assuming each time that b and σ^2 are s-regular (in a Sobolev-sense; for low-frequency even linking both regularities appropriately) and $\Delta_N = o(N^{-1/2})$ in the high-frequency case. These rates are provably optimal in an asymptotic minimax sense, see Gobet, Hoffmann and Reiß [1] and the references therein. We see that different observation schemes induce different degrees of ill-posedness and thus structurally different inverse problems.

For concrete data it is a priori difficult to choose among the low- and high-frequency estimators. One unifying estimation strategy, regardless of the asymptotic scheme, is therefore desirable. A first such estimator for σ^2 has been constructed by Chorowski [2]. See also the references therein for further recent developments, *e.g.* random observations times and a nonparametric Bayes approach.

Finally, let us point out the d-dimensional case $d > 1$. For continuous and high-frequency observations the estimators and their theory readily transfer, but

the spectral approach is more involved. Assuming again stationarity on a bounded domain $D \subset \mathbb{R}^d$ with reflecting boundary and a *divergence form* (with respect to the invariant density μ) of the generator

$$L^{b,\Sigma} f(x) = \frac{\operatorname{div}(S(x)\nabla f(x))}{\mu(x)} \text{ with some positive definite } S(x) \in \mathbb{R}^{d\times d}, \quad x \in D,$$

the Markov semigroup is again self-adjoint in $L^2(\mu)$ with $\Sigma(x) = 2S(x)/\mu(x)$ and $b(x) = (\sum_i \partial_i S_{ij}(x))_j/\mu(x)$. Then eigenfunction-eigenvalue pairs (u_k, ν_k) of $L^{b,\Sigma}$ satisfy the Poisson equation

$$\operatorname{div}(S(x)\nabla u_k(x)) = \nu_k \mu(x) u_k(x), \ x \in D, \text{ with Neumann boundary conditions.}$$

We face the inverse problem of estimating the matrix-valued function S from these equations for $k = 1, \dots, K$ (K to be determined) and empirical (noisy) versions of (ν_k, u_k) and μ. A convergence analysis of this approach poses a fascinating open problem.

References

[1] E. Gobet, M. Hoffmann, M. Reiß, Nonparametric estimation of scalar diffusions based on low-frequency data, *Annals of Statistics* **32** (2004), 2223–53.
[2] J. Chorowski, Nonparametric volatility estimation in scalar diffusions: Optimality across observation frequencies, *Bernoulli* (2017), to appear.

Nonparametric estimation in stochastic differential equations by penalized maximum likelihood

FABIAN DUNKER

(joint work with Thorsten Hohage)

We develop nonparametric estimators for coefficients in time homogeneous stochastic differential equation

$$d\mathbf{X}_t = \boldsymbol{\mu}(\mathbf{X}_t)dt + \sigma(\mathbf{X}_t)d\mathbf{W}_t.$$

The data are assumed to be either independent, identically distributed (i.i.d.) realizations of X_t at some point in time $t = t_1$ or i.i.d. observations of the invariant measure of X_t for $t \to \infty$. Hence, neither continuous nor high frequency observations of X_t are assumed. This means that our estimators are suitable for low frequency observations.

The problem is formulated as a nonlinear ill-posed operator equation with a deterministic forward operator described by the Fokker-Planck equation. Regularization is needed for a stable inversion of the operator equation. We propose an iteratively regularized Newton method with maximum likelihood data misfit and general convex regularization term to get stable reconstructions.

We derive convergence rates in terms of the Bregman distance with respect to the regularization functional. The central assumptions of the convergence rate

theorem are a smoothness condition on the true solution and a nonlinearity condition on the operator. These assumptions are verified for estimation of the drift coefficient μ with Sobolev-type regularization terms.

The advantages of maximum likelihood data misfit are demonstrated in Monte-Carlo simulations. We used the iteratively regularized Gauss-Newton method with quadratic data fidelity and quadratic regularization terms as the benchmark method.

REFERENCES

[1] A. De Cezaro, O. Scherzer, and J. P. Zubelli, *Convex regularization of local volatility models from option prices: convergence analysis and rates*, Nonlinear Anal. **75**(4) (2012), 2398–2415.
[2] F. Dunker, and T. Hohage, *On parameter identification in stochastic differential equations by penalized maximum likelihood*, Inverse Problems **30** (2014), 095001.
[3] E. Gobet, M. Hoffmann, and M. Reiß, *Nonparametric estimation of scalar diffusions based on low frequency data*, Ann. Statist. **32**(5) (2004), 2223–2253.
[4] T. Hohage, and F. Werner, *Iteratively regularized Newton-type methods for general data misfit functionals and applications to Poisson data*, Numer. Math. **123**(4) (2013), 745–779.
[5] A. Hurn, J. Jeisman, and K. Lindsay, *Teaching an old dog new tricks: Improved estimation of the parameters of stochastic differential equations by numerical solution of the Fokker-Planck equation.*, NCER Working Paper Series, 9 (2007).
[6] O. Papaspiliopoulos, Y. Pokern, G. O. Roberts, and A. M. Stuart, *Nonparametric estimation of diffusions: a differential equations approach*, Biometrica **99**(3) (2012), 511–531.

Electrical impedance tomography imaging via the Radon transform

SAMULI SILTANEN

(joint work with Allan Greenleaf, Andreas Hauptmann, Matti Lassas, Matteo Santacesaria, Gunther Uhlmann)

Electrical impedance tomography (EIT) images the internal electric conductivity distribution from current-to-voltage boundary measurements.

In [5], a method was introduced for recovering jumps in conductivity values using EIT. The method is based on *complex geometrical optics* (CGO) solutions introduced by Sylvester and Uhlmann [7], and it is capable of detecting inclusions within inclusions in an unknown inhomogeneous background conductivity.

The inverse conductivity problem of Calderón [4] is the mathematical model of EIT. Take a bounded, simply connected domain $\Omega \subset \mathbb{R}^2$ with smooth boundary. Let the scalar conductivity $\sigma \in L^\infty(\Omega)$ satisfy $\sigma(x) \geq c > 0$. Applying a voltage distribution f at the boundary leads to

$$(1) \qquad \nabla \cdot \sigma \nabla u = 0 \quad \text{in } \Omega, \qquad u|_{\partial\Omega} = f.$$

EIT measurements are modeled by the Dirichlet-to-Neumann map

$$(2) \qquad \Lambda_\sigma : f \mapsto \sigma \frac{\partial u}{\partial \vec{n}}\Big|_{\partial\Omega},$$

where $\vec{n}$ is the outward normal vector of $\partial\Omega$.

(a)

(b)

(c)

$T_0^{a,+}\mu(t,1)$ $T_2^{a,+}\mu(t,1)$

(d)
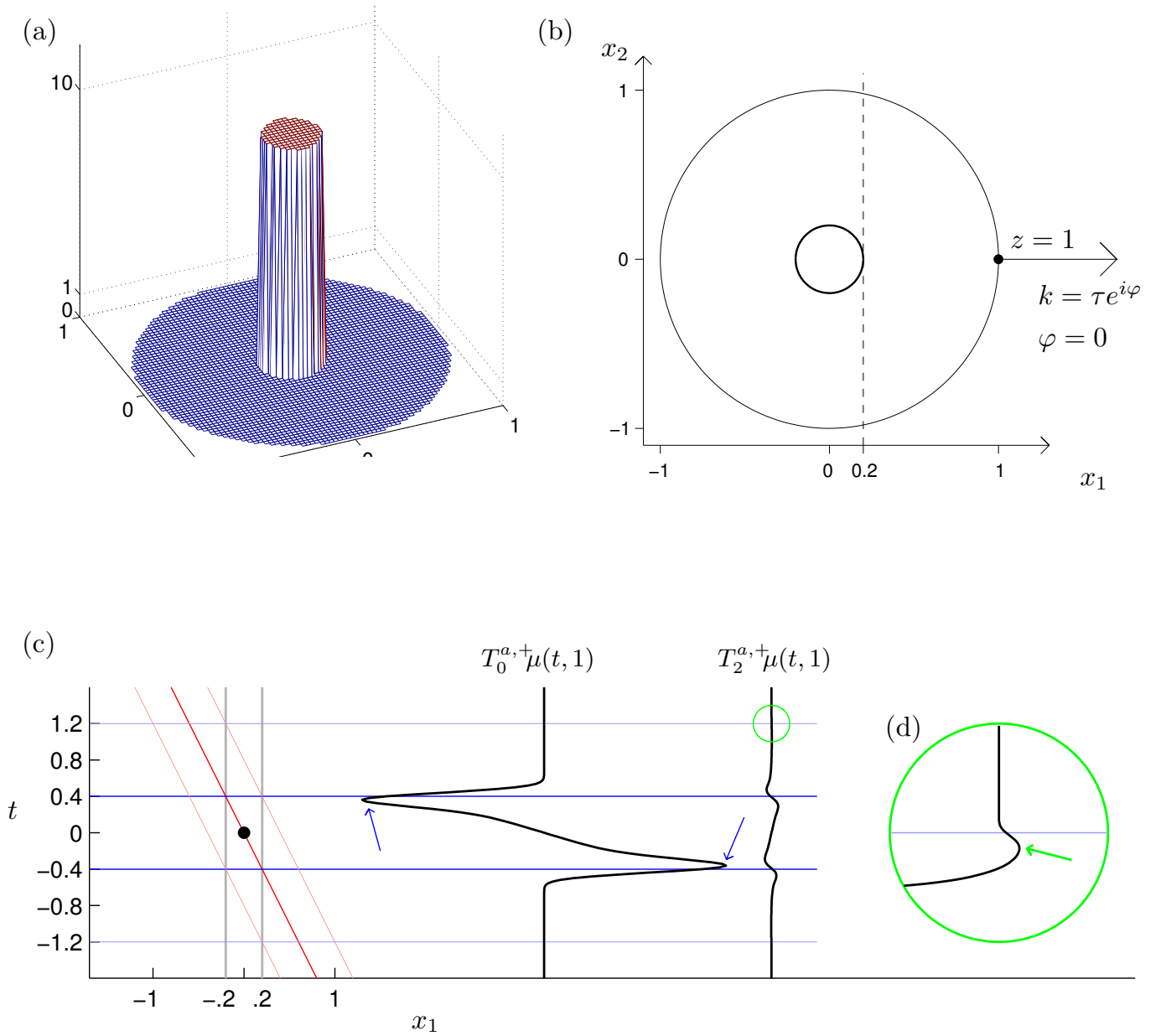
FIGURE 1.   (a) Three-dimensional plot of the conductivity having a jump along the circle with radius $\rho = 0.2$ and center at the origin. (b) Unit disc and singular support of the conductivity in the (x_1, x_2) plane. (c) The term $T_0^{a,+}\mu(t,1)$ has peaks, indicated by blue arrows, at $t = \pm 2\rho$ corresponding to the locations of the main singularities in μ. The higher-order term $T_2^{a,+}\mu(t,1)$, smaller than $T_0^{a,+}\mu(t,1)$ in amplitude, exhibits singularities caused by reflections at both $t = \pm 2\rho$ and $t = \pm 4\rho$. (d) The singularities of the term $T_2^{a,+}\mu(t,1)$ at $t = \pm 4\rho$ are very small. Shown is the zoom-in near $t = 4\rho$, with amplitude increased by a factor of 70.

In [2], the construction of the CGO solutions was done via a Beltrami equation. Identify $\mathbb{R}^2$ with $\mathbb{C}$ by setting $z = x_1 + ix_2$ and define a Beltrami coefficient by

$$\mu(z) = (1 - \sigma(z))/(1 + \sigma(z)).$$

We have $|\mu(z)| \leq 1 - \epsilon$ for some $\epsilon > 0$. Further, if we assume $\sigma \equiv 1$ outside some $\Omega_0 \subset\subset \Omega$, then $\text{supp}(\mu) \subset \overline{\Omega_0}$. Now consider the unique solution of

$$(3) \qquad \bar{\partial}_z f_\pm(z, k) = \pm\mu(z)\overline{\partial_z f_\pm(z, k)}; \qquad e^{-ikz} f_\pm(z, k) = 1 + \omega^\pm(z, k),$$

where $ikz = ik(x_1 + ix_2)$ and $\omega^\pm(z, k) = \mathcal{O}(1/|z|)$ as $|z| \to \infty$. Here z is a spatial variable and $k \in \mathbb{C}$ a spectral parameter. Also, $u = \text{Re} f_+$ satisfies (1).

The new idea is to apply a partial Fourier transform in the radial direction of k. Write $k = \tau e^{i\varphi}$ and define

$$(4) \qquad \widehat{\omega}^\pm(z, t, e^{i\varphi}) = \mathcal{F}_{\tau \to t}\big(\omega^\pm(z, \tau e^{i\varphi})\big).$$

Recall that the traces of CGO solutions can be recovered perfectly from Λ_σ [2, 1] and approximately from practical EIT data [3].

Formally one can view the Beltrami equation (3) as a scattering equation, where μ is considered as a compactly supported scatterer and the "incident field" is the constant function 1. Consider a "scattering series" for the unaveraged $\omega^\pm$,

$$(5) \qquad \omega^\pm = \sum_{j=0}^{\infty} \omega_j^\pm$$

and set $\widehat{\omega}_j^\pm = \mathcal{F}_{\tau \to t}\omega_j^\pm$ as in (4). The derivation of (5) makes use of [6].

Figure 1 suggests that jumps in conductivity produce certain useful singularities in the terms of the scattering series.

Actually, what we can recover from EIT data resembles parallel-beam X-ray projection data of the singularities of σ. Indeed, in [5] reconstruction formulae are derived for σ analogous to the classical filtered back-projection method of X-ray tomography.

Define averaged operators $T_j^{a,\pm}$ for $j = 1, 2, 3, \ldots$ and $T^{a,\pm}$ by the complex contour integral,

$$(6) \qquad T_j^{a,\pm}\mu(t, e^{i\varphi}) = \frac{1}{2\pi i}\int_{\partial\Omega} \widehat{\omega}_j^\pm(z, t, e^{i\varphi})dz,$$

$$(7) \qquad T^{a,\pm}\mu(t, e^{i\varphi}) = \frac{1}{2\pi i}\int_{\partial\Omega} \widehat{\omega}^\pm(z, t, e^{i\varphi})dz,$$

Now $T^{a,\pm}$ are recoverable from EIT data, and one can (to some extent) understand its singularities, and derive approximate reconstruction formulas, by analyzing the operators $T_j^{a,\pm}$. See [5] for more details.

References

[1] K. Astala and L. Päivärinta, *A boundary integral equation for Calderón's inverse conductivity problem*, in Proc. 7th Intern. Conf. on Harmonic Analysis, Collectanea Mathematica, 2006.

[2] K. Astala and L. Päivärinta, *Calderón's inverse conductivity problem in the plane*, Annals of Math., **163** (2006), 265–299.

[3] K. Astala, J. Mueller, L. Päivärinta, A. Perämäki, and S. Siltanen, *Direct electrical impedance tomography for nonsmooth conductivities*, Inverse Probl. Imag., **5** (2011), 531–549.

[4] A.-P. Calderón, *On an inverse boundary value problem*, in Seminar on Numerical Analysis and its Applications to Continuum Physics (Rio de Janeiro, 1980), Soc. Brasil. Mat., Rio de Janeiro, 1980, 65–73.

[5] Greenleaf A, Lassas M, Santacesaria M, Siltanen S, Uhlmann G. Propagation and recovery of singularities in the inverse conductivity problem. arXiv preprint arXiv:1610.01721. 2016 Oct 6.

[6] M. Huhtanen and A. Perämäki, *Numerical solution of the R-linear Beltrami equation*, Math. of Comp., **81** (2012), 387–397.

[7] J. Sylvester and G. Uhlmann, A global uniqueness theorem for an inverse boundary value problem, Ann. of Math. **125** (1987), 153–169.

Exterior Shape Calculus

Ralf Hiptmair

(joint work with Jing-Zhi Li)

1. Basic Concepts

Shape differentiation according to Zolesio's velocity method proceeds as follows [10, Sect 2.9], [2, Ch. 4]: Let $(\mathsf{T}_s(\mathbf{v}))_{s \in \mathbb{R}}$ be the flow, that is the 1-parameter group of diffeomorphisms $\mathsf{T}_s : D \to D$ of a bounded "hold all" domain $D \subset \mathbb{R}^d$, $d \in \mathbb{N}$, generated by the C^2-smooth and compactly supported velocity field $\mathbf{v} \in C_0^2(D, \mathbb{R}^d)$. Given some C^2-domain Ω strictly contained in D we introduce the set of admissible domains

$$\mathcal{A} := \{\mathsf{T}_s(\mathbf{v})(\Omega) : s \in \mathbb{R}, \mathbf{v} \in C_0^1(D, \mathbb{R}^d)\} .$$

Writing $X(\Lambda^\ell, B)$ for a space of ℓ-forms, $0 \le \ell \le d$ on $B \subset D$, which is invariant under pullbacks $\mathsf{T}_s(\mathbf{v})^*$ for any $\mathbf{v} \in C_0^2(D, \mathbb{R}^d)$, we consider a shape-dependent ℓ-form $\boldsymbol{\omega}(\Omega) \in X(\Lambda^\ell, B)$, $B = D$ or $B = \Omega$, and define its *material derivative* in the direction $\mathbf{v}$ at Ω as (if the limit exists) [10, Sect. 2.25]

$$\left\langle \frac{D\boldsymbol{\omega}}{D\Omega}(\Omega), \mathbf{v} \right\rangle := \lim_{s \to 0} \frac{\mathsf{T}_s(\mathbf{v})^* \boldsymbol{\omega}(\mathsf{T}_s(\Omega)) - \boldsymbol{\omega}(\Omega)}{s} \in X(\Lambda^\ell, B) .$$

Whereas the material derivative belongs to the Lagrangian realm, the *shape derivative* of $\boldsymbol{\omega}$ at Ω in the direction $\mathbf{v}$ is an Eulerian concept, pointwise defined in the sense of distributions by [10, Sect. 2.30]

$$\left\langle \frac{d\boldsymbol{\omega}}{d\Omega}, \mathbf{v} \right\rangle := \lim_{s \to 0} \frac{\boldsymbol{\omega}(\mathsf{T}_s(\mathbf{v})(\Omega)) - \boldsymbol{\omega}(\Omega)}{s} \quad \text{in} \quad \mathcal{D}'(B, \Lambda^\ell), \quad B = \Omega, D .$$

Both derivatives are connected by the *Lie derivative* through the fundamental formula [8, Sect. 1.1]

$$\boxed{\left\langle \frac{d\boldsymbol{\omega}}{d\Omega}, \mathbf{v} \right\rangle = \left\langle \frac{D\boldsymbol{\omega}}{D\Omega}(\Omega), \mathbf{v} \right\rangle - \boldsymbol{\mathcal{L}}_\mathbf{v} \, \boldsymbol{\omega}(\Omega)} .$$

This tells us (i) how to compute the shape derivative, and (ii) that the shape derivative may not belong to $X(\Lambda^\ell, \Omega)$, because taking the Lie derivavtive involves (exterior) differentiation. For instance, if $\boldsymbol{\omega}$ maps into the Sobolev space $H^1\Lambda^\ell(D)$, then its shape derivative at Ω may be in $L^2\Lambda^\ell(D)$ only: taking the shape derivative may incur a loss of smoothness.

2. Shape Gradients of Integrals

Let $\boldsymbol{\omega}$ be a shape-dependent ℓ-form and $\Sigma \subset \Omega$ an oriented, C^1-smooth ℓ-dimensional manifold. Then, following [7], we find using Cartan's formula $\mathcal{L}_{\mathbf{v}}\,\omega = \mathsf{d} \circ \imath_{\mathbf{v}} + \imath_{\mathbf{v}} \circ \mathsf{d}$, $\imath_{\mathbf{v}}$ the contraction of a form with the vectorfield $\mathbf{v}$, [3, Sect. 4.2]

$$
\left. \frac{d}{ds} \int_{\mathsf{T}_s(\mathbf{v})(\Sigma)} \boldsymbol{\omega}(\mathsf{T}_s(\mathbf{v})(\Omega)) \right|_{s=0} = \int_\Sigma \left\langle \frac{D\boldsymbol{\omega}}{D\Omega}(\Omega), \mathbf{v} \right\rangle = \int_\Sigma \left\langle \frac{d\boldsymbol{\omega}}{d\Omega}(\Omega), \mathbf{v} \right\rangle + \mathcal{L}_{\mathbf{v}}\,\boldsymbol{\omega}(\Omega)
$$

$$
= \int_\Sigma \left\langle \frac{d\boldsymbol{\omega}}{d\Omega}(\Omega), \mathbf{v} \right\rangle + \int_{\partial\Sigma} \imath_{\mathbf{v}}\,\boldsymbol{\omega}(\Omega) + \int_\Sigma \imath_{\mathbf{v}}\,\mathsf{d}\,\boldsymbol{\omega}(\Omega) \ .
$$

To render the shape derivative meaningful, traces on $\partial\Sigma$ must exist, which alludes to tighter regularity requirements on ω.

3. Shape Derivative of Solutions of Boundary Value Problems

A Neumann boundary value problem for an ℓ-form ω reads in variational form: for given $\gamma \in H\Lambda^{d-\ell-1}(D)$ seek $\omega \in H\Lambda^\ell(\Omega)$ such that [8, Sect. 3.3.1]

$$
(1) \qquad \int_\Omega *\,\mathsf{d}\,\omega \wedge \mathsf{d}\,\eta + *\,\omega \wedge \eta = \int_{\partial\Omega} \mathbf{t}(\gamma \wedge \eta) \quad \forall \eta \in H\Lambda^\ell(\Omega) \ ,
$$

where $*$ is a Hodge operator and $H\Lambda^\ell(B)$ is a Sobolev space of ℓ-forms on B. Note that the Neumann data γ have to be defined everywhere in D and that the test space does not depend on Ω. This paves the way for *implicit shape differentiation* of (1), relying on the formulas from Section 2: Abbreviating $\delta\omega := \left\langle \frac{d\boldsymbol{\omega}}{d\Omega}(\Omega), \mathbf{v} \right\rangle$ for given deformation velocity field $\mathbf{v} \in C_0^2(D, \mathbb{R}^d)$ we end up with a variational characterization of the shape derivative [8, Sect .4.3]:

$$
(2) \quad \int_\Omega *\,\mathsf{d}\,\delta\omega \wedge \mathsf{d}\,\eta + *\,\delta\omega \wedge \eta
$$

$$
= \int_{\partial\Omega} -\mathbf{t}\,\imath_{\mathbf{v}}(*\,\mathsf{d}\,\omega \wedge \mathsf{d}\,\eta + *\,\omega \wedge \eta) + \mathbf{t}\,\imath_{\mathbf{v}}\,\mathsf{d}(\gamma \wedge \eta)
$$

$$
= \int_{\partial\Omega} \underbrace{\left\{ (-1)^{d-\ell}\,\mathsf{d}\,\mathbf{t}(\imath_{\mathbf{v}} *\,\mathsf{d}\,\omega) + \mathbf{t}(\imath_{\mathbf{v}} *\,\omega + \imath_{\mathbf{v}}\,\mathsf{d}\,\gamma) + (-1)^{d-\ell-1}\,\mathsf{d}\,\mathbf{t}(\imath_{\mathbf{v}}\,\gamma) \right\}}_{=:\nu(\omega) \in \Lambda^{d-\ell-1}, \text{``Neumann data'' for } \delta\omega} \wedge \mathbf{t}\,\eta
$$

for all $\eta \in H\Lambda^\ell(D)$. The final identity relies on product rules for d and $\imath_{\mathbf{v}}$ plus the strong form of the equation $(-1)^{d-\ell}\,\mathsf{d} * \mathsf{d}\,\omega + *\,\omega = 0$ and of the boundary conditions $\mathbf{t}(*\,\mathsf{d}\,\omega) = \mathbf{t}\,\gamma$ on $\partial\Omega$. This is possible, because we have to assume *extra regularity* of ω and γ anyway, in order to render the trace expressions meaningful.

This is the case, for instance, for $\omega \in H^1\Lambda^\ell(\Omega)$, $\gamma \in H^1\Lambda^\ell(D)$. Since we have restricted ourselves to C^2-domains, the required smoothness of ω is guaranteed by elliptic regularity theory. From the above formulas we conclude that the shape derivative of ω solution of (1) at Ω in direction $\mathbf{v}$ solves a veriational problem of the same structure with Neumann data given by $\nu(\omega) \in L^2\Lambda^{d-\ell-1}(\partial\Omega)$ from (2).

Remark 1. The approach to shape derivatives of solutions of Dirichlet problems cannot rely on the standard variational formulation whose trial space will depend on Ω. Instead one may use a mixed variational formulation [7] or Lagrange multipliers to enforce the boundary conditions weakly.

Remark 2. For transmission problems the loss of smoothness under shape differentiation manifests itself in the failure of the shape derivative to satisfy the usual transmission conditions. This rules out the use of standard variational formulations. Instead the transmission conditions have to be imposed weakly through Lagrange multipliers, see [8, Sect. 3.3.3].

4. Translation to Vector Proxies

Classical vector analysis offers an isomorphic model for exterior calculus in Euclidean space, with d and $\imath_{\mathbf{v}}$ incarnated by familiar operations on functions and vector fields, see [8, Sect. 5.2]. This permits us, for a concrete degree ℓ of the form ω, to translate the general formulas derived by means of exterior calculus to expressions for functions and vector fields. For instance for the Neumann problem for $\ell = 1$, which is related to the so-called eddy current equations for an unknown vector field $\mathbf{u}$, we arrive at the boundary condition on $\partial\Omega$ [8, Sect. 5.2]

$$\mathbf{curl}\,\delta\mathbf{u} \times \boldsymbol{n} = \mathbf{curl}_\Gamma((\mathbf{v}\cdot\boldsymbol{n})(\mathrm{curl}_\Gamma\,\mathbf{u_t} + \mathbf{g}\cdot\boldsymbol{n})) - (\mathbf{v}\cdot\boldsymbol{n})(\mathbf{u} + \mathbf{curl}\,\mathbf{g})_{\boldsymbol{t}}\,,$$

where $\boldsymbol{n}$ is the exterior unit normal to $\partial\Omega$, and $\mathbf{g} : \Omega \to \mathbb{R}^3$ e vector representative of the data 1-form γ.

Thus, using the fundamental operations of exterior calculus, it takes only a few general formulas to find boundary value problems satisfied by shape derivatives of solutions of many second order boundary value problems. In one fell swoop we recover the results of a host of articles, see [5, 4, 9, 1, 6].

References

[1] M. Costabel and F. Le Louër, *Shape derivatives of boundary integral operators in electromagnetic scattering. Part II: Application to scattering by a homogeneous dielectric obstacle*, Integral Equations and Operator Theory, 73 (2012), pp. 17–48.

[2] M. Delfour and J.-P. Zolésio, *Shapes and Geometries*, vol. 22 of Advances in Design and Control, SIAM, Philadelphia, 2nd ed., 2010.

[3] T. Frankel, *The Geometry of Physics*, Cambridge University Press, Cambridge, second ed., 2004.

[4] H. Haddar and R. Kress, *On the Fréchet derivative for obstacle scattering with an impedance boundary condition*, SIAM Journal on Applied Mathematics, 65 (2004), pp. 194–208.

[5] F. Hettlich, *Fréchet derivatives in inverse obstacle scattering*, Inverse Problems, 11 (1995), pp. 371–382.

[6] ———, *The domain derivative of time-harmonic electromagnetic waves at interfaces*, Math. Methods Appl. Sci., 35 (2012), pp. 1681–1689.

[7] R. Hiptmair and J. Li, *Shape derivatives in differential forms I: An intrinsic perspective*, Ann. Mat. Pura Appl. (4), 192 (2013), pp. 1077–1098.

[8] R. Hiptmair and J.-Z. Li, *Shape derivatives in differential forms II: Application to scattering problems*, Report 2017-24, SAM, ETH Zürich, 2017.

[9] R. Potthast, *Domain derivatives in electromagnetic scattering*, Math. Methods Appl. Sci., 19 (1996), pp. 1157–1175.

[10] J. Sokolowski and J.-P. Zolesio, *Introduction to shape optimization*, vol. 16 of Springer Series in Computational Mathematics, Springer, Berlin, 1992.

Imaging small scatterers with electromagnetic waves

Fernando Guevara Vasquez

(joint work with Maxence Cassier)

We consider the problem of imaging small scatterers in a homogeneous medium by probing the medium with electric dipoles located at an array and recording the resulting scattered electric field at the same array. For well separated scatterers, the scattered field can be well described in terms of a polarization tensor per scatterer [1], i.e. a 3×3 complex symmetric matrix. For N scatterers located at points $\vec{y}_1, \ldots, \vec{y}_N$ with polarization tensors $\boldsymbol{\alpha}_1, \ldots, \boldsymbol{\alpha}_N$, the array data (ignoring multiple scattering) is the matrix valued field

$$(1) \qquad \boldsymbol{\Pi}(\boldsymbol{x}_r, \boldsymbol{x}_s, k) = \sum_{j=1}^{N} \mathbb{G}(\vec{\boldsymbol{x}}_r, \vec{\boldsymbol{y}}_j, k) \boldsymbol{\alpha}_N \mathbb{G}(\vec{\boldsymbol{y}}_j, \vec{\boldsymbol{x}}_s, k),$$

for all receiver $\vec{\boldsymbol{x}}_r = (\boldsymbol{x}_r, 0)$ and source $\vec{\boldsymbol{x}}_s = (\boldsymbol{x}_s, 0)$ positions in an array $\mathcal{A} \times 0$, located in the $x_3 = 0$ plane. Here we write vectors with three components in bold with arrows, and vectors with two components in bold only, so that $\vec{\boldsymbol{x}} = (\boldsymbol{x}, x_3)$. Also $\mathbb{G}(\vec{\boldsymbol{x}}, \vec{\boldsymbol{y}}, k) \in \mathbb{C}^{3\times3}$ is the dyadic Green function for the Maxwell equation at wavenumber $k = 2\pi/\lambda = \omega/c$. As usual λ is the wavelength, ω is the angular frequency and c is the wave speed (see e.g. [4]).

We presented a resolution study of the Kirchhoff imaging function adapted to electromagnetics:

$$(2) \qquad \mathcal{I}(\vec{\boldsymbol{y}}, k) = \int_{\mathcal{A}} d\boldsymbol{x}_r \int_{\mathcal{A}} d\boldsymbol{x}_s \overline{\mathbb{G}(\vec{\boldsymbol{x}}_r, \vec{\boldsymbol{y}}, k)} \boldsymbol{\Pi}(\boldsymbol{x}_r, \boldsymbol{x}_s, k) \overline{\mathbb{G}(\vec{\boldsymbol{y}}, \vec{\boldsymbol{x}}_s, k)},$$

which is a matrix valued field instead of a scalar one in acoustics. For an array of aperture a used to image an object at a distance L, the acoustics Kirchhoff imaging function is known to have a resolution of $\lambda L/a$ in the cross-range plane (the plane parallel to the array) and of c/B in the range direction (the direction perpendicular to the array). Here B is the bandwidth of the measurements and the image for multi-frequency data is obtained by integrating the single frequency image over the bandwidth. We show in [3] that the imaging function (2) obeys the same resolution estimates as the Kirchhoff imaging function in acoustics, if we consider the scalar field consisting of the norm of the matrix field (2) at each

imaging point. Moreover we give a simple post-processing step that can extract from (2) a matrix field that approximates the polarization tensor of a scatterer if it were located at the imaging point. The analysis in [3] is done in the Fraunhofer asymptotic regime, which assumes that the propagation distance is large compared to the array, and that the object we want to image is small compared to the array (among other assumptions). The key quantity we study is the matrix valued field

$$(3) \qquad \mathbb{H}(\vec{\boldsymbol{y}}, \vec{\boldsymbol{y}}', k) = \int_{\mathcal{A}} d\boldsymbol{x}_r \overline{\mathbb{G}(\vec{\boldsymbol{x}}_r, \vec{\boldsymbol{y}}, k)} \mathbb{G}(\vec{\boldsymbol{x}}_r, \vec{\boldsymbol{y}}', k),$$

which plays the role of a *point spread function*, i.e. the image of a point. This concept is easier to explain if we switch to the passive imaging case where the array consists of only receivers and the goal is to image a collection of small sources. In this case $\mathbb{H}(\vec{\boldsymbol{y}}, \vec{\boldsymbol{y}}', k)\vec{\boldsymbol{p}}$ is the Kirchhoff image at a point $\vec{\boldsymbol{y}}$ of a single point source located at $\vec{\boldsymbol{y}}'$ and with polarization vector $\vec{\boldsymbol{p}}$. We show that in the Fraunhofer asymptotic regime and if $\vec{\boldsymbol{y}}$ and $\vec{\boldsymbol{y}}'$ are in the same $x_3 = L$ plane, the point spread function decays as $1/\|\boldsymbol{y} - \boldsymbol{y}'\|$ at a rate consistent with the resolution estimate $\lambda L/a$. Similarly if we integrate over a frequency band $\omega_0 + [-B/2, B/2]$, we obtain a sinc like behavior in the range direction that gives the c/B range resolution estimate. Another conclusion of the asymptotic study is that $\mathbb{H}(\vec{\boldsymbol{y}}, \vec{\boldsymbol{y}}, k)$ is singular but that its 2×2 block corresponding to the cross-range coordinates is well-conditioned. Thus the problem of finding the polarization vector $\vec{\boldsymbol{p}}$ of a point source from the Kirchhoff image is ill-conditioned. However the linear system obtained by keeping only the cross-range components of $\mathbb{H}$ and the image is well-conditioned. Similarly for the active case, the problem of finding the cross-range components $\boldsymbol{\alpha}_{1:2,1:2}$ of a polarization tensor $\boldsymbol{\alpha}$ is stable. We note that only the cross-range components of the electric field are needed to image these quantities.

Examples of matrix valued images are given in figures 1 and 2, where we imaged two point scatterers located at $\vec{\boldsymbol{y}}_1 = (6\lambda_0, 6\lambda_0, 100\lambda_0)$, $\vec{\boldsymbol{y}}_2 = (6\lambda_0, -6\lambda_0, 106\lambda_0)$ and with polarization tensors

$$\boldsymbol{\alpha}_1 = \begin{bmatrix} 2+2\imath & 1-\imath/2 & 0 \\ 1-\imath/2 & 1+2\imath & 1+\imath/2 \\ 0 & 1+\imath/2 & 1+\imath \end{bmatrix} \text{ and } \boldsymbol{\alpha}_2 = \begin{bmatrix} 2+\imath & \imath/2 & 1/2 \\ \imath/2 & 1+\imath & 0 \\ 1/2 & 0 & 1+\imath \end{bmatrix}.$$

In both figures 1 and 2, we visualize 2×2 symmetric matrices by ellipses with principal axis and dimensions given by the matrices' eigenvectors and eigenvalues.

We are currently adapting a technique for Kirchhoff imaging without phases [2] to the Maxwell equations (joint with Patrick Bardsley and Maxence Cassier). The experimental setup consists of a single electric dipole point source located at $\vec{\boldsymbol{x}}_s$ and a passive array that are used to image the position and polarization tensors of a collection of small scatterers. The electric field generated by the source is

$$\vec{\boldsymbol{E}}_{\text{inc}}(\vec{\boldsymbol{x}}, k) = \mathbb{G}(\vec{\boldsymbol{x}}, \vec{\boldsymbol{x}}_s, k)\vec{\boldsymbol{j}}_s$$

where the polarization vector $\vec{\boldsymbol{j}}_s(k)$ is a zero mean, stationary, ergodic Gaussian process with known correlation matrix $J(k) = \langle \vec{\boldsymbol{j}}_s(k)\vec{\boldsymbol{j}}_s(k)^* \rangle$. We assume the array can only measure polarization data in the cross-range plane. That is only the 2×2
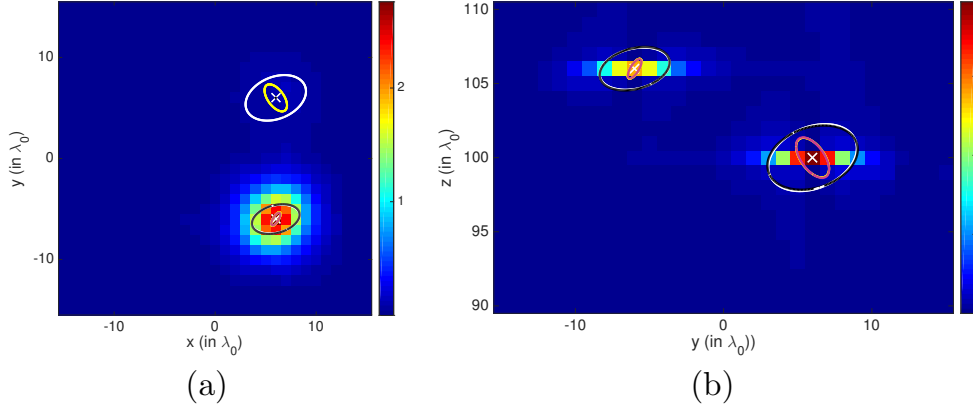
FIGURE 1. (a) Cross-range ($z = 106\lambda_0$) and (b) range ($x = 6\lambda_0$) images of scatterers. The color indicates the norm of the recovered polarization tensor. The white/black ellipses represent the true/calculated real part of the polarization tensor. The yellow/pink ellipses represent the true/calculated imaginary part.
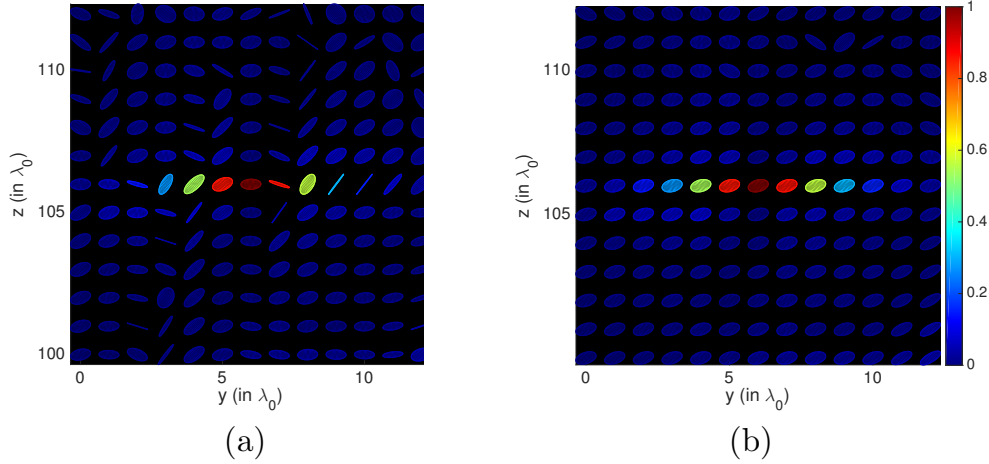

FIGURE 2. Images of the polarization tensor in range ($x = 6\lambda_0$). The analysis in [3] shows that a straightforward solution of the system for the polarization tensor $\boldsymbol{\alpha}$ is afflicted by oscillatory artifacts (a). These can be removed by fixing the phase of the recovered polarization tensor by enforcing e.g. that $\alpha_{1,1}$ be real (b). The ellipses' color represents the polarization tensor norm.

Hermitian auto-correlation matrices $C(\boldsymbol{x}_r, k) = \langle \boldsymbol{E}(\vec{\boldsymbol{x}}_r, k)\boldsymbol{E}(\vec{\boldsymbol{x}}_r, k)^* \rangle$ are known. Here $\boldsymbol{E}(\vec{\boldsymbol{x}}_r, k)$ is the cross-range total field evaluated at the array location $\vec{\boldsymbol{x}}_r$. Hence the data we work with is equivalent to measuring the Stokes parameters of the electric field at the array [4]. We have preliminary results showing that the resolution estimates apply to this setting, but the information that can be recovered stably about the polarization tensors $\boldsymbol{\alpha}$ corresponds to a 2×2 projection

of $\boldsymbol{\alpha}$ in left and right bases determined by the positions of the receiver array, the source and the scatterer.

REFERENCES

[1] H. Ammari, M. S. Vogelius, and D. Volkov, *Asymptotic formulas for perturbations in the electromagnetic fields due to the presence of inhomogeneities of small diameter II. The full Maxwell equations.*, Journal de mathématiques pures et appliquées, 80 (2001), pp. 769–814, doi:10.1016/S0021-7824(01)01217-X.
[2] P. Bardsley and F. Guevara Vasquez, *Kirchhoff migration without phases*, Inverse Problems, 32 (2016), p. 105006, doi:10.1088/0266-5611/32/10/105006
[3] M. Cassier and F. Guevara Vasquez, *Imaging Polarizable dipoles*, ArXiv:1703.03544.
[4] L. Novotny and B. Hecht, *Principles of nano-optics*, Cambridge University Press, 2012.

The monotonicity method for inverse scattering

BASTIAN HARRACH

(joint work with Mikko Salo, Valter Pohjola)

We consider the problem of determining the support of an unknown scatterer in a bounded domain from knowledge of the associated Neumann-Dirichlet-operator for the Helmholtz equation. We show that the support can be uniquely reconstructed from operator comparisons in the sense of operator definiteness up to finitely many eigenvalues. This extends previous works on coercive equations such as EIT [4] to coercive-plus-compact equations, and yields a constructive characterization of scatterers, that is numerically stable in the sense that is allows convergent implementations for noisy data. The results that we present herein have to be considered work-in-progress, and we only sketch the main ideas for a sample case.

The setting. Let

$$\text{(1)} \qquad \Lambda_0 : \ L^2(\partial\Omega) \to L^2(\partial\Omega), \quad g \mapsto u_0^{(g)}|_{\partial\Omega}$$

be the Neumann-Dirichlet-operator for the homogeneous Helmholtz equation in a bounded domain $\Omega \subseteq \mathbb{R}^n$, $n \geq 2$, with smooth boundary $\partial\Omega$, i.e. $u_0^{(g)} \in H^1(\Omega)$ solves

$$\text{(2)} \qquad \Delta u_0^{(g)}(x) + k^2 u_0^{(g)}(x) = 0 \quad \text{in } \Omega, \quad \partial_\nu u_0^{(g)}|_{\partial\Omega} = g.$$

We also consider the case where the domain contains an open scatterer $D \subset \Omega$ with $\overline{D} \subset \Omega$ and $\Omega \setminus \overline{D}$ is connected. We assume that the refractive index in D is real-valued and strictly larger than the background, so that the scattering coefficient is given by $1 + q(x)$, where $q \in L^\infty(\Omega)$ is assumed to fulfill that $q(x) = 0$ (a.e.) outside D and

$$0 < q_{\min} \leq q(x) \leq q_{\max} \quad \text{for all } x \in D \text{ (a.e.)}$$

Then the scattering field $u^{(g)} \in H^1(\Omega)$ solves

$$\text{(3)} \qquad \Delta u_q^{(g)}(x) + k^2(1 + q(x))u_q^{(g)}(x) = 0 \quad \text{in } \Omega, \quad \partial_\nu u_q^{(g)}|_{\partial\Omega} = g,$$

and the corresponding Neumann-Dirichlet-operator is denoted by

$$(4) \qquad \Lambda_q : \ L^2(\partial\Omega) \to L^2(\partial\Omega), \quad g \mapsto u_q^{(g)}|_{\partial\Omega}.$$

We assume that k^2 is not a resonance, neither for the homogeneous nor for the inhomogeneous problem, so that both, (2) and (4), are uniquely solvable for all $g \in L^2(\partial\Omega)$ and the Neumann-Dirichlet-operators are well-defined.

The main result. Our main result is a constructive proof that D is uniquely determined from comparing Λ_q with Λ_0. For an open set B (e.g., a small ball), we introduce the self-adjoint compact test operator

$$T_B : \ L^2(\partial\Omega) \to L^2(\partial\Omega), \quad \int_{\partial\Omega} g T_B h := \int_B k^2 u_0^{(g)} u_0^{(h)}.$$

Theorem 1. *There exists a number $d_{max} \in \mathbb{N}$ such that*

(a) if $B \subseteq D$ then

$$\alpha T_B \leq_{d_{max}} \Lambda(q) - \Lambda(0) \quad \text{for all } \alpha \leq q_{min}.$$

(b) if $B \nsubseteq D$ then, for all $\alpha > 0$, $\Lambda(q) - \Lambda(0) - \alpha T_B$ has infinitely many negative eigenvalues,

where $\alpha T_B \leq_{d_{max}} \Lambda(q) - \Lambda(0)$ denotes that the difference $\Lambda(q) - \Lambda(0) - \alpha T_B$ has at most d_{max} negative eigenvalues. The number d_{max} only depends on q_{max} and can be calculated without knowledge of D.

Proof of the main result. The proof of theorem 1 follows the approach in [4] (see also [2, 3, 5] for uniqueness proofs based on this approach) and combines a monotonicity estimate with the idea of localized potentials from [1].

Lemma 2 (Monotonicity). *There exists a number $d_{max} \in \mathbb{N}_0$ such that*

$$\int_{\partial\Omega} g \left(\Lambda(q) - \Lambda(0) \right) g \geq_{d_{max}} \int_{\Omega} k^2 q |u_0^{(g)}|^2$$

Proof. From the variational formulations of (1) and (3) one obtains that

$$\int_{\partial\Omega} g \left(\Lambda(q) - \Lambda(0) \right) g - \int_{\Omega} k^2 q |u_0^{(g)}|^2$$

$$\geq \int_{\Omega} \left(\left| \nabla(u_q^{(g)} - u_0^{(g)}) \right|^2 - k^2 (1 + q_{max}) |u_q^{(g)} - u_0^{(g)}|^2 \right)$$

$$= \langle \left(I - (1 + k^2(1 + q_{max}))K \right) (u_q^{(g)} - u_0^{(g)}), u_q^{(g)} - u_0^{(g)} \rangle_{H^1(\Omega)},$$

where I is the identity on $H^1(\Omega)$ and

$$K : \ H^1(\Omega) \to H^1(\Omega), \quad \langle Ku, v \rangle_{H^1(\Omega)} := \int_{\Omega} uv,$$

is compact. The assertion now follows from the fact that $I - (1 + k^2(1 + q_{max}))K$ can only have a finite number $d_{max} \in \mathbb{N}_0$ of negative eigenvalues. $\square$

Lemma 3 (Localized potentials). *If $B \subseteq \Omega$ is open and $B \nsubseteq D$ then for each finite dimensional subspace $V \subseteq L^2(\partial\Omega)$,*

(5) $\qquad \exists (g_k)_{k\in\mathbb{N}} \subseteq V^\perp : \quad \int_B k^2 |u_0^{(g_k)}|^2 \to \infty \quad but \quad \int_D k^2 |u_0^{(g_k)}|^2 \to 0.$

Moreover, for this sequence also $\int_D k^2 |u_q^{(g_k)}|^2 \to 0$.

Proof. By shrinking B, we can assume w.l.o.g. that $\overline{B} \subseteq \Omega$, $\overline{B} \cap \overline{D} = \emptyset$ and that $\Omega \setminus (\overline{B} \cup \overline{D})$ is connected. We then argue by contradiction, and assume that (5) is not true. Then, with the Neumann-to-Solution operators

$$L_D : \ L^2(\partial\Omega) \to L^2(D), \quad g \mapsto u_0^{(g)}|_D,$$
$$L_B : \ L^2(\partial\Omega) \to L^2(B), \quad g \mapsto u_0^{(g)}|_B,$$

there would exist a constant $C > 0$ such that

$$\|L_B g\| \le C \|L_D g\| \quad \text{for all } g \in V^\perp.$$

This would yield that there exists a self-adjoint compact F with $\dim(F) < \infty$ and

$$\|L_B g\|^2 \le C^2 \|L_D g\|^2 + \|Fg\|^2 \quad \text{for all } g \in L^2(\partial\Omega).$$

Using a powerful relation between norms of operator evaluations and the ranges of their adjoints [1, Lemma 2.5]), this would imply that

(6) $\qquad\qquad\qquad \mathcal{R}(L_B^*) \subseteq \mathcal{R}(L_D^*) + \mathcal{R}(F).$

However, the adjoints L_D^* and L_B^* can be characterized as Source-to-Dirichlet operators, and using a unique continuation argument as in part (b) of the proof of theorem 3.6 in [4], one can show that

$$\mathcal{R}(L_D^*) \cap \mathcal{R}(L_B^*) = \{0\},$$

and that $\mathcal{R}(L_D^*), \mathcal{R}(L_B^*) \subseteq L^2(\partial\Omega)$ are both dense and thus infinite-dimensional. By a dimension argument, it thus follows that (6) cannot be true. This proves (5).

Defining $\tilde{L}_D : \ L^2(\partial\Omega) \to L^2(D)$, $g \mapsto u_q^{(g)}|_D$ and using that $q = 0$ outside of D, one can show that $\mathcal{R}(\tilde{L}_D^*) = \mathcal{R}(L_D^*)$. Hence, the additional assertion $\int_D k^2 |u_q^{(g_k)}|^2 \to 0$ follows by the same arguments. $\qquad\square$

Proof of theorem 1. If $B \subseteq D$ and $\alpha \le q_{\min}$ then lemma 2 yields that

$$\alpha \int_{\partial\Omega} g T_B g = \alpha \int_B k^2 |u_0^{(g)}|^2 \le \int_\Omega k^2 q |u_0^{(g)}|^2 \le_{d_{\max}} \int_{\partial\Omega} g \left(\Lambda(q) - \Lambda(0)\right) g,$$

which shows (a). Interchanging u_q and u_0 in lemma 2, it also follows that

$$\int_{\partial\Omega} g \left(\Lambda(q) - \Lambda(0)\right) g \le_{d_{\max}} \int_\Omega k^2 q |u_q^{(g)}|^2$$

Hence, if $B \nsubseteq D$, but $\Lambda(q) - \Lambda(0) \ge_{\mathrm{fin}} \alpha T_B$, then this would imply that

$$\alpha \int_B k^2 |u_0^{(g)}|^2 \le \int_\Omega k^2 q |u_q^{(g)}|^2 = \int_D k^2 q_{\max} |u_q^{(g)}|^2$$

holds for all $g \in V^\perp$ with some finite-dimensional space $V \subset L^2(\partial\Omega)$. But this contradicts lemma 3 and thus proves (b). □

REFERENCES

[1] B. Gebauer, *Localized potentials in electrical impedance tomography*, Inverse Probl. Imaging **2** (2008), 251–269.
[2] B. Harrach, *On uniqueness in diffuse optical tomography*, Inverse problems **25** (2009), 055010.
[3] B. Harrach, *Simultaneous determination of the diffusion and absorption coefficient from boundary data*, Inverse Probl. Imaging **6** (2012), 663–679.
[4] B. Harrach and M. Ullrich, *Monotonicity-based shape reconstruction in electrical impedance tomography*, SIAM Journal on Mathematical Analysis **45** (2013), 3382–3403.
[5] B. Harrach and M. Ullrich, *Local uniqueness for an inverse boundary value problem with partial data*, Proceedings of the American Mathematical Society **145** (2017), 1087–1095.

Stekloff Eigenvalues in Inverse Scattering

SHIXU MENG

(joint work with Fioralba Cakoni, David Colton, Peter Monk)

We consider a problem in non-destructive testing in which small changes in the (possibly complex valued) refractive index $n(x)$ of an inhomogeneous medium of compact support are to be determined from changes in measured far field data due to incident plane waves.

It is known that transmission eigenvalues can be determined from the measured scattering data and carry information about the refractive index of non-absorbing media [3]. However the use of transmission eigenvalues in nondestructive testing has two major drawbacks. The first drawback is that in general only the first transmission eigenvalue can be accurately determined from the measured data [2] and the determination of this eigenvalue means that the frequency of the interrogating wave must be varied in a frequency range around this eigenvalue. In particular, multi-frequency data must be used in an a priori determined frequency range. This also requires the medium to be non-dispersive. The second drawback is that only real transmission eigenvalues can be conveniently determined from the measured scattering data which means that transmission eigenvalues cannot be used for the non-destructive testing of inhomogeneous absorbing media.

To overcome these difficulties, we consider a modified far field operator $\mathcal{F}$ whose kernel is the difference of the measured far field pattern due to the scattering object and the far field pattern of an auxiliary scattering problem with the Stekloff boundary condition imposed on the boundary of a domain B where B is either the support of the scattering object or a ball containing the scattering object in its interior. It is shown that $\mathcal{F}$ can be used to determine the Stekloff eigenvalues corresponding to B where if $B \neq D$ the refractive index is set equal to one in $B \setminus \overline{D}$. For fixed k, $\lambda := \lambda(k) \in \mathbb{C}$ is called a Stekloff eigenvalue if there exists a

nontrivial solution $u \in H^1(B)$ to

$$\Delta w + k^2 n(x) w = 0 \text{ in } B,$$
$$\frac{\partial w}{\partial \nu} + \lambda w = 0 \text{ on } \partial B.$$

In the simple case when the refractive index is real valued, we establish the existence of Stekloff eigenvalues in this case and derive a relationship between small changes in the refractive index and the corresponding change in the Stekloff eigenvalue. The case that the refractive index can be complex valued is more complicated. We study this non-selfadjoint Stekloff eigenvalue problem using Agmon's theory of non-selfadjoint eigenvalue problems [1] and the Dirichlet to Neumann map [5], we show that there exist infinitely many Stekloff eigenvalues. Finally a formula is obtained relating changes in $n(x)$ to changes in the Stekloff eigenvalues and numerical examples are given [4] showing the effectiveness of determining changes to the refractive index in this way.

References

[1] S. Agmon, *Lectures on Elliptic Boundary Value Problems*, AMS Chelsea Publications, Providence, RI, (2010).
[2] F. Cakoni and D. Colton, *A Qualitative Approach to Inverse Scattering Theory*, Springer, New York, (2014).
[3] D. Colton and R. Kress, *Inverse Acoustic and Electromagnetic Scattering Theory*, 3rd, Springer-Verlag, New York, (2013).
[4] A. Girouard and R. S. Laugesen and B. A. Siudeja, Steklov Eigenvalues and Quasiconformal Maps of Simply Connected Planar Domains, *Archive for Rational Mechanics and Analysis*, **219**, 903–936, (2016).
[5] J. M. Lee and G. Uhlmann, Determining anisotropic real-analytic conductivities by boundary measurements, *Communications on Pure and Applied Mathematics*, **42**, 8 (1097-1112), (1989).

Problems in computational helioseismology

Laurent Gizon

(joint work with Damien Fournier, Thorsten Hohage)

The Sun supports acoustic oscillations continuously excited by near-surface turbulent convection. *Global helioseismology* consists of inverting the measured frequencies of the normal modes of oscillation to infer the sound speed and rotation as a function of radius and unsigned latitude [1]. Techniques of *local helioseismology* based on correlations of the wave field at the surface are being developed to infer the structure and dynamics of the Sun in three dimensions [2, 3].

Forward problem. Time-distance helioseismology [4] is a particular technique of local helioseismology, analogous to geophysical seismic interferometry. Ignoring terms that involve gravity, the oscillations at position $\mathbf{r}$ and frequency ω can be described by a scalar field $\psi(\mathbf{r}, \omega)$, which solves the acoustic wave equation [5]

$$(1) \quad L_{\mathbf{r},\omega}[\psi] := -(\omega^2 + 2i\omega\gamma)\psi - 2i\omega\mathbf{u} \cdot \nabla_{\mathbf{r}}\psi - c\nabla_{\mathbf{r}} \cdot \left(\frac{1}{\rho}\nabla_{\mathbf{r}}(\rho c\psi)\right) = s(\mathbf{r}, \omega),$$

where $\gamma(\mathbf{r}, \omega)$ is attenuation and the steady background medium is represented by density $\rho(\mathbf{r})$, sound speed $c(\mathbf{r})$, and flow $\mathbf{u}(\mathbf{r})$. Waves are excited by a stationary random process (granulation) represented by the function $s(\mathbf{r}, \omega)$. The above equation is supplemented by a radiative boundary condition [6]. The basic input data in time-distance helioseismology is the covariance function $C(\mathbf{r}', \mathbf{r}, \omega) = \psi^*(\mathbf{r}', \omega)\psi(\mathbf{r}, \omega)$ between two points on the solar surface. Under the assumption that sources are spatially uncorrelated and of the form $\mathbb{E}[s^*(\mathbf{r}', \omega)s(\mathbf{r}, \omega)] = \delta(\mathbf{r} - \mathbf{r}')P(\omega)\gamma(\mathbf{r}, \omega)/\rho(\mathbf{r})$ we have (to within a surface term)

$$(2) \qquad C(\mathbf{r}', \mathbf{r}, \omega) = \frac{P(\omega)}{4i\omega} \left[G(\mathbf{r}, \mathbf{r}', \omega) - G^\dagger(\mathbf{r}, \mathbf{r}', \omega) \right] + \text{noise},$$

where $L_{\mathbf{r}, \omega}[G(\mathbf{r}, \mathbf{r}', \omega)] = \delta(\mathbf{r} - \mathbf{r}')/\rho(\mathbf{r})$ and $G^\dagger = G^*(\mathbf{u} \to -\mathbf{u})$ is obtained by switching the sign of $\mathbf{u}$ and taking the complex conjugate. The linear forward problem consists in computing the perturbations to the covariance function caused by infinitesimally small perturbations in the background medium. Combining the first Born approximation [7, 8] and Eq. (2), Gizon et al. [5] expressed sensitivity kernels in terms of only four Green's functions in the reference medium, computed using the finite-element code Montjoie [9].

Inverse problem. The inverse problem consists of reconstructing $\gamma(\mathbf{r}, \omega)$, $c(\mathbf{r})$, $\rho(\mathbf{r})$, and $\mathbf{u}(\mathbf{r})$ in the interior, starting from a reference solar model. This requires knowledge of the noise covariance matrix [10, 11]. Linear inversions are traditionally performed using Tikhonov regularization [12] or the method of approximate inverse (called optimally localized averaging, see ref. [13]). Under the assumption of local horizontal translation invariance of the sensitivity kernels, multichannel inversions in Fourier space enable to solve problems that would otherwise require too much computer memory [14]. Minimax estimators have been computed for this problem using the Pinsker method [15, 16].

The non-linear inverse problem of time-distance helioseismology (finite perturbations to the medium) has not been studied in full detail yet. Future studies should build on existing theoretical uniqueness results, in particular on the Novikov-Agaltsov reconstruction algorithm [17], which combines measurements of G at several frequencies (see table below). For measurements of C instead of G, we have conducted numerical experiments to determine the number of frequencies required to reconstruct ρ and c. For realistic noise levels, more frequencies will be needed to obtain useful reconstructions.

Outstanding problems. Further advances in local helioseismology will require improved forward solvers for vector MHD wave equations (see refs. [22, 23]) and homogenized wave equations [24], as well as improved inversion methods that minimize the number of forward solves [25, 26]. A major challenge in local helioseismology is the very large size of the input dataset, e.g. $\sim 10^{12}$ pairs of points times $\sim 10^2$ frequencies in time-distance helioseismology. As a result, it is important to either select or average the input data before inverting them. One interesting averaging scheme that deserves further attention is helioseismic holography [27, 28, 29], which uses Green's second identity to image scatterers in the Sun, as in Porter-Bojarski holography [30, 31].

TABLE 2. Number of frequencies needed for reconstruction

	Observable: G		Observable: C	
	theory	experiment	theory	experiment
c	1 (ref. [18])	1 (ref. [19])	?	2 (this work)
ρ	1 (ref. [18])	1 (ref. [19])	?	2 (this work)
c, ρ	2 (ref. [18])	2 (ref. [19])	?	4 (this work)
$\mathbf{u}$	2 (ref. [17])	2 (ref. [20])	?	2 (ref. [20])
c, ρ, γ, $\mathbf{u}$	3 (ref. [17])	≥ 3 (ref. [21])	?	?

REFERENCES

[1] S. Basu, *Global seismology of the Sun*, Living Reviews in Solar Physics, **13** (2016), 2.

[2] L. Gizon, A. C. Birch, H. C. Spruit, *Local helioseismology: three-dimensional imaging of the solar interior*, Annual Review of Astronomy and Astrophysics **48** (2010), 289–338.

[3] S. Hanasoge, L. Gizon, K. R. Sreenivasan, *Seismic sounding of convection in the Sun*, Annual Review of Fluid Mechanics **48** (2016), 191–217.

[4] T. L. Duvall Jr., S. M. Jeffferies, J. W. Harvey, M. A. Pomerantz, *Time-distance helioseismology*, Nature **362** (1993), 430–432.

[5] L. Gizon, H. Barucq, M. Duruflé, C. S. Hanson, M. Leguèbe, A. C. Birch, J. Chabassier, D. Fournier, T. Hohage, E. Papini, *Computational helioseismology in the frequency domain: acoustic waves in axisymmetric solar models with flows*, Astronomy and Astrophysics **600** (2017), A35.

[6] H. Barucq, J. Chabassier, M. Duruflé, L. Gizon, M. Leguèbe, *Atmospheric radiation boundary conditions for the Helmholtz equation*, Mathematical Modelling and Numerical Analysis (2017), submitted.

[7] L. Gizon, A. C. Birch, *Time-Distance Helioseismology: the forward problem for random distributed sources*, The Astrophysical Journal **571** (2002), 966–986.

[8] V. G. A. Böning, M. Roth, W. Zima, A. C. Birch, L. Gizon, *Sensitivity kernels for flows in time-distance helioseismology: extension to spherical geometry*, The Astrophysical Journal **824** (2016), 49.

[9] M. Duruflé, *Numerical integration and high-order finite element methods applied to time-harmonic Maxwell equations*, PhD Thesis (2006), ENSTA ParisTech, France.

[10] L. Gizon, A. .C. Birch, *Time-distance helioseismology: noise estimation*, The Astrophysical Journal **614** (2004), 472–489.

[11] D. Fournier, L. Gizon, T. Hohage, A. C. Birch, *Generalization of the noise model for time-distance helioseismology*, Astronomy and Astrophysics **567** (2014), A137.

[12] A. G. Kosovichev, *Tomographic imaging of the Sun?s interior*, Astrophys. J. Lett. **461** (1996), L55.

[13] F. P. Pijpers, M. J. Thompson, *Faster formulations of the optimally localized averages method for helioseismic inversion*, Astronomy and Astrophysics **262** (1992), L33–L36.

[14] J. Jackiewicz, A. C. Birch, A. C., Gizon, S. M. Hanasoge, T. Hohage, J.-B. Ruffio, M. Švanda. *Multichannel three-dimensional SOLA inversion for local helioseismology*, Solar Physics **276** (2012), 19–33.

[15] M. S. Pinsker, *Optimal filtering of square integrable signals in Gaussian white noise*, Problems of Information Transmission **16** (1980), 120–133.

[16] D. Fournier, L. Gizon, M. Holzke, T. Hohage. *Pinsker estimators for local helioseismology: inversion of travel times for mass-conserving flows*, Inverse Problems **32** (2016), 105002.

[17] A. Agaltsov, *Méthodes de reconstruction pour des problèmes inverses pour des équations de type Helmholtz*, PhD Thesis (2016), Université Paris-Saclay, France.

[18] R. G. Novikov, *Multidimensional inverse spectral problem for the equation* $-\Delta\psi + (v(x) - Eu(x))\psi = 0$, Functional Analysis and Its Applications **22** (1988), 263–272.

[19] A. I. Nachman, *Reconstruction from boundary measurements*, Annals of Mathematics **128** (1988), 531–576.

[20] D. I. Zotov, A. S. Shurup, O. D. Rumyantseva, *Vector field reconstruction of flows using the Novikov-Agaltsov functional algorithm and the additive correlation method*, Bulletin of the Russian Academy of Sciences: Physics **81** (2017), 101–105.

[21] A. S. Shurup, O. D. Rumyantseva, *Joint reconstruction of sound speed, attenuation and currents by Novikov-Agaltsov functional algorithm*, Acoustical Physics (2017), in press.

[22] R. Cameron, L. Gizon, T. L. Duvall Jr. *Helioseismology of sunspots: confronting observations with three-dimensional MHD simulations of wave propagation*, Solar Physics **251** (2008), 291–308.

[23] S. M. Hanasoge, D. Komatitsch, L. Gizon, *An absorbing boundary formulation for the stratified, linearized, ideal MHD equations based on an unsplit, convolutional perfectly matched layer*, Astronomy and Astrophysics **522** (2010), A87.

[24] S. M. Hanasoge, L. Gizon, G. Bal, *Propagation of seismic waves through a spatio-temporally fluctuating medium: homogenization*, The Astrophysical Journal **773** (2013), 101.

[25] Hanasoge, S. M., Birch, A., Gizon, L., Tromp, J. *The Adjoint Method Applied to Time-distance Helioseismology*, The Astrophysical Journal **738** (2011), 100.

[26] T. Hohage, S. Langer, *Acceleration techniques for regularized Newton methods applied to electromagnetic inverse medium scattering problems*, Inverse Problems, **26** (2010), 074011.

[27] C. Lindsey, C., D. C. Braun, *Basic Principles of Solar Acoustic Holography*, Solar Physics **192** (2000), 261–284.

[28] C. Lindsey, D. C. Braun, *Seismic Images of the far side of the Sun*, Science **287** (2000), 1799–1801.

[29] R. Skartlien, Local helioseismology as an inverse source-inverse scattering problem, The Astrophysical Journal **565** (2002), 1348–1365.

[30] R. P. Porter and A. J. Devaney, *Holography and the inverse source problem*, Journal of the Optical Society of America **72** (1982), 327–330.

[31] A. J. Devaney, R. P. Porter, *Holography and the inverse source problem. Part II: Inhomogeneous media*, Journal of the Optical Society of America A **2** (1985), 2006–2012.

Beyond Kirchhoff migration in 2D seismic imaging

Andreas Rieder

(joint work with Christine Grathwohl, Peer Kunstmann, Eric Todd Quinto)

In seismic imaging one wants to identify material parameters of a medium from measurements of reflected waves. If the medium does not support shear stress and has constant mass density (say 1) then the acoustic wave equation governs wave propagation: the acoustic potential $u(t; \mathbf{x}, \mathbf{x_s}) \in \mathbb{R}$ at location $\mathbf{x} \in \mathbb{R}^2$ and time $t \geq 0$ satisfies

$$(1) \qquad \frac{1}{\nu^2}\, \partial_t^2 u - \Delta_{\mathbf{x}} u = \delta(\mathbf{x} - \mathbf{x_s})\delta(t)$$

where $\nu = \nu(\mathbf{x})$ is the speed of sound and $\mathbf{x_s}$ is the excitation (source) point. The task is to reconstruct ν from the backscattered (reflected) field $u(t; \mathbf{x_r}, \mathbf{x_s})$, $(t; \mathbf{x_r}, \mathbf{x_s}) \in [0, T_{\max}] \times \mathcal{R} \times \mathcal{S}$ where $\mathcal{S}$ and $\mathcal{R}$ are the sets of source and receiver (microphone) positions, respectively, and $T_{\max}$ is the recording time.

This inverse problem is nonlinear. We linearize by the Born ansatz

$$\frac{1}{\nu^2(\mathbf{x})} = \frac{1 + n(\mathbf{x})}{c^2(\mathbf{x})}$$

with a smooth, a priori known background velocity $c = c(\mathbf{x})$. Now, n is the quantity we seek. The Born approximation is justified when no multiple scatterings occur.

Using principles of wave propagation we can show that n may be determined as a solution of the integral equation

(2) $$Fw(T; \mathbf{x_r}, \mathbf{x_s}) = \frac{1}{\pi} \int_0^T (u - \widetilde{u})(t; \mathbf{x_r}, \mathbf{x_s}) \mathrm{d}t$$

with the reference solution $\widetilde{u}$ which has to be computed from (1) with ν replaced by c. In (2), the operator F is a generalized Radon transform

$$Fw(T; \mathbf{x_r}, \mathbf{x_s}) = \int \frac{w(\mathbf{x})}{c^2(\mathbf{x})} a(\mathbf{x}, \mathbf{x_s}) a(\mathbf{x}, \mathbf{x_r}) \delta\big(T - \tau(\mathbf{x}, \mathbf{x_s}) - \tau(\mathbf{x}, \mathbf{x_r})\big) \mathrm{d}\mathbf{x}$$

where the travel time τ and the amplitude a can be computed from

$$|\nabla_{\mathbf{x}} \tau| = c^{-1} \quad \text{and} \quad \mathrm{div}(a^2 \nabla_{\mathbf{x}} \tau) = 0,$$

see, e.g. [6]. So, Fw integrates w over reflection isochrones: $T = \tau(\cdot, \mathbf{x_s}) + \tau(\cdot, \mathbf{x_r})$.

Since the 1950's Kirchhoff migration is the standard technique to approximately solve the integral equation. Beylkin [1] gave Kirchhoff migration a mathematical foundation: the reconstructed n_{rec} can be expressed as $n_{\mathrm{rec}} = F^\# K g$ where $g = Fn$ are the data (measurements), K is a convolution operator, and $F^\#$ denotes a dual transform (generalized backprojection). Further, he could prove that

$$n_{\mathrm{rec}} = F^\# K F n = I_{\mathrm{partial}} n + \Psi n$$

where I_{partial} is a kind of band pass filtering (operator of partial reconstruction) and Ψ is smoothing. Further, the imaging operator $F^\# K F$ is a pseudo-differential operator of order 0.

We propose a different approach which we think is more flexible, allows a better control of the involved parameters, and gives a better understanding of the propagation of singularities. As we cannot hope to recover n from the data completely we consider imaging operators Λ which differ from $F^\# K F$:

$$\Lambda = P^* F^* \Phi F$$

where Φ is a smooth cutoff function, F^* is (smoothly weighted) L^2-dual, and P^* is the dual of a local operator such that Λ is of order 1. Our reconstruction technique based on Λ also differs from Kirchhoff migration, see [2].

In what follows we assume that the background velocity is constant, $c = 1$, yielding $\tau(\mathbf{x}, \mathbf{y}) = |\mathbf{x} - \mathbf{y}|$ as well as $a(\mathbf{x}, \mathbf{y}) = 1/|\mathbf{x} - \mathbf{y}|$. Further, let n be compactly supported in $\mathbb{R}_+^2$, the lower half space $x_2 > 0$ ($x_2 > 0$ points downwards). Source and receiver positions are given by the common offset scanning geometry

$$\mathbf{x_s}(s) = (s - \alpha, 0)^\top \quad \text{and} \quad \mathbf{x_r}(s) = (s + \alpha, 0)^\top$$

where $\alpha \geq 0$ is the common offset. In this situation the generalized Radon transform integrates over ellipses and may be written as

$$Fw(s,t) = \int A(s,\mathbf{x})w(\mathbf{x})\delta\big(t - \varphi(s,\mathbf{x})\big)\mathrm{d}\mathbf{x}, \quad t > 2\alpha,$$

with

$$\varphi(s,\mathbf{x}) := |\mathbf{x_s}(s) - \mathbf{x}| + |\mathbf{x_r}(s) - \mathbf{x}| \quad \text{and} \quad A(s,x) = \frac{1}{|\mathbf{x_s}(s) - \mathbf{x}|\,|\mathbf{x_r}(s) - \mathbf{x}|}.$$

We start with the imaging operator

$$\Lambda = \Delta F^* \Phi F$$

where Δ is the Laplacian. From the elliptic means $g = Fn$ we can recover

$$\Lambda n = \Delta F^* \Phi g.$$

We have composed Λ as a pseudo-differential operator of order 1 and Λn emphasizes singularities (e.g., jumps along curves) of n which are tangent to ellipses being integrated over. To see this note that – under the Bolker assumption – any hypersurface Radon transform R on $\mathbb{R}^d$ and its (formal, smoothly weighted) L^2-adjoint R^* are Fourier integral operators of order $-(d-1)/2$ [3]. If they can be composed, then R^*R is a pseudo-differential operator. Our F on $\mathbb{R}^2$ satisfies the Bolker assumption [4] and, hence, $F^*\Phi F$ is of order -1.

Theorem 1. *The top order symbol of $\Lambda = \Delta F^* \Phi F$ is*

$$\sigma(\mathbf{x},\xi) = -2\pi\,|\xi|^2\,\frac{A^2(s,\mathbf{x})\Phi(s,\varphi(s,\mathbf{x}))}{|\omega|\,B(s,\mathbf{x})}$$

where

$$B(s,\mathbf{x}) = \big|\det\big(\nabla_\mathbf{x}\varphi(s,\mathbf{x}), \partial_s\nabla_\mathbf{x}\varphi(s,\mathbf{x})\big)\big|.$$

The symbol is evaluated at $(\mathbf{x},\xi)$ where $s \in \mathbb{R}$ and $\omega \in \mathbb{R}$ are defined uniquely by

$$\xi = \omega\nabla_\mathbf{x}\varphi(s,\mathbf{x}).$$

For positive α the explicit expression for σ is rather complicated. Therefore, we restrict ourselves here to $\alpha = 0$.

Corollary 2. *Let $\alpha = 0$. Then,*

$$\sigma(\mathbf{x},\xi) = -\pi\frac{\xi_2^2}{|\xi|}\frac{1}{x_2^3}\,\Phi\Big(x_1 - \tfrac{\xi_1}{\xi_2}x_2, 2x_2\tfrac{|\xi|}{|\xi_2|}\Big).$$

If

$$\xi \in C(\mathbf{x}) := \Big\{\xi \in \mathbb{R}^2 : \xi_2 \neq 0,\ \Phi\Big(x_1 - \tfrac{\xi_1}{\xi_2}x_2, 2x_2\tfrac{|\xi|}{|\xi_2|}\Big) > 0\Big\}.$$

then Λ is micro-locally elliptic at $\mathbf{x}$ in direction ξ. Thus, the next corollary follows from a general result [5]. By $\mathrm{WF}^s(u)$ we denote the H^s-wave front set of the distribution u.

Corollary 3. *Let* $\alpha = 0$ *and* $\xi \in C(\mathbf{x})$ *for* $\mathbf{x} \in \mathbb{R}_+^2$. *Then, for* $u \in \mathcal{D}_0'(\mathbb{R}_+^2)$

$$(\mathbf{x}, \xi) \in \mathrm{WF}^s(u) \iff (\mathbf{x}, \xi) \in \mathrm{WF}^{s-1}(\Lambda u).$$

Loosely speaking, u fails to be in H^s at $\mathbf{x}$ in direction ξ iff Λu fails to be in H^{s-1} at $\mathbf{x}$ in direction ξ.

Since the symbol of Λ goes to zero rapidly with increasing depth x_2, the wave fronts farther down are also reconstructed more weakly than those closer to the surface. We compensate for this deficiency by introducing a modified imaging operator

$$\Lambda_{\mathrm{mod}} = \Delta M F^* \Phi F \quad \text{where } M \text{ is multiplication by } x_2^3.$$

The top order symbol of Λ_{mod} is $x_2^3 \sigma(\mathbf{x}, \xi)$ and depends on x_2 only via the term involving the cutoff function. The set $C(\mathbf{x})$ is the same for both imaging operators.

References

[1] G. Beylkin, *Imaging of discontinuities in the inverse scattering problem by inversion of a causal generalized Radon transform*, J. Math. Phys. **26** (1985), 99–108.

[2] C. Grathwohl, P. Kunstmann, A. Rieder, E. T. Quinto, *Approximate inverse for the common offset acquisition geometry in 2D seismic imaging*, CRC1173-Preprint, Dept. of Mathematics, Karlsruhe Institute of Technology (2016). `http://www.waves.kit.edu/downloads/CRC1173_Preprint_2016-37.pdf`

[3] V. Guillemin, S. Sternberg, *Geometric asymptotics*, Mathematical Surveys **14** (1977), American Mathematical Society.

[4] V. P. Krishnan, H. Levinson, E. T. Quinto, *Microlocal analysis of elliptical Radon transforms with foci on a line*, in I. Sabadini and D. Struppa, editors, *The Mathematical Legacy of Leon Ehrenpreis, 1930-2010*, Springer Proceedings in Mathematics **16** (2012), 163–182.

[5] B. E. Petersen, *Introduction to the Fourier transform and pseudo-differential operators*, Monographs and Studies in Mathematics **19** (1983), Pitman, Boston.

[6] W. W. Symes, *Mathematics of reflection seismology*, Technical report, The Rice Inversion Project, Rice University, Houston, TX, USA (1998). `http://www.trip.caam.rice.edu/downloads/preamble.pdf`.

Stability and convergence for seismic reconstruction using full waveform inversion

Florian Faucher

(joint work with Hélène Barucq, Henri Calandra, Guy Chavent, Maarten V. de Hoop)

We study the seismic inverse problem associated with the time-harmonic wave equations for the reconstruction of subsurface media. The reconstruction is conducted using the full waveform inversion (FWI) method and relies on iterative minimization algorithm, which we adapt for large scale situation. Considering the Dirichlet-to-Neumann map as the data, the inverse problem shows a conditional

Lipschitz-type stability when assuming piecewise constant representation of the parameters. We obtain the analytical lower and upper bounds for the stability constant and provide quantitative numerical estimates to demonstrate the sharpness of these bounds, in the geophysical context. We further study the convergence of the minimization problem and are able to numerically estimate the size of the basin of attraction, depending on the frequency. From these stability and convergence results, we design a multi-level algorithm with simultaneous progression in frequency and scale. Eventually we carry out numerical experiments for acoustic and elastic parameters reconstruction assuming no prior information in the initial models, in two and three dimensions.

1. Time-harmonic inverse problem for the wave equation

The seismic inverse problem aims the recovery of subsurface materials from the measurements of waves at the surface. The underlying inverse problem can be formulated as an optimization problem, as initiated by the work of Tarantola [5, 6]. Such techniques are referred to as full waveform inversion (FWI). Let us consider a bounded domain Ω of $\mathbb{R}^2$ or $\mathbb{R}^3$, the propagation of wave is given by u solution of

$$(1) \qquad\qquad -\omega^2 \rho(\mathbf{x}) u(\mathbf{x}) - \nabla \cdot \underline{\sigma}(\mathbf{x}) = f(\mathbf{x}),$$

where ω is the frequency, ρ the density, $\underline{\sigma}$ the stress tensor and f the source. The medium properties (Lamé, Thomsen parameters, etc) are referred to as m and contained in $\underline{\sigma} := \underline{\sigma}(m, \mathbf{x})$. The number of parameters to recover depends on the type of medium (i.e. acoustic, elastic, anisotropic, etc). For example in acoustic isotropic case, the propagation of waves follows the Helmholtz equation

$$(2) \qquad\qquad \left(-\Delta - \frac{\omega^2}{c(\mathbf{x})^2} \right) u(\mathbf{x}) = f(\mathbf{x}),$$

where the medium is defined by a single parameter: the wavespeed c.

In the seismic context, measurements are acquired on a portion Σ of the domain, which is standardly a discrete set of surface locations; we denote the corresponding data d. The forward problem $\mathcal{F}$ associated with parameter m is defined such that

$$(3) \qquad\qquad \mathcal{F} \ : \ m \quad \rightarrow \quad \mathcal{F}(m) = \{ u(\mathbf{x}) \, |_\Sigma \}.$$

The reconstruction follows an iterative minimization of the cost function defined as the difference between the data and simulation using an approximate model:

$$(4) \qquad\qquad \min_m \mathcal{J}(m) = \frac{1}{2} \| \mathcal{F}(m) - d \|^2.$$

2. Conditional Lipschitz-type stability

We consider the inverse problem associated with the Helmholtz equation using the Dirichlet-to-Neumann map as the data. [1] shows conditional Lipschitz-type

stability when taking a piecewise constant representation for the model:

$$(5) \qquad c^{-2}(\mathbf{x}) = m(\mathbf{x}) = \sum_{k=1}^{N} \alpha_k \chi_k(\mathbf{x}),$$

where α_k stands for constant coefficient and χ_k the characteristic function. In this configuration the stability result gives

$$(6) \qquad \|m_1 - m_2\| \leq \mathcal{C}\|\mathcal{F}(m_1) - \mathcal{F}(m_1)\|.$$

In [2] we have been able to precisely characterize the stability constant $\mathcal{C}$,

$$(7) \qquad \frac{1}{4\omega^2} e^{K_1 N^{1/5}} \leq \mathcal{C} \leq \frac{1}{\omega^2} e^{(K_2(1+\omega^2 c_{\min}^{-2})N^{4/7})},$$

where K_1 and K_2 are mathematical constant.

We confront the analytical bounds to numerical estimation of the stability constant and demonstrate their sharpness, in particular for a geophysical setup. The stability analysis helps conduct the iterative algorithm by providing insight on frequency and scale dependency. Namely the use of low frequencies requires the use of low scale (low N) to limit the growth of the stability constant.

3. Convergence of the iterative algorithm

We motivate the frequency progression in our algorithm by a local analysis of convergence properties based on weakly nonlinear inverse problem as defined in [3, 4].

Assuming an initial model m_0, we focus on the interval $[m_0 - \Delta_{m_0}, m_0 + \Delta_{m_0}]$ where Δ_{m_0} is a distance chosen to obtain the deflection condition (which indicates advantageous convergence properties). We define numerical estimate of Δ_{m_0} after the discretization of the wave equation,

$$(8) \qquad \Delta_{m_0} \geq \frac{\pi}{4} \frac{\|D\mathcal{F}(m_0)\|}{\|D^2\mathcal{F}(m_0)\|}.$$

Hence it allows us to estimate the size of the basin of attraction with respect to the frequency. In particular we show that low frequencies give a larger convergence radius, which is particularly crucial when no initial information is known on the model to be recovered.

4. Numerical experiments

From the stability and convergence results we define a multi-level algorithm where the frequency progresses with scale in order to conduct the iterative minimization algorithm. We carry out experiments in two and three dimensions for the reconstruction of seismic coefficients, in acoustic and elastic media. In the Figure 1 we illustrate the recovery of P-wavespeed model in elastic medium.
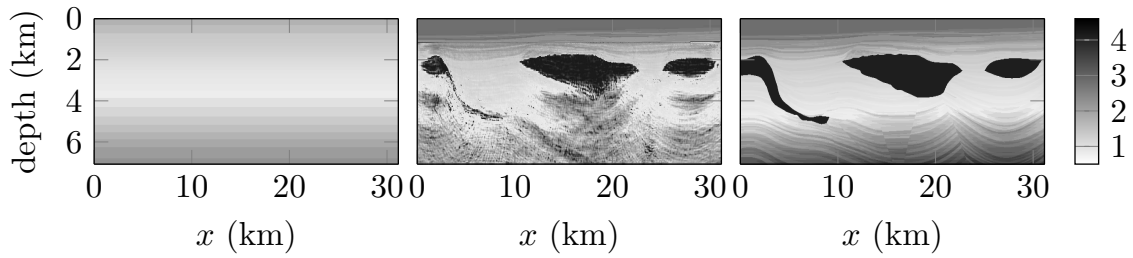
FIGURE 1. Elastic reconstruction of a two dimensional seismic model, initial (left), reconstructed (center) and true (right) P-wavespeed coefficients (km s^{-1}).

5. PERSPECTIVES

We aim to extend the stability result in the case of partial data and absorbing boundary conditions on some part of the domain boundary. It involves the use of Cauchy data and piecewise linear representation. We will discuss the current progress and illustrate the numerical benefits.

A precise relation between frequency and scale, from the stability and convergence, is the natural extension but necessitates further analysis. We also aim at anisotropic coefficients reconstruction, which is numerically feasible but would greatly benefit from analytical results.

REFERENCES

[1] G. Alessandrini and S. Vessella, *Lipschitz stability for the inverse conductivity problem*, Adv. in Appl. Math. **35** (2005), 207–241.
[2] E. Beretta, M. V. de Hoop, F. Faucher and O. Scherzer, *Inverse boundary value problem for the Helmholtz equation: quantitative conditional Lipschitz stability estimates*, SIAM Journal on Mathematical Analysis **48** (2016), 3962–3983.
[3] G. Chavent and K. Kunisch, *On weakly nonlinear inverse problems*, SIAM Journal on Applied Mathematics **56** (1996), 542–572.
[4] M. V. de Hoop, L. Qiu and O. Scherzer *An analysis of a multi-level projected steepest descent iteration for nonlinear inverse problems in Banach spaces subject to stability constraints*, Numerische Mathematik **129** (2015), 127–148.
[5] A. Tarantola, *Inversion of seismic reflection data in the acoustic approximation*, Geophysics **49** (1984), 135–157.
[6] A. Tarantola, *Inversion of travel times and seismic waveforms*, Seismic tomography (1987), 1259-1266.

Bayesian Inversion for the Drift in Stochastic Differential Equations

Yvo Pokern

(joint work with Tjun Y. Hoh, Ioanna Manolopoulou)

For a stochastic differential equation (SDE) of Ito type of the form

$$\mathrm{d}V_t = \xi(V_t)\mathrm{d}t + \sigma(V_t)\mathrm{d}W_t, \qquad V_0 = v_0,$$

the problem considered here is to estimate the term $\xi(\cdot)$ known as the drift term as well as the term $\sigma(\cdot)$ known as the diffusivity based on observations of the stochastic process $(V_t)_{t\in[0,T]}$ at time points $t_i \in [0,T]$. In the statistical context, it has frequently been assumed that the unknown functions $\xi(\cdot)$ and $\sigma(\cdot)$ can be described by a finite-dimensional parameter $\theta \in \Theta$, usually of small dimension and with each component readily interpretable in the application domain. Interest then shifts to finding good values for this parameter, an approach known as parametric inference. Such a parameterization limits flexibility and if this is to be avoided, a nonparametric approach can be adopted instead, where the whole functions $\xi(\cdot), \sigma(\cdot)$, or at least their values at a set of points are estimated. The Bayesian approach is to assume *a priori*, i.e. before having taken the observations (V_{t_i}) into account, that the function is an element of a suitable function space H and to construct a probability measure π_0, referred to as a *prior*, on this function space which reflects a scientific consensus belief elicited from interaction with application area experts. The SDE gives rise to a probability measure on the observations $P((V_{t_i})|\xi,\sigma)$ which is combined with the prior measure π_0 using Bayes' theorem to yield the posterior measure; see [2] for the Bayesian viewpoint in general and [10] for an exposition in the context of nonparametric estimation and inverse problems.

If observations are available at all points of the interval $[0,T]$, this is known as continuous time observation and a rich theory exists to address this problem, see [6]. This setting has also been considered in [8] as its relative simplicity enables a study of the frequentist behaviour of the Bayesian procedure proposed in dimension one. If observations are available at a finite number of time points with maximal inter-observation time $\Delta t = \max\{t_{i+1} - t_i\}$ and it is acceptable to consider the limit $\Delta t \to 0$, $T \to \infty$, then many results are available, see [9] in the parametric case and e.g. [5] in the nonparametric case.

This work assumes a simpler parametric form for the diffusivity $\sigma(v) \equiv \Sigma \in \mathbb{R}^{2\times 2}$ and presents fully nonparametric estimation of the drift $\xi(\cdot)$. In extension of [7, 8], the state space considered is the two-dimensional torus, or equivalently the unit square with periodic boundary conditions but the work differs from [4] by defining the process on the torus rather than mapping a diffusion on $\mathbb{R}^2$ to the torus by a modulus operation. The prior measure is Gaussian and described by the prior mean function $\xi_0 \equiv 0$ and the prior precision operator

$$\mathcal{A}_0 = \eta_o I + \eta(\partial_x^8 + \partial_y^8),$$

where x and y refer to the two coordinates describing the state space $S = [0,1]^2 \ni (x,y)^T$ and $\eta > 0$, $\eta_o > 0$ are so-called hyperparameters that are chosen to more carefully reflect prior beliefs on the drift.

As in the univariate case, conditional on continuous time observations and diffusivity, the posterior follows a Gaussian measure and the update equations connecting prior to posterior mean and precision are of the same form given in [7], i.e. the posterior mean is given as the solution of

$$(1) \qquad \int_S \varphi(v)\mathcal{A}\hat{\xi}(v)\mathrm{d}v = \frac{1}{2}\int_0^T \varphi(V_t)\mathrm{d}V_t \qquad \forall \varphi \in \mathcal{D}(\mathcal{A}),$$

where the posterior precision is given by

$$\mathcal{A} = \mathcal{A}_0 + \gamma_T,$$

where, in turn, γ_T is the empirical measure of the process $\{V_t\}_{t=0}^T$:

$$\int_0^T \varphi(V_t)\mathrm{d}t = \int_S \varphi(v)\mathrm{d}\gamma_T(v) \qquad \forall \varphi \in \mathbb{C}(S).$$

Discretization is carried out via a truncated Fourier representation using preconditioned conjugate gradient methods to solve the PDE (1) and to sample from the posterior measure using the Krylov-based methods reviewed in [1]. The algorithm is complemented by a Langevin-based sampling method for data augmentation and a Gibbs sampler. Finally, an application to animal movement modelling is displayed briefly where position observations of a single Capuchin monkey are obtained at not quite regularly spaced observation times. It is found that acceptable model fit is obtained only upon sub-sampling of the data and the drift appears non-conservative (i.e. it contains a rotational component) which precludes simpler models present in the literature on animal movement ecology where the drift is modelled as the gradient of a potential, e.g. [3].

References

[1] E. Aune, J. Eidsvik, Y. Pokern, *Iterative numerical methods for sampling from high dimensional Gaussian distributions*, Statistics and Computing, (2012).

[2] J. M. Bernardo, A. F. M. Smith *Bayesian Theory*, Wiley (2000).

[3] D. R. Brillinger, H. K. Preisler, A. A. Ager, J. G. Kie *The Use of Potential Functions in Modelling Animal Movement*, In: Data Analysis from Statistical Foundations, Nova Science, Huntington (2007), pp. 369–386

[4] E. Garcia-Portugues, M. Sorensen, K. V. Mardia, T. Hamelryck, *Langevin Diffusion on the Torus: estimation and applications*, arxiv1705.00296

[5] F. Comte, V. Genon-Catalot, Y. Rozenholc, *Penalized nonparametric mean square estimation of the coefficients of diffusion processes*, Bernoulli, **13**, 2, (2007), 514–543.

[6] Y. A. Kutoyants, *Statistical Inference for Ergodic Diffusion Processes*, Springer (2004).

[7] O. Papaspiliopoulos, Y. Pokern, G. O. Roberts, A. M. Stuart, *Nonparametric estimation of diffusions: a differential equations approach*, Biometrika **99**, 2 (2012), 511–531.

[8] Y. Pokern, A. M. Stuart, H. J. van Zanten *Posterior consistency via precision operators for Bayesian nonparametric drift estimation in SDEs*, Stochastic Processes and Their Applications **132**, 2 (2013), 603–628.

[9] B .L. S. Prakasa Rao, *Statistical Inference for Diffusion Type Processes*, Arnold Publishers, London (1999).

[10] A. M. Stuart, *Inverse Problems: A Bayesian perspective*, Acta Numerica **19**, (2010), 451–559.

Inverse homogenization: Inverse problem for the structure of composites

Elena Cherkaev

Subscale processes in microstructured media are of concern in a variety of physical and biological imaging and inverse problems. Modeling of transport phenomena (electromagnetic, thermal, fluid, etc.) in such medium involves homogenization of the fine scale problem. Solution of the corresponding inverse problem provides the homogenized or effective parameters of the medium. Inverse homogenization is a problem of deriving characteristics of the underlying microlevel process or geometry of a finely structured composite material from the known effective properties. The approach is based on the reconstruction of the matrix-valued spectral measure in the Stieltjes integral representation of the homogenized parameters of the media. This representation relates the n-point correlation functions of the microstructure to the moments of the spectral measure of an operator depending on the composite's geometry. We show that the matrix-valued spectral measure that contains all information about the fine scale geometry, together with its moments, can be uniquely reconstructed from the effective properties of the medium measured in an interval of frequency.

As an example of a problem with processes on a subscale, we consider interaction of low frequency electromagnetic wave with a finely structured medium. We assume that a heterogeneous material occupying a domain Ω in $\mathbb{R}^3$, is ε-periodic with the cell of periodicity Ω^ε, and consider the time-harmonic Maxwell's equations in the ε-periodic medium:

$$\begin{cases} \nabla \times E^\varepsilon(x) - i\omega\mu(x/\varepsilon)H^\varepsilon(x) = 0, & \nabla \cdot \epsilon(x/\varepsilon)E^\varepsilon(x) = 0 \\ \nabla \times H^\varepsilon(x) + i\omega\epsilon(x/\varepsilon)E^\varepsilon(x) = 0, & \nabla \cdot \mu(x/\varepsilon)H^\varepsilon(x) = 0 \end{cases}$$

Here E^ε and H^ε are electric and magnetic fields, ϵ is complex permittivity, μ is magnetic permeability, and ω is the frequency. Two-scale asymptotic expansions method with $y = x/\varepsilon \in \Omega^\varepsilon$ results in homogenized Maxwell's equations [11]:

$$\begin{cases} \nabla \times E(x) - i\omega\mu^* H(x) = 0, & \nabla \cdot \epsilon^* E(x) = 0 \\ \nabla \times H(x) + i\omega\epsilon^* E(x) = 0, & \nabla \cdot \mu^* H(x) = 0 \end{cases}$$

Functions E, H are the homogenized electric and magnetic fields, and ϵ^* and μ^* are effective permittivity and permeability of the medium,

(1) $\qquad \epsilon^* = < \epsilon(y)\left(I_3 + \nabla_y \phi_{\mathrm{e}}(y)\right) >, \qquad \mu^* = < \mu(y)\left(I_3 + \nabla_y \phi_{\mathrm{h}}(y)\right) >$

where $< \cdot >$ denotes averaging over Ω^ε, and functions ϕ_{e} and ϕ_{h} are solutions of local elliptic equations:

(2) $\quad \nabla_y \cdot \epsilon(y)\nabla_y \phi_{\mathrm{e}}^k(y) = -\nabla_y \cdot \epsilon(y)e_k, \qquad \nabla_y \cdot \mu(y)\nabla_y \phi_{\mathrm{h}}^k(y) = -\nabla_y \cdot \mu(y)e_k$

As the electric and magnetic problems are decoupled on the fine scale, we further consider only the local problem for the electric field. We assume that on the fine scale, the medium is a two-phase composite, χ is the characteristic function of the domain occupied by the first material. Permittivity $\epsilon(y)$ takes values $\epsilon_i, i = 1, 2$, in domains occupied by the i-th material, $\epsilon(y) = \epsilon_1\chi(y) + \epsilon_2(1 - \chi(y))$. The

local problem (2) can be rewritten as $\nabla \cdot (\epsilon_1 \chi(y) + \epsilon_2(1 - \chi(y))) E = 0$ for $E = e_k + \nabla \phi$ and brought to the form: $\nabla \cdot \chi E = s \nabla \cdot E$ with a complex parameter $s = 1/(1 - \epsilon_1/\epsilon_2)$. Then, $\nabla \cdot \chi (\nabla \phi + e_k) = s \Delta \phi$, where $(-\Delta)$ is the Laplacian. Introducing an operator Γ projecting vector fields onto a subspace of curl free, zero mean fields, $\Gamma = \nabla(-\Delta)^{-1}(\nabla \cdot)$, we can express E as a function of the operator $\Gamma \chi$,

$$(3) \qquad E = (I + \frac{1}{s}\Gamma \chi)^{-1} e_k = s(sI + \Gamma \chi)^{-1} e_k.$$

With the function χ in the inner product, $\Gamma \chi$ is a bounded self-adjoint operator. The spectral resolution of $\Gamma \chi$ with the projection valued measure Q results in the spectral representation for the field E. Using (1), (3), and the spectral representation of the resolvent, we represent the function $F(s) = 1 - \epsilon^*(s)/\epsilon_2$ as

$$(4) \qquad F_{jk}(s) = \langle \chi \, (sI + \Gamma \chi)^{-1} e_j, e_k \rangle = \int_0^1 \frac{\langle \chi \, dQ(z) \, e_j, \, e_k \rangle}{s - z} = \int_0^1 \frac{d\mu_{jk}(z)}{s - z}$$

where μ is the *spectral measure* of $\Gamma \chi$, $d\mu_{jk}(z) = \langle \chi \, dQ(z) e_j, e_k \rangle$.

   This integral representation was developed to derive *forward bounds* on ϵ^* given permittivity values ϵ_1, ϵ_2 and partial information on the composite geometry [1, 7, 6]. Since then it was used in a variety of forward and inverse homogenization problems (see [8, 3, 9, 10] and references therein). For the discussed inverse problem, it is important that the representation (4) separates the parameter information in s from information about the microgeometry contained in μ. Information about the structure of the subscale process is incorporated into μ via its moments μ^n, depending on the $(n+1)$-point correlation functions of the medium:

$$(5) \qquad \mu_{jk}^n = \int_0^1 z^n d\mu_{jk}(z) = (-1)^n \langle \chi[(\Gamma \chi)^n e_j] \cdot e_k \rangle$$

   In the case when the homogenized medium is isotropic with a scalar effective permittivity, $F(s)$ is a scalar function of s, and the spectral measure μ is a scalar measure. Also, if the function χ is axisymmetric with respect to the spatial coordinates, the matrix of measures μ is diagonalizable, and we can consider separately diagonal elements μ_{kk} and $F_{kk}(s)$ of μ and $F(s)$ as scalar functions of s. In this case, the following uniqueness theorems hold.

Theorem 1 ([2])**.** *The measure μ can be uniquely reconstructed if the function $F(s)$ is known on an open set of the complex variable s with a limiting point.*

Theorem 2 ([4])**.** *The moments of the measure μ can be uniquely reconstructed if the function $F(s)$ is known on an open set of the complex variable s with a limiting point. Moreover, function μ and its moments are uniquely reconstructed if the effective complex permittivity ϵ^* is known in an interval of frequency ω.*

   Here we extend these results to the general case of a non-diagonalizable matrix-valued measure $\mu = \{\mu_{jk}\}$ corresponding to an anisotropic medium.

Theorem 3. *A determinate matrix measure μ together with its moments (5), can be uniquely reconstructed if the matrix function $F(s)$ is known on an open set of the complex variable s with a limiting point. In particular, sufficient data are provided by the effective complex permittivity tensor ϵ^* (1) known in an interval of frequency ω.*

An efficient numerical method of reconstruction of the function μ is based on Padé approximation. In the case of scalar function μ, the convergence of the Padé approximants is asserted by Markov's theorem (A. Markov, 1895).

$$\lim_{n \to \infty} \frac{q_n(s)}{p_n(s)} = \int_0^1 \frac{d\mu(z)}{s - z}, \qquad \text{for} \quad s \in \mathbb{C} \setminus [0, 1]$$

Here $\{p_n\}_n$ is a sequence of polynomials orthogonal with respect to μ and $\{q_n\}_n$ is a sequence of polynomials of the second kind,

$$q_n(t) = \int_0^1 \frac{p_n(t) - p_n(z)}{t - z} \, d\mu(z), \quad n \geq 0$$

The Padé approximant for a matrix-valued analytic function is constructed using matrix polynomials P_n orthogonal with respect to measure μ:

$$\int_0^1 P_n(z) \, d\mu(z) \, P_m^*(z) = \delta_{nm} I, \quad n, m \geq 0, \quad \mu(z) = \mu_{jk}(z)$$

and matrix polynomials of the second kind $Q_n(s)$.

Theorem 4 ([5]). *For a determinate matrix measure μ*

$$\lim_{n \to \infty} P_n^{-1}(s) \, Q_n(s) = \int_0^1 \frac{d\mu(z)}{s - z}, \quad for \quad s \in \mathbb{C} \setminus [0, 1]$$

Convergence is uniform for s in compact subsets of $\mathbb{C} \setminus [0, 1]$.

Moreover, for a given sequence of polynomials $\{P_n\}_n$, the corresponding measure can be found as weak accumulation points of a sequence of discrete measures with support in a set of zeros of $\{P_n\}$, $\mu_n = \sum_{k=1}^m \delta_{z_{n,k}} G_{n,k}$, where G_{nk} are matrices:

$$G_{nk} = \frac{1}{\det(P_n(z))^{l_k}(z_{nk})} \left(Adj(P_n(z))\right)^{l_k - 1}(z_{nk}) \, Q_n(z_{nk})$$

and z_{nk} are the zeros of $P_n(z)$ (in increasing order) of multiplicity l_k. Then the matrix Padé approximant can be written as:

$$P_n^{-1}(s) \, Q_n(s) = \sum_{k=1}^m G_{nk} \frac{1}{s - z_{nk}}$$

where m is the number of zeros of $P_n(z)$. Using these results, we show that:

Theorem 5. *The moments μ^k of the matrix-valued spectral measure μ of the operator $\Gamma\chi = \nabla(-\Delta)^{-1}(\nabla \cdot \chi)$ are given by*

$$\mu_k = \sum_{j=1}^m G_{nj} z_{nj}^k .$$

The formulas are exact for $k = 0, 1, ..., 2n - 1$.

References

[1] D.J. Bergman, *The dielectric constant of composite material - a problem in classical physics*, Phys.Rep. C, **43** (1978), 377–407.

[2] E. Cherkaev, *Inverse homogenization for evaluation of effective properties of a mixture*, Inverse Problems, **17** (2001), 1203–1218.

[3] E. Cherkaev, C. Bonifasi-Lista, *Characterization of structure and properties of bone by spectral measure method*, J Biomech., 2011, **44** (2011), 2, 345–351.

[4] E. Cherkaev, M-J. Ou, *De-homogenization: reconstruction of moments of the spectral measure of composite*, Inverse Problems, **24** (2008), 065008.

[5] A. Duran, *Markov's theorem for orthogonal matrix polynomials*, Canad. J. Math., **48** (1996), 1180–1195.

[6] K. Golden, G. Papanicolaou, *Bounds for effective parameters of heterogeneous media by analytic continuation*, Commun. Math. Phys., **90** (1983), 473–491.

[7] G.W. Milton, *Bounds on the complex dielectric constant of a composite material*, Appl. Phys. Lett., **37** (1980), 3, 300–302.

[8] G.W. Milton, *The Theory of Composites*, Cambridge University Press (2002), Cambridge.

[9] N.B. Murphy, E. Cherkaev, K. Golden, *Anderson transition for classical transport in composite materials*, Phys. Rev. Lett., **118** (2017), 036401.

[10] N.B. Murphy, E. Cherkaev, J. Zhu, J. Xin, K. Golden, *Spectral analysis and computation of effective diffusivities in space-time periodic incompressible flows*, Annals of Mathematical Sciences and Applications, **2** (2017), 1, 3–66.

[11] N. Wellander, G. Kristensson, *Homogenization of the Maxwell equations at fixed frequency*, SIAM J. Appl. Math., **64** (2003), 1, 170–195.

Quantitative Photoacoustic Imaging of Two-photon Absorption

Kui Ren

(joint work with Patrick Bardsley, Rongting Zhang)

Two-photon absorption photoacoustic tomography (TP-PAT) [4, 7, 9, 11, 12, 13, 14] is a variant of photoacoustic tomography (PAT) that uses photoacoustic effects to determine two-photon optical absorption properties of biological tissues. Here the term two-photon optical absorption refers to the phenomenon that an electron transfers to an excited state after simultaneously absorbing two photons whose total energy exceed the electronic energy band gap. It is obvious that two-photon absorption occurs much less frequently than single-photon absorption when the photon density is not particularly high. That is the main reason that two-photon absorption is often neglected in traditional modeling of light propagation in biological tissues. However, the two-photon absorption phenomenon can be very useful in molecular imaging since it can often be tuned to be associated with specific molecular signatures. We can therefore use it to visualize particular cellular functions and molecular processes inside biological tissues if we have a way to image two-photon absorption.

The main difference between TP-PAT and the regular PAT is that two-photon absorption, in addition to single-photon absorption, needs to be considered in the model for light propagation. Let $\Omega \subseteq \mathbb{R}^d$ ($d \geq 2$) be the medium to be probed,

and $u(\mathbf{x})$ be the density of photons at position $\mathbf{x} \in \Omega$. Then, in diffusive regime, $u(\mathbf{x})$ solves the following semilinear diffusion equation:

(1)
$$\begin{aligned} -\nabla \cdot \gamma(\mathbf{x})\nabla u(\mathbf{x}) + \sigma(\mathbf{x})u(\mathbf{x}) + \mu(\mathbf{x})|u|u(\mathbf{x}) &= 0, & \text{in } \Omega \\ u &= g(\mathbf{x}), & \text{on } \partial\Omega \end{aligned}$$

where the function $g(\mathbf{x})$ models the incoming NIR photon source, the function $\gamma(\mathbf{x})$ is the diffusion coefficient of the medium, $\sigma(\mathbf{x})$ is the usual single-photon absorption coefficient of the medium, and $\mu(\mathbf{x})$ is the intrinsic two-photon absorption coefficient. The total two-photon absorption coefficient is given by the product $\mu(\mathbf{x})|u|$ where the absolute value operation is taken to ensure that the total two-photon absorption coefficient is non-negative, a property that needs to be preserved for the diffusion model to correctly reflect the physics.

The initial pressure field generated by the photoacoustic effect in TP-PAT is the product of the Grüneisen coefficient of the medium, Γ, and the total energy absorbed locally by the medium, $\sigma u + \mu|u|u$ [3, 5]. Note that here the total absorbed energy consists of two components, the contribution from single-photon absorption, σu, and the contribution from two-photon absorption, $\mu|u|u$. Therefore, we write the initial pressure field as [2, 3, 5]:

(2)
$$H(\mathbf{x}) = \Gamma(\mathbf{x})\Big[\sigma(\mathbf{x})u(\mathbf{x}) + \mu(\mathbf{x})|u|u(\mathbf{x})\Big], \qquad \mathbf{x} \in \Omega.$$

The Grüneisen coefficient is non-dimensionalized. It describes the efficiency of the photoacoustic effect of the underlying medium.

The change of pressure field generates ultrasound waves that propagate following the standard acoustic wave equation [3]:

(3)
$$\begin{aligned} \frac{1}{c^2(\mathbf{x})}\frac{\partial^2 p}{\partial t^2} - \Delta p &= 0, & \text{in } (0, +\infty) \times \mathbb{R}^d \\ p(t, \mathbf{x}) = H(\mathbf{x})\chi_\Omega, \quad \frac{\partial p}{\partial t}(t, \mathbf{x}) &= 0, & \text{in } \{t = 0\} \times \mathbb{R}^d \end{aligned}$$

where $p(t, \mathbf{x})$ is the pressure field, $c(\mathbf{x})$ is the speed of the ultrasound waves, and χ_Ω is the characteristic function of the domain Ω. The ultrasound speed c is assumed known. The objective of TP-PAT is to reconstruct the optical coefficients from measured ultrasound signal on the surface of the medium, $p|_{(0,T)\times\partial\Omega}$ for T long enough.

We investigated numerically the inverse problem using the nonlinear least-square framework. For instance, in the case of reconstructing (σ, μ) from $J \geq 1$ data sets generated by sources $\{g_j\}_{j=1}^J$, we search for (σ, μ) that minimizes the functional

(4)
$$\Phi(\sigma, \mu) \equiv \frac{1}{2}\sum_{j=1}^J \int_0^T \int_{\partial\Omega} (p_j - p_j^*)^2 d\mathbf{x}dt + \kappa R(\sigma, \mu),$$

where $(0, T)$ is the measurement time interval, p_j^* is the measured acoustic data generated by source g_j ($1 \leq j \leq J$), and the regularization term $R(\sigma, \mu) = \frac{1}{2}\left(\int_\Omega |\nabla\sigma|^2 d\mathbf{x} + \int_\Omega |\nabla\mu|^2 d\mathbf{x}\right)$. In Fig. 1, we show some typical reconstructions of the absorption coefficients in a numerical experiment with four data sets.
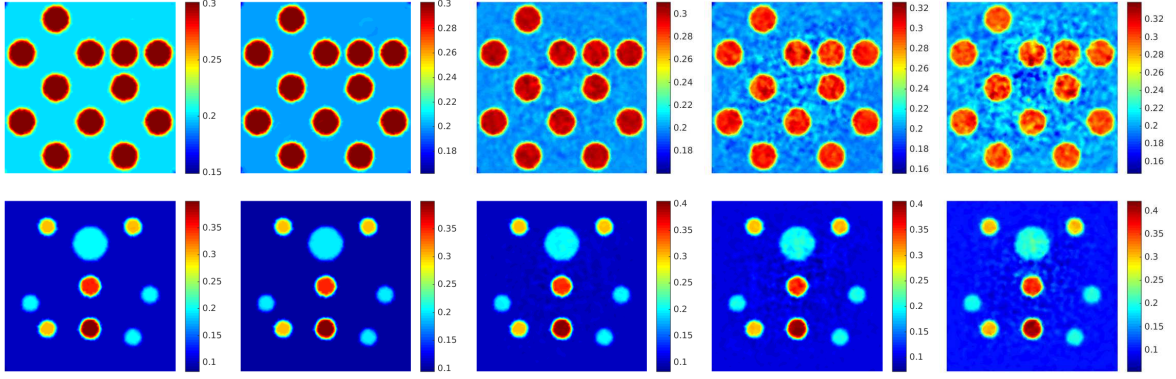
FIGURE 1. The true absorption coefficients (σ (top row), μ (bottom row)) (first column) and the reconstructions with data at different noise levels ($\epsilon = 0\%, 2\%, 5\%, 10\%$ from the second column to the fifth column). Data collected from four different illuminations are used in each reconstruction.

We also analyzed mathematically the quantitative step of the inverse problem: to reconstruct information on the coefficients $(\Gamma, \gamma, \sigma, \mu)$ from $J \geq 1$ internal data sets:

$$H_j(\mathbf{x}) = \Gamma(\mathbf{x})\Big[\sigma(\mathbf{x})u_j(\mathbf{x}) + \mu(\mathbf{x})|u_j|u_j(\mathbf{x})\Big], \quad 1 \leq j \leq J,$$

generated with boundary sources g_j $(1 \leq j \leq J)$

$$\begin{aligned}
-\nabla \cdot \gamma(\mathbf{x})\nabla u_j(\mathbf{x}) + \sigma(\mathbf{x})u_j(\mathbf{x}) + \mu(\mathbf{x})|u_j|u_j(\mathbf{x}) &= 0, && \text{in } \Omega \\
u_j &= g_j(\mathbf{x}), && \text{on } \partial\Omega
\end{aligned}$$

The results can be summarized as follows.

(a) Nonuniqueness in reconstructing $(\Gamma, \gamma, \sigma, \mu)$**.** It is not possible to reconstruct all four coefficients simultaneously, no matter how much data we have. The precise statement is as follows.

Theorem 1. *Let $\gamma^{1/2}|_{\partial\Omega}$ be given and assume that $\gamma^{1/2} \in \mathcal{C}^2(\Omega)$. Define the following functionals:*

$$\alpha = \frac{\Delta\gamma^{1/2}}{\gamma^{1/2}} + \frac{\sigma}{\gamma}, \qquad \beta = \frac{\mu}{\gamma^{3/2}}, \qquad \zeta_1 = \Gamma\frac{\sigma}{\gamma^{1/2}}, \qquad \zeta_2 = \Gamma\frac{\mu}{\gamma}.$$

Assume that either (α, β, ζ_1) or (α, β, ζ_2) is known, and H is among the data used to determine them. Then for any given new illumination $\widetilde{g}$, the corresponding datum $\widetilde{H}$ is uniquely determined by $(\widetilde{g}, H)$.

This result says that once we know (α, β, ζ_1) (or (α, β, ζ_2)), which is not enough to uniquely determine all four coefficients, introducing more data will not provide new information in terms of uniqueness.

(b) Uniqueness and stability in reconstructing (σ, μ)**.** If we are only interested in the reconstruction of the absorption coefficients, we can show that two "well-chosen" data sets are sufficient to uniquely and stably reconstruct (σ, μ) as stated in the following result.

Theorem 2. *Let Γ and γ be given. Let (H_1, H_2) and $(\widetilde{H}_1, \widetilde{H}_2)$ be the data sets corresponding to the coefficients (σ, μ) and $(\widetilde{\sigma}, \widetilde{\mu})$ respectively that are generated with the pair of sources (g_1, g_2). Assume that $g_i \geq \varepsilon > 0$, $i = 1, 2$, and $g_1 - g_2 \geq \varepsilon' > 0$ for some ε and ε'. Then $(H_1, H_2) = (\widetilde{H}_1, \widetilde{H}_2)$ implies $(\sigma, \mu) = (\widetilde{\sigma}, \widetilde{\mu})$ provided that all coefficients involved are sufficiently smooth. Moreover, we have*

$$(5) \quad \|\sigma - \widetilde{\sigma}\|_{L^\infty(\Omega)} + \|\mu - \widetilde{\mu}\|_{L^\infty(\Omega)} \leq \widetilde{C}\left(\|H_1 - \widetilde{H}_1\|_{L^\infty(\Omega)} + \|H_2 - \widetilde{H}_2\|_{L^\infty(\Omega)}\right),$$

for some constant $\widetilde{C}$.

(c) Local uniqueness in determining (γ, σ, μ)**.** It turns out that we can in fact simultaneously reconstruct three of the four coefficients. However, the analysis of the inverse problem in this case is much more complicated technically. In the case of reconstructing (γ, σ, μ), assuming Γ is known, we can establish a local uniqueness result using the tools of complex geometric optics (CGO) solutions [6, 8]. Our analysis is based on the study of the linearized system for the perturbations $\{\delta\gamma, \delta\sigma, \delta\mu, \{\delta u_j\}_{j=1}^J\}$, consisting of the governing equations as well as the internal data, around background (γ, σ, μ):

$$\begin{aligned}
-\nabla \cdot (\delta\gamma \nabla u_j) - \nabla \cdot (\gamma \nabla \delta u_j) &= -\delta H_j/\Gamma, \quad \text{in } \Omega \\
u_j \delta\sigma + |u_j| u_j \delta\mu + (\sigma + 2\mu |u_j|)\delta u_j &= +\delta H_j/\Gamma, \quad \text{in } \Omega
\end{aligned}$$

with appropriate boundary conditions.

Theorem 3. *Let $d = 3$. Let $\{\delta H_j\}_{j=1}^J$ and $\{\widetilde{\delta H_j}\}_{j=1}^J$ be the data sets generated with $(\delta\gamma, \delta\sigma, \delta\mu)$ and $(\widetilde{\delta\gamma}, \widetilde{\delta\sigma}, \widetilde{\delta\mu})$ respectively. Assume that the background coefficients are smooth enough. Then there exists a set of $J \geq d+1$ boundary illuminations, $\{g_j\}_{j=1}^J$, such that $\{\delta H_j\}_{j=1}^J = \{\widetilde{\delta H_j}\}_{j=1}^J$ implies $(\delta\gamma, \delta\sigma, \delta\mu) = (\widetilde{\delta\gamma}, \widetilde{\delta\sigma}, \widetilde{\delta\mu})$ if $\delta\gamma_{|\partial\Omega} = \widetilde{\delta\gamma}_{|\partial\Omega}$.*

A general stability result can be derived following the theory of Douglis-Nirenberg on over-determined elliptic systems [1, 10]; see [5] for more details.

References

[1] G. Bal, *Hybrid inverse problems and redundant systems of partial differential equations*, in Inverse Problems and Applications, P. Stefanov, A. Vasy, and M. Zworski, eds., vol. 615 of Contemporary Mathematics, American Mathematical Society, 2013, pp. 15–48.

[2] P. Bardsley, K. Ren, and R. Zhang, *Quantitative photoacoustic imaging of two-photon absorption*, Submitted, (2017).

[3] A. R. Fisher, A. J. Schissler, and J. C. Schotland, *Photoacoustic effect for multiply scattered light*, Phys. Rev. E, 76 (2007). 036604.

[4] G. Langer, K.-D. Bouchal, H. Grün, P. Burgholzer, and T. Berer, *Two-photon absorption-induced photoacoustic imaging of Rhodamine B dyed polyethylene spheres using a femtosecond laser*, Optics Express, 21 (2013), pp. 22410–22422.

[5] K. Ren and R. Zhang, *Nonlinear quantitative photoacoustic tomography with two-photon absorption*, SIAM J. Appl. Math., 77 (2017).

[6] J. Sylvester and G. Uhlmann, *Global uniqueness theorem for an inverse boundary value problem*, Ann. Math., 125 (1987), pp. 153–169.

[7] G. J. Tserevelakis, D. Soliman, M. Omar, and V. Ntziachristos, *Hybrid multiphoton and optoacoustic microscope*, Opt. Lett., 39 (2014), pp. 1819–1822.

[8] G. Uhlmann, *Electrical impedance tomography and Calderon's problem*, Inverse Problems, 25 (2009). 123011.

[9] B. E. Urban, J. Yi, V. Yakovlev, and H. F. Zhang, *Investigating femtosecond-laser-induced two-photon photoacoustic generation*, J. Biomed. Opt., 19 (2014). 085001.

[10] T. Widlak and O. Scherzer, *Stability in the linearized problem of quantitative elastography*, Inverse Problems, 31 (2015). 035005.

[11] P. W. Winter, A. G. York, D. D. Nogare, M. Ingaramo, R. Christensen, A. Chitnis, G. H. Patterson, and H. Shroff, *Two-photon instant structured illumination microscopy improves the depth penetration of super-resolution imaging in thick scattering samples*, Optica, 1 (2014), pp. 181–191.

[12] Y. Yamaoka, M. Nambu, and T. Takamatsu, *Fine depth resolution of two-photon absorption-induced photoacoustic microscopy using low-frequency bandpass filtering*, Optics Express, 19 (2011), pp. 13365–13377.

[13] Y. Yamaoka and T. Takamatsu, *Enhancement of multiphoton excitation-induced photoacoustic signals by using gold nanoparticles surrounded by fluorescent dyes*, in Photons Plus Ultrasound: Imaging and Sensing, A. A. Oraevsky and L. V. Wang, eds., SPIE, 2009. 71772A.

[14] C. S. Yelleswarapu and S. R. Kothapalli, *Nonlinear photoacoustics for measuring the nonlinear optical absorption coefficient*, Optics Express, 18 (2010), pp. 9020–9025.

Coherent acousto-optic imaging

John C. Schotland

(joint work with Jeremy Hoskins)

The acousto-optic effect refers to the scattering of light from a medium whose optical properties are modulated by an acoustic wave. Brillouin scattering from density fluctuations in a fluid [1] and the ultrasonic modulation of multiply-scattered light [2] are familiar examples of this effect. It is well known that the scattered optical field carries information about the medium. This principle has been exploited to develop an imaging modality, known as acousto-optic imaging, which combines the spectroscopic sensitivity of optical methods with the spatial resolution of ultrasonic imaging. Two forms of acousto-optic imaging are usually distinguished. Direct imaging employs a focused ultrasound beam for image formation [3, 4, 5, 6, 7, 8, 9, 10, 11, 12, 13, 14, 15, 16, 17]. The image is created by scanning the focus of the beam and recording the intensity of the scattered light at a fixed detector. Tomographic imaging utilizes an inverse scattering method to reconstruct images of the optical properties of the medium [20, 22, 32, 33, 34, 29, 31, 30, 35].

The theory of the acousto-optic effect begins with a model for the propagation of electromagnetic waves in a material medium. The most general such model is based on the Maxwell equations for a dielectric whose permittivity is modulated by an acoustic wave [1]. Alternatively, for multiply-scattered light, a phenomenological theory based on the radiative transport equation (RTE) or the diffusion approximation (DA) to the RTE may be employed [18, 20, 21, 19]. In this paper,

we develop a *first-principles* theory of the acousto-optic effect. We begin by constructing a model for the acoustic modulation of the dielectric permittivity of a medium consisting of small scatterers suspended in a fluid. Next, we consider the propagation of light in the medium and obtain the wave equations obeyed by the frequency components of the optical field at harmonics of the acoustic frequency. We then obtain the corresponding RTE by asymptotic analysis of the Wigner transform of the field in a random medium. We note that the problem is challenging because the random medium acquires a time-dependence due to the presence of the acoustic field. We apply our results to estimating the minimum detectable size of a small inhomogeneity in acousto-optic imaging. Since the scatterers in the medium are displaced by the acoustic wave, the scattered light undergoes a frequency shift which permits the localization of the resulting so-called tagged photons to the volume containing the focus.

References

[1] M. Born and E. Wolf, *Principles of Optics* (Cambridge University Press, Cambridge, England, 1999).

[2] W. Leutz and G. Maret, Physica B **204**, 14 (1995).

[3] F.A. Marks, H.W. Tomlinson and G.W. Brooksby, Proc. SPIE **1888**, 500 (1993).

[4] M. Kempe, M. Larionov, D. Zaslavsky and A.Z. Genack, J. Opt. Soc. Am. 14, 1151 (1997).

[5] E. Granot, A. Lev, Z. Kotler, B.G. Sfez and H. Taitelbaum, J. Opt. Soc. Am. A **18**, 1962 (2001).

[6] L.H. Wang, S.L. Jacques and X. Zhao, Opt. Lett. **20**, 629 (1995).

[7] L.H. Wang and Q. Shen, Opt. Lett. **23**, 561 (1998).

[8] L.-H.V. Wang and G. Ku, Opt. Lett. **23**, 975 (1998).

[9] G. Yao, S. Jiao and L.-H.V. Wang, Opt. Lett. **25** 734 (2000).

[10] J. Li and L.-H.V. Wang, Appl. Opt. **41**, 2079 (2002).

[11] J. Li, G. Ku and L.-H.V. Wang, Appl. Opt. **41** 6030 (2002).

[12] S. Leveque, A.C. Boccara, M. Lebec and H. Saint-Jalmes, Opt. Lett. **24**, 181 (1999).

[13] S. Leveque-Fort, J. Selb, L. Pottier and A.C. Boccara, Opt. Comm. **196**, 127 (2001).

[14] M. Atlan, B.C. Forget, F. Ramaz, A.C. Boccara and M. Gross, Opt. Lett. **30**, 1360 (2005).

[15] M. Gross, M. Lesaffre, F. Ramaz, P. Delaye, G. Roosen and A.C. Boccara, Eur. Phys. J. E **28**, 173 (2009).

[16] A. Lev, Z. Kotler and B.G. Sfez, Opt. Lett. **25** 378 (2000).

[17] A. Lev and B.G. Sfez, Opt. Lett. **27**, 473 (2002).

[18] G. D. Mahan, W. E. Engler, J. J. Tiemann, and E. Uzgiris, Proc. Natl. Acad. Sci USA **95**, 14015 (1998)

[19] S. Sakadzic and L. V. Wang, Phys. Rev. Lett. **96**, 163902 (2006).

[20] G. Bal and J. C. Schotland, Phys. Rev. Lett. **104**, 043902 (2010).

[21] Hollmann, J. L., Horstmeyer, R., Yang, C. H. and DiMarzio, C. A., J. Biomed. Opt. **19**, 035005 (2014).

[22] H. M. Varma, K. P. Mohanan, N. Hyvonen, A. K. Nandakumaran and R. M. Vasu J. Opt. Soc. Am. A **28**, 2322-2332 (2011).

[23] M. C. W. van Rossum and Th. M. Nieuwenhuizen, Rev. Mod. Phys. **71**, 313 (1999).

[24] P. de Vries, D. van Coevorden and A. Lagendijk, Rev. of Mod. Phys. **70**, 447-466 (1998).

[25] L. Ryzhik, G. Papanicolaou and J.B. Keller, Wave Motion **24**, 327 (1996).

[26] A. Caze and J. C. Schotland, J. Opt. Soc. Am. A **32**, 1475-1484 (2015).

[27] J. Duderstadt and W. Martin, *Transport Theory* (John Wiley and Sons, New York, 1979).

[28] V. A. Markel and J. C. Schotland, Phys. Rev. E **70**, 056616 (2004).

[29] G. Bal and J. Schotland, Phys. Rev. E. **89**, 031201 (2014).

[30] G. Bal, F. Chung and J. C. Schotland, SIAM J. Math. Analysis **48**, 1332-1347 (2016).

[31] G. Bal and S. Moskow, Inverse Problems, **30**, 025005 (2014).

[32] Ammari, H., Bossy, E., Garnier, J, Nguyen, L. H. and Seppecher, L., Proc. American Mathematical Society, **142**, 3221-3236 (2014).

[33] Ammari, H., Nguyen, L. H. and Seppecher, L., J. Functional Analysis **267**, 4361-4398 (2014).

[34] Ammari, H., Garnier, J, Nguyen, L. H. and Seppecher, L., Communications in Partial Differential Equations **38**, 1737-1762 (2013).

[35] F. J. Chung and J. C. Schotland, Inverse Transport and Acousto-Optic Imaging, arXiv:1609.08118

Reporter: Frederic Weidling